SVENSKA GEOFYSISKA FÖRENINGEN

VOLUME II, NUMBER 4 **Tellus** NOVEMBER 1959

A QUARTERLY JOURNAL OF GEOPHYSICS

The Yearly Circulation of Chloride and Sulfur in Nature; Meteorological, Geochemical and Pedological Implications. Part I

By ERIK ERIKSSON

International Meteorological Institute, Stockholm

(Manuscript received May 28, 1959)

Abstract

The circulation of air borne oceanic constituents is discussed to the extent available data permit. From data on sea salt particles in the atmosphere and their fall rate it is estimated that they are produced at a rate of the order of magnitude 1000 million tons a year over the ocean areas. About 90 per cent of this is precipitated over the oceans, the rest is carried into continents and is brought back to the sea in rivers. The estimated residence time for sea salt particles in the atmosphere is only a few days, higher for smaller particles, which lose their identity through coalescence, and lower for larger particles, lost by rainout or fallout. From the rate of production of sea salt particles in breaking waves it is concluded that about 0.3 per cent of the ocean areas is covered by breaking waves. On land the residence time of sea salt may vary from a few years in peripherally, drained humid areas to thousands of years in arid areas or areas without peripheral run-off.

Geochemical balance computations indicate that a major part of the sulfur in the atmosphere is of oceanic origin but does not originate as chloride through spray emitted from breaking waves. Of chemical reactions taking place in the atmosphere between sea salt constituents the release of HCl from sea salt particles due to absorption of oxidized sulfur dioxide seems to be quantitatively important and mainly responsible for variations in the Cl/Na ratio in precipitation. The deposition of chloride in precipitation over continents shows nicely the main areas of inflow of maritime air. Dry deposition of sea salt components seems to be an important process. The rate of which these constituents are carried to the ground from the air is about 1—2 cm per second, a figure concordant with the turbulent nature of air close to the ground.

As for proportions of sea salt components in precipitation some fractionation processes seems to take place at the sea surface (probably involving organic matter derived from surface films). In typical maritime areas there is always an excess cations over inorganic anions suggesting association of some cations with organic acid material in precipitation. The presence of sea salt components in groundwater can be taken advantage of in the estimation of regional evaporation using chloride as an indicator. Reduction of sulfur in groundwaters can cause precipitation of calcium and magnesium, thus modifying the chemical properties of groundwaters considerably. The role of air borne sea salt components for the development and properties of soils is discussed in principle.

Contents

Part 1. Tellus 11 : 4

I Introduction

II General features
1. Average composition of tropospheric air
2. Circulation of atmospheric constituents
3. Vertical transports
4. Sources of chemical constituents in the atmosphere

III Sea salt particles in the atmosphere
1. General
2. Vertical variations over ocean areas
3. Sea salt particles over land
4. Rate of production of sea salt particles
5. Advection of sea salt as a function of altitude

Part 2. Tellus 12 : 1

IV The yearly circulation of sea salts between continents and the oceans
1. Introduction
2. Weathering and the composition of the oceans
3. Average rate of weathering of igneous rocks and volcanic production
4. Actual rate of weathering
5. Human production
6. General balance
7. The "air borne" sulfur

V Chemical reactions in the atmosphere involving oceanic components
1. Oxidation of chloride by ozone
2. Release of HCl by absorption of SO_3 or H_2SO_4
3. Rate of oxidation of SO_2
4. Transfer of oxidized SO_2 sea salt particles
5. Other possible reactions
6. Conclusions

VI Deposition by gravitational fallout, impingement and gaseous absorption
1. Dry deposition of particulate matter
2. Absorption of gaseous compounds

VII Deposition of chloride and sulfur over the continents
1. Chloride
2. Sulfur
3. Yearly circulation of sulfur in nature

VIII The proportions of sea salt components in precipitation
1. The Cl/Na ratio
2. Possible separation processes at the surface

IX On chemical hydrology
1. Evaporation and chloride concentration
2. Reduction of sulfate and precipitation of calcium and magnesium carbonates

X Soils and airborne salts

I. Introduction

It has been known for some time that oceanic salts are present in the atmosphere over continents and are found in precipitation, the earliest measurements dating back to the middle of the nineteenth century. The geochemical implication of this transport was visualized by Posephny, a Hungarian geologist already in 1877. In an extremely well written paper he discussed the origin of chloride in river water and recent saline deposits. At that time not much was known about the chemical composition of precipitation but he concluded from geological evidence that chloride in river water and various saline deposits must have originated in the sea and were carried inland by the atmosphere. He discussed also at some length the saline deposits of the Bonneville Basin—the present Great Salt Lake region in North America—an area which he visited and found that the older saline formations could not account for the present amounts of chloride.

Later investigations on rain-water in different places gave a qualitative support to Posephny's views. KÖHLER's (1921, 1922, 1925) investigations on cloud droplets and the role of sea salt particles in condensation processes stimulated the development of cloud physics in which field a good deal of recent useful data are found.

In the meantime the question about the circulation of oceanic salts in nature was discussed on occasions. In his well-known book "Data on Geochemistry" CLARKE (1924) discusses the oceanic elements in river water but gives a rather low estimate of the airborne part. He is, however, somewhat embarrassed by the presence of so much chloride and sulfur in river water. Clarke's attitude can be understood from his belief in the method of computing the age of the oceans by means of sodium in river water and his sceptical attitude towards the now acknowledged isotope methods of geological age determination.

A splendid effort was made by CONWAY in 1942 to reconstruct quantitatively the evolution of oceans. In this procedure he regarded all chloride in river water as cyclical, because weathering can hardly supply any. Most of this cyclical chloride he was led to believe is airborne, and, furthermore, he found that also a large part of the sulphur in river water must originate in the sea generated by some other mechanism than chloride is generated.

At present there is more information available on the composition of air and precipitation and on various physical and chemical processes in the atmosphere, allowing a rather complete reconstruction of the yearly circulation of oceanic salts in nature and the role of the atmosphere in this circulation. To some readers the present paper may seem to contain too much of speculation. There is, admittedly, some but only in the sense of trying to tie all pieces of information into a comprehensible pattern, resembling to a high degree of probability the pattern actually existing.

The present paper is thus mainly concerned with the release and transport of sea salts from oceans into continental areas. To understand these processes better a short description of

significant chemical and physical properties of the atmosphere is given. Investigations on sea salt particles over the oceans are reviewed rather thoroughly as well as the generation of sea salt particles. After that a section is devoted to considerations on the yearly circulation of sea salts between oceans and continents as revealed by the use of geochemical data. Mechanisms of transfer to and removal by the ground of sea salt components are given in another section followed by considerations on the possible separation of sea salt components from sea salt particles. Existing data on precipitation of chloride and sulphur over land are then reviewed and their circulation schematically outlined.

The two last sections touch briefly on some problem of great interest in hydrology and soil science. They do not explore the subjects by any means but do show that such problems are intimately tied to atmospheric chemistry.

Some of the present material was included in a review report to UNESCO in 1957 (Eriksson 1958) like parts of section II and III, section IX and the whole of section X.

II. General features

1. *Average Composition of Tropospheric Air*

Available average data for minor constituents in the atmosphere have been compiled in table 2.1. This table is intended to give an impression of the order of magnitude of the constituents present. The table is by no means complete as it excludes among other things organic compounds which, presumably, are very numerous.

The estimates in the latter part of the table are based partly on data from the European chemical network described by Egnér and Eriksson (1955) and since then somewhat extended, and partly on data from a similar table compiled by Hutchinson (1959).

Gaseous constituents of principal interest here are those of carbon, nitrogen, sulfur and chlorine. The presence of sulfur dioxide has been known for quite a long time but does not exclude also some other forms of sulfur like H_2S. Its presence is mostly ascribed to industrial and domestic combustion of fossil carbon though, as will be shown later, this source is by no means sufficient to explain its incidence on a global scale.

The presence of *gaseous forms* of *chlorine* was indicated very recently in investigations by Junge (1956). There are only two possible gaseous compounds of chlorine in the atmosphere, namely hydrochloric acid and ammonium chloride. Free chlorine, Cl_2, can hardly exist in an atmosphere where hydrogen is present at a fifty times higher pressure.

The constituents in *particulate* state listed in table 2.1 are components of so called *condensation nuclei* which have recently been thoroughly discussed by Junge (1958), as well as of substances which normally would be classified as dust. All listed elements of the particulate matter may occur as soluble salts, and as such they can be components of the *hygroscopic particles* called condensation nuclei. Sodium, potassium, calcium and magnesium are, however, also constituents in common minerals, and as such they can be derived also from atmospheric dust which is, mainly, finely divided mineral matter.

Components invariably to be expected in particles of *marine origin* are primarily chloride, sodium and sulphate. These particles which are also called *sea salt particles* have been investigated quite extensively during the last years and will be discussed at some length in a later section. They occur as crystals or liquid droplets, depending on the relative humidity of the air, in a size range from about 0.1 μ (1 μ = micron = 10^{-4} cm) to 20 μ or even greater or, in weight, from 10^{-14} to 10^{-8} g or greater. The actual size distribution has been investigated on many occasions especially by Woodcock and co-workers (1949, 1950 a, 1950 b, 1952, 1953, 1955, 1957). The size distribution can within not too wide limits, be approximately described by the so-called inverse r^3 law originally proposed by Junge (1952).

$$\frac{dN}{d(\log r)} = \frac{k}{r^3} \qquad (2.1)$$

where N is the number of particles equal to or greater than the radius and k is a constant. The simple formula above implies that each logarithmic size interval contains the same mass of sea salts (see fig. 2.1.) Considering a wider range of particle sizes it can, however, be inferred when the frequency of particles is expressed as a function of the logarithm of

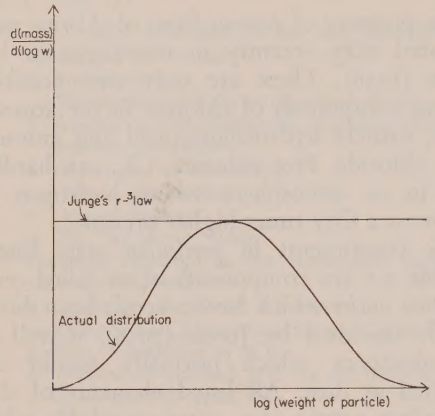

Fig. 2.1. Schematic mass-weight distributions of particles in the atmosphere.

size (or weight) that the mass is more or less normally distributed. (See fig. 2.1.)

The term *sea salt particles* should not be taken as indicating that the relative composition is exactly that of sea water. JUNGE (1956, fig. 2) has found that the larger particles contain sodium and chloride in approximately the same proportion as sea salts, but in smaller particles, sulphate is present in a greater proportion than in the sea. This phenomenon, which does not exclude the marine origin of the excess sulphate, will be discussed in more detail later. At present it will be understood that sea salt particles largely if not altogether represent constituents derived from the sea, though the proportions of these are not quite the same as in sea water.

Besides sea salt particles there are also smaller hygroscopic condensation nuclei, the so-called *Aitken nuclei* of a size less than 0.1 μ. Practically nothing is known about their chemistry but it has been inferred from experiments that condensation nuclei of similar size and properties can be produced in a number of processes such as combustion, photochemical reactions, etc. Their concentration in densely populated areas is very great, generally amounting to several ten thousands per cm^3. Over the sea as well as over sparsely populated areas they

TABLE 2.1

The chemical composition of the troposphere (1 atm. pressure)

	Compound	Partial pressure in atmospheres	Concentration in microgram per m^3	Remarks
Nitrogen	N_2	0.78101		constant
Oxygen	O_2	0.20946		constant
Water	H_2O	$\sim$ 0.02		very variable
Argon	Ar	0.00917		constant
Carbon dioxide	CO_2	3.3×10^{-4}		somewhat variable
Neon	Ne	1.82×10^{-5}		constant
Helium	He	5.24×10^{-6}		constant
Methane	CH_4	1.5×10^{-6}		constant
Krypton	Kr	1.14×10^{-6}		constant
Nitrous oxide	N_2O	5×10^{-7}		constant
Hydrogen	H_2	5×10^{-7}		constant
Ozon	O_3	$\sim 5 \times 10^{-7}$		very variable
Carbon monoxide	CO	1×10^{-7}		variable
Xenon	Xe	8.6×10^{-8}		constant
Sulfur dioxide	SO_2	1×10^{-8}		somewhat variable
Ammonia	H_2N	$\sim 5 \times 10^{-9}$		variable
Hydrochloric acid	HCl	$\sim 10^{-8}$		variable
Nitrogen dioxide	NO_2	$\sim 10^{-9}$		variable
Iodine	J_2	$\sim 2 \times 10^{-13}$		variable
Chloride	Cl		$\sim$ 1	very variable
Sulfate-sulfur	SO_4-S		$\sim$ 1	very variable
Ammonia nitrogen	H_3N-N		$\sim$ 1	very variable
Nitrate nitrogen	NO_3-N		$\sim$ 1	very variable
Sodium	Na^+		$\sim$ 1	very variable
Calcium	Ca^{2+}		$\sim$ 1	very variable
Magnesium	Mg^{2+}		$\sim$ 0.5	very variable
Potassium	K^+		$\sim$ 0.5	very variable

are usually low in number (cf. LETTAU 1939). An extensive review of Aitken nuclei distribution is given by LANDSBERG (1938). Quantitatively they cannot be as important as sea salt particles as they are mainly products of combustion.

Another important category of particles, which has been mentioned before, is the group of insoluble mineral particles classified meteorologically as *atmospheric dust*. Too little attention has been given to these, as it usually has been inferred that they are of local origin. They range in size from 10 to 0.1 μ. Obviously they are derived from soils and, more important, the bulk of them must originate in arid regions with little or no vegetative cover or in semi-arid areas with well developed agriculture. Conditions in humid regions do not as a rule favour the release of these particles from the soil surface.

Some information exists about dust in the atmosphere although no systematic collections have been made. The reports mostly concern "dust falls", i.e. cases where precipitation contains appreciable concentrations of dust. But actually it appears that dust is normally just as common as sea salts in precipitation. This can be inferred from analyses of snow collected in Finland during the late winter, published by VIRO (1953). The amount of silica (SiO_2) in his analyses, which must come from such dust, is quite substantial and is of equal geochemical importance as the sea salts.

2. *Circulation of atmospheric constituents*

The *circulation* of an *element* is defined as net transports of the element or a compound containing the element along closed paths in nature. It is clear from this definition that purely molecular exchange between, for instance, the atmosphere and the sea surface is not a part of a circulation unless a net transport takes place.

It can be shown (cf. ERIKSSON 1959) that practically all constituents in the atmosphere take part in circulations. They are added to the atmosphere in certain regions and withdrawn from the atmosphere in other regions. Every constituent thus spends a certain average time in the atmosphere, between the addition and the subtraction, this time being called *residence time* and is generally defined as the ratio of the amount of the constituent in the atmosphere divided by the rate at which it is added to the atmosphere in the particular circulation studied.

In many of the circulations the transported amount returns quantitatively to the regions where it is added to the atmosphere. A few elements, however, are radioactive and are consequently subjected to decay during the circulation. Of special interest are those who are formed in the atmosphere by cosmic radiation. In their circulations they resemble the corresponding inactive isotopes except for the continuous disappearance by decay.

Other radioactive isotopes, added from land surfaces are radon and thoron which, by their decay forms a series of elements that partly will accumulate on the deep sea floor as lead isotopes. This circulation is not closed in the sense defined but represents a net transport from one region to another without any foreseeable return.

Localities where a net addition of chemical constituents to the atmosphere takes place will be referred to as *source regions* as they often are of considerable areal extent. The regions where a net subtraction of chemical constituents from the atmosphere takes place are, consequently, called *sink regions*, also those of large areal extent.

The circulation path in the atmosphere can be both *zonal*, i.e. along latitude circles, or *meridional*, i.e. across latitude circles. The distinction between these two transports is significant for the following reason. The average air circulation is zonal and one could imagine a planet where it was strictly zonal. In such a case zonal transports would be simple advections but meridional circulations would be strongly impeded. The air circulation on the earth has, however, meridional components though no net transport of air takes place meridionally. These components can be rather steady features as in the subtropical high pressure systems over the oceans and, to some degree, in the blocking situations that can build up at higher latitudes. They can also be irregular in time and space as in the travelling cyclones or in the meandering jet stream at higher altitudes. All these features of the atmospheric motion greatly facilitates meridional transports of chemical and physical properties. In regions where they are irregular in

time and space their effect can be looked upon as a large scale *diffusion process* (often called *large scale eddy flux*).

The large scale eddy flux of a compound in a region where irregular features of the air circulation prevail will manifest itself by time variations in the concentration of the compound in the air that passes a fixed point on the earth's surface. These variations are, of course, irregular, but their relative average magnitude defined in a suitable manner seems to be inversely related to the atmospheric residence time of the constituent studied.

Examples on meridional circulations of elements have been given recently by ERIKSSON (1959) who infers that all permanent gaseous constituents in the atmosphere must show a net transport in the atmosphere from equatorial-subtropical regions to temperate-polar regions, the return taking place in the oceans. The reason for this is the variation of solubility of gases in water with temperature, the difference in temperature of ocean surface water in low and high latitudes and the ocean circulation as manifested by the salinity distribution in the sea and the net evaporation pattern over the sea surface.

A typical and well recognized *meridional* circulation is shown by water, low latitudes being its source region for the atmosphere and high latitudes its sink regions. The residence time of water in the atmosphere in its meridional circulation is short, about a month, and the relative variations of water vapor pressure in the atmosphere are very large. Carbon dioxide has a similar circulation but as its residence time in this meridional circulation may be of the order of 100 years or so, its relative variation in the atmosphere is quite moderate, amounting to only a few per cent. Finally, a gas like argon, that also must circulate in the same manner, has a residence time of perhaps 100,000 years or more and any variation would probably be hard to detect by any known analytical procedure.

When illustrating the circulation of an element it is convenient to do this on a global scale and divide the nature into *reservoirs* between which the element is transferred. One of these reservoirs is logically the *atmosphere*, i.e. the gaseous phase of the globe. The liquid phase or the *hydrosphere*, represented practically entirely by the oceans, is another logical reservoir. The *solid inorganic phase* may be divided into two reservoirs, one is the *litosphere* and the other the *pedosphere*, i.e. the soil where plants are rooted and which is a medium where all three phases plus organic dead and living matter are intimately mixed. *Living plants* that use the sun's energy in assimilating carbon dioxide may be divided into a reservoir of land plants and another for marine plants. The distinction is significant because land plants take the carbon dioxide and possibly other elements from the atmosphere while marine plants use dissolved carbon dioxide and other elements in sea water.

The decay of plants takes place in many steps in which animals and other parasitic organisms take part. As they together with undecomposed organic matter represent a certain storage of not only carbon dioxide but also nutrients like nitrogen and sulphur they are conveniently regarded as a reservoir of *undecomposed organic matter* in nature. Again, a distinction should be made between a land reservoir and a marine reservoir of undecomposed organic matter.

3. *Vertical transports*

Vertical transport of properties in the atmosphere depends on four processes, namely convection, turbulent diffusion and molecular diffusion and in the case of particles, fall by gravity. Convection is a selective vertical transport of warmer air through the environment and is ultimately dependent on the vertical stability of the air.

Turbulent diffusion can be pictured as a random motion of air parcels of different size and is caused by wind shear which, together with the inertia of the air causes instabilities in an air stream leading to formation of eddies which move in all directions relative to the mean wind. These eddies are finally elongated to long filaments and across their large surfaces molecular diffusion causes them rapidly to lose their identity (cf. WELANDER 1955). By this mechanism rapid transports of properties can take place vertically, provided the earth's surface acts as a sink or a source. Close to the surface, however, in the so-called laminar boundary layer turbulent elements disappear so that molecular diffusion, or in the case of particulate matter, the fall by gravity and impingement are the ultimate transport mech-

anisms. The thickness of this layer is of the order of magnitude 0.1 cm.

Near the ground the effect of convection is difficult to separate from turbulent diffusion. For this reason it is included in the turbulent diffusion which then depends strongly on the vertical stability of the air. This is, of course, also true when vertical stability is such that no convection occurs. Even then the vertical stability influences the turbulent diffusion. But the dependence of turbulent diffusion on the stability cannot be of the same nature in a stable stratification and in an unstable.

The transport by turbulent diffusion can be expressed mathematically in the same way as molecular diffusion. If F is the vertical turbulent flux of a property present at a density of ϱ, the flux is related to the gradient of the property by

$$F = -K\frac{\partial \varrho}{\partial z} \tag{2.2}$$

z being the vertical height coordinate and K the turbulent diffusion coefficient. Generally K increases rapidly with height which means that $\frac{\partial \varrho}{\partial z}$ decreases if F is the same at all levels. K is further a function of the wind velocity and the stability of the air. In general, K changes so rapidly near the earth's surface that $\frac{\partial \varrho}{\partial z}$ for any property is difficult to evaluate already at a few meters' height above the surface.

As K can be assumed to be the same for the vertical transport of all chemical constituents in the atmosphere the following relation can be taken advantage of. For a compound a and b we can write

$$F_a = -K\frac{\partial \varrho_a}{\partial z} \tag{2.3}$$

$$F_b = -K\frac{\partial \varrho_b}{\partial z} \tag{2.4}$$

and consequently

$$\frac{d\varrho_a}{d\varrho_b} = \frac{F_a}{F_b} \tag{2.5}$$

Integrating between two levels z_1 and z_2 one gets (assuming F_a and F_b to be constant)

$$\Delta\varrho_a = (\varrho_a)_{z_2} - (\varrho_a)_{z_1} = \frac{F_a}{F_b}\left[(\varrho_b)_{z_2} - (\varrho_b)_{z_1}\right] =$$

$$= \frac{F_a}{F_b}\Delta\varrho_b$$

or

$$F_a = F_b\frac{\Delta\varrho_a}{\Delta\varrho_b} \tag{2.6}$$

For many chemical constituents of interest their density at the interface air-ground (the ground taken to represent also surfaces of vegetation) may be zero. The density in free air at normal observation height ($\sim$ 2 m) can be easily assessed experimentally. Thus if F_b and $\Delta\varrho_b$ represent a property like water vapor and is known, merely measurements of the density in air of any other property makes it possible to calculate its flux. Assuming that we know $\Delta\varrho_{H_2O}$ and F_{H_2O} we can obviously define a kind of a vertical transport velocity w by

$$w = \frac{F_{H_2O}}{\Delta\varrho_{H_2O}}$$

which can be interpreted as the rate at which fresh air is steadily brought in immediate contact with the ground. This concept of a vertical velocity in the case of vertical transports of chemical quantities has been used earlier by EGNÉR (1932) when discussing nitrogen losses from soils and manure and recently by CHAMBERLAIN & CHADWICK (1953) in connection with absorption of radioiodine by soil and vegetation. If w is known, then apparently

$$F_a = w\Delta\varrho_a \tag{2.7}$$

The velocity w averaged over a longer period also depends on the roughness of the ground. A value for the subtropical ocean regions can be estimated crudely in the following way. The evaporation in trade wind regions between 15 and 25° S or N of the equator is according to WÜST (1954) about 130 cm per year. This means that the daily flux is $\frac{130}{365} = 0.356$ g $\times$ cm^{-2} $\times$ day^{-1}. In these regions the relative humidity from ship measurements, averaged over a year is around 80 per cent and as the water temperature is around 25° the density of water vapor at the

surface must be 23×10^{-6} g × cm^{-3}. Thus, $\Delta\varrho_{H_2O} = 4.6 \times 10^{-6}$. Then w becomes 7.5×10^4 cm × day^{-1} or 0.87 cm × sec^{-1}.

This value may be regarded as a minimum value as the air is always slightly stable in trade wind regions (WYMAN-WOODCOCK expedition, unpublished). Over land, especially when heated in summer, the turbulent exchange is presumably greater due to convectional processes. On the other hand, low air inversion due to nocturnal cooling of land will reduce the turbulent exchange considerably at times. So from these points of view the value around 1,000 m per day may apply also to continents, maybe except for wooded regions where the roughness of the ground leads to very strong turbulence.

Particulate matter has also a certain settling velocity which will ultimately bring particles to the ground. For such particles the vertical transport is given by

$$F = -K\frac{\partial\varrho}{\partial z} + V\varrho \qquad (2.8)$$

where V is the fall velocity and is negative. From this

$$F = w\Delta\varrho + V\varrho \qquad (2.9)$$

which shows that the transport is made up of two quantities, one turbulent and one due to settling. In the case of particles, however, conditions in the laminar boundary layer differ vastly from conditions in the case of transport of molecules. Particles are practically uninfluenced by molecular processes so that no gradient whatsoever can be developed in the laminar boundary layer where fall velocity is the only transport means. This means that in a steady state process where the surface does not generate particles, $\Delta\varrho$ will be zero unless the fall rates are increased in the boundary layer.

When air is moving over land covered with vegetation, the inertia of particles can increase the apparent fall rate near the ground due to impingement of particles on leaves, needles and other obstacles. With the normally occurring wind speeds it can be shown that objects of a diametre of 1—2 mm are effective for removing larger particles by impingement. Pine and spruce needles should be effective in removing particles by impingement and in such a case a turbulent transport from higher levels will take place. One prerequisite for removal by impingement is, however, that the particles are retained for some specific reasons. This is mostly the case for sea salt particles because they are hygroscopic and wet even at low relative humidities.

A turbulent transport of gases can only take place if the gases are absorbed, or released, by the ground, i.e. soil and vegetation. Absorption can be predicted from the known properties of gases once the chemical properties of soil and vegetation are known.

4. *Sources of chemical constituents in the atmosphere*

a. Continental sources

We have been concerned so far only with the removal of chemical constituents from the atmosphere. The ground can also act as a source which is apparent from the existence of particulate matter or dust in the atmosphere. It is also clear that the ground can be a source of gaseous constituents.

Very obvious sources of both particulate and gaseous material due to human activities are found in densely populated districts with much industrial activity. Important areas in this regard can be found in western Europe and the north-eastern United States. The output of material into the atmosphere from these regions is obviously of great local importance and much work assessing atmospheric pollution has consequently been done. On the other hand the importance of these source areas on a global scale may have been considerably overestimated.

α. Sources of particulate matter. Atmospheric dust has been discussed earlier to some extent and it was inferred that the source regions must be the arid parts and agricultural areas of our continents. Dust appears in precipitation as well, therefore it may influence its composition. This influence depends, however, on the technique of analysis of precipitation samples as well as on the kind of dust which is carried by the atmosphere.

The composition of atmospheric dust must reflect the composition of the top soils in arid and agricultured regions. From the composition of these it can be inferred that the insoluble

material consists of the three most common minerals, quartz, feldspar and mica, probably with a greater weight of quartz. Arid regions often contain calcium carbonate and calcium sulphate in the top layer; in this case these two could be present in the air representing compounds which are not readily soluble but still found in solution. Calcium carbonate, which is more frequent and which is probably easier to get into the air, would probably not exist as such for long when much sulphur dioxide is present in the air which on oxidation converts the carbonate into sulphate. Calcium sulphate is comparatively soluble, at least when considering such dilute systems as rain water. It is, however, of no use to speculate further on these two compounds as there is too little evidence concerning their presence in the atmosphere at present. It can be mentioned, however, that carbonate particles, which are easy to identify, have been detected in dust collected by impingement on glass slides in northern Sweden (unpublished results).

Salt efflorescences occur in large areas of the arid regions in top soils. It could perhaps be expected that these salts would be carried up into the air together with dust particles and thus be transported away from the arid regions. There is, however, some evidence that such a transport of easily soluble salts is not too important. Some salt particles may be carried into the air as observed by CROZIER & SEELY (1952) above the Mojave Desert in western United States. The number of such particles, however, was generally low compared to the number of salt particles encountered in maritime air masses above this region, and seemed to be correlated with the number of dust particles. In Quetta, situated on the Beluchistan highland in Pakistan, thick dust haze coming from the deserts to the west where large areas of salt waste are found is often experienced during summer. FOURNIER D'ALBE (1955) investigated the salt nuclei content in the surface air layer at this place and found no significant rise in the number of hygroscopic nuclei during these occasions. He thinks that the salts in the salt wastes are present on the surface as fairly large grains which, though raised by strong winds, rapidly fall out again under the influence of gravity. Therefore very little is actually carried away by wind from these regions. They may, however, influence the composition of precipitation locally.

There is thus far no evidence of any substantial transport of easily soluble salts from the arid regions.

The transport of insoluble mineral matter from arid regions into humid areas is, of course, a transport of great geochemical importance. The windborn soil material known as loess must be derived from such transports. The classical example of such soils is the extensive loess deposits in parts of China which are believed to be derived from the arid central part of Asia. The yearly amounts transported need not be great; in a few million years substantial deposits will be the result even if the yearly amount precipitated is of the order of only $kg \times ha^{-1} \times year^{-1}$.

From the fact that loess deposits are calcareous, i.e. contain calcium carbonate, it might be inferred that calcium carbonate is a significant constituent of atmospheric dust.

β. Sources of gaseous compounds. The land surfaces, or better, the continental surfaces can be sources of gaseous compounds. A well known example is the escape of radon from soil, produced by desintegration of radium in rock material. Other gaseous compounds produced in the soil are ammonia, carbon dioxide, nitrous oxide and probably hydrogen sulfide.

Hydrogen sulfide is easily formed by bacterial reduction of sulphate. This occurs where organic substances are present but oxygen is absent. The bacteria use the oxygen of the sulphate for oxidizing organic matter, and thereby gain energy necessary for their sustenance. This process occurs most frequently in swamps, bogs, soils with a high water table and in lakes with stable stratification. Even in normal well drained soils reduction processes can occur which may produce hydrogen sulfide. A good soil consists of aggregates of soil material and when wet, these are sites of anaerobic processes in which sulfur may participate.

In the reduction of sulphate ferrous sulphide may be formed. This is a rather common mineral in many soils high in organic matter, formed by sedimentation in water (for instance the "gyttja" soils of Sweden). If there is not a sufficient amount of ferrous iron present H_2S

will form. As the solubility of H_2S in water is rather moderate, its escaping tendency is great and it gradually diffuses into the atmosphere. Hydrogen sulfide is also formed during decomposition of sulfur containing organic matter.

The best known example of sulphate reduction in water is given by the Black Sea where the content of H_2S in deep water is very great (NIKITIN, 1931).

Lakes in tropical and subtropical regions often contain very stable stratified water as a result of warm surface conditions. This deprives deep layers of water of oxygen, and hydrogen sulphide forms as a consequence. Large lakes in tropical Africa, investigated by BEAUCHAMP (1953), are remarkably low in sulphate when compared with chlorine. It seems likely that large quantities of hydrogen sulphide are being released to the atmosphere. Similarly ANDERSON (1945) noticed a deficiency of sulphate in some south Australian lakes where he also was able to smell hydrogen sulphide. The limit of detection of H_2S by its odor is near 20 $\mu g \times m^{-3}$, consequently there must be appreciable concentrations in the atmosphere around these lakes.

The reduction of sulphate in ground waters makes them alkaline as pointed out by RIFFENBURG (1925). He found that when water seeps through sedimentary beds high in organic matter it becomes alkaline. Since H_2S is formed in such processes certainly some, if not the main part, must reach the atmosphere. H_2S which escapes to the atmosphere is oxidized to SO_2 and finally SO_3 which in turn is brought to earth again.

Release of HCl from the ground may occur with the help of sulphur trioxide. Sulphur trioxide which is very hygroscopic, is formed by oxidation of SO_2. With water it forms sulphuric acid which has a very low escaping tendency. Therefore both SO_3 and H_2SO_4 can be rapidly removed from the atmosphere or added to condensation nuclei. In salt waste regions rich in sodium chloride the presence of SO_2 in the air may lead to a loss of HCl. As SO_3 is formed it reacts with NaCl and water forming sodium sulphate and hydrochloric acid. This process is actually employed in the most common commercial method for the manufacture of hydrochloric acid.

b. Oceanic sources

The open ocean areas can contribute chemical constituents to the atmosphere in two ways. One is by mechanical disintegration of water into small droplets which evaporate, leaving droplets of concentrated solutions or crystalline matter as small particles in the atmosphere. The other is by gaseous diffusion through the interface water-air.

In addition to the open sea areas there are the borders of the sea in which the same two processes occur on a magnified scale. Production of sea salt particles in a surf has been known for long and the role of intertidal flats for production of various gases is obvious, considering the abundance of organic material and the anaerobic character of these deposits.

As to the mechanical processes of water disintegration these have been studied relatively recently by WOODCOCK, KIENTZLER, ARONS and BLANCHARD (1953a) who discovered that bursting bubbles in sea water eject a number of small droplets into the air which, upon evaporation, form small sea salt particles. Bubbles are, of course, produced by breaking waves which always occur frequently when the wind force exceeds four (Beaufort). BLANCHARD & WOODCOCK (1956) have, however, also discovered other processes of bubble formation. One is by impaction of drops on a water surface, another which produces very small bubbles takes place when snow flakes fall into water, air being entrapped as small bubbles.

All these processes have been studied in detail by BLANCHARD & WOODCOCK (l.c.) who related the number of particles produced and their size to the size of the bursting bubbles and they account satisfactorily for the amount and distribution of sea salt particles in air over ocean areas. Breaking waves seem to be quantitatively the most important and naturally one would expect the production of sea salt particles to be related to the wind force which is also the case as shown by WOODCOCK (1953).

Thus, a satisfactory mechanism exists by which disintegrated sea water is carried into the air. Once in the air the droplets formed are influenced by gravity which tends to carry them back to the sea surface. On the other hand they are influenced by the turbulence of

the air which tends to distribute them in all directions. At the same time evaporation sets in which tends to reduce the gravitational settling by increasing their specific surface. The final distribution of sea salt particles in the atmosphere over a source region will largely depend on the rate of production of sea water droplets, their rate of evaporation and the turbulence of the air.

In the steady state which requires a constant source of the surface we have

$$-K\frac{\partial n}{\partial z}+Vn=0 \qquad (2.10)$$

where K is the turbulent diffusion coefficient, n the volume concentration of particles of a certain size, V the fall velocity and z the vertical coordinate. It is seen that provided K is constant the distribution will be simply exponential (V being negative), namely

$$n=n_0 \exp\,(Vz/K) \qquad (2.11)$$

As the flux down to the surface where K is very small is Vn_0, the rate of production must be the same. But this is the rate of production of sea salt particles, *in equilibrium with the relative humidity of the environment.* The equilibrium mass and volume of a sea salt particle (relative to the mass and volume of the corresponding sea water droplet of 35 % salinity) at different relative humidities can be calculated from available data on the vapor pressure of sea water at different salinities (Arons & Kientzler 1954) and from the densities of sodium chloride solutions found in chemical handbooks. Table 2.2 gives the results of these computations for relative humidities between 75 and 100 per cent. RH is the relative humidity under equilibrium conditions, S the salinity in g · kg^{-1}, ϱ the density of sodium chloride solutions of the same satinity, ϱ/ϱ_0 the relative density, W/W_0 the relative volume, r/r_0 the relative radius and $V/V_0=\varrho/\varrho_0\,(r/r_0)^2$ the relative fall velocity. The last hold within the size range of particles considered here.

Table 2.2 shows that the decrease in fall velocity is appreciable already at 97 % RH when it has decreased to about 2/3 of the original. To decrease this value at 97 % RH to half, one has to decrease RH to 88 %. From 90 to 80 % the change in fall velocity is rather small, but an appreciable reduction occurs at around 75 % when NaCl crystallizes. Altogether, the fall velocity is reduced by a factor of about 7 by the complete evaporation of a sea water droplet.

TABLE 2.2

Salinity, density, relative volume, radius and fall velocity of sea salt particles at different relative humidities all at 25° C

RH per cent	Salinity S in g · kg^{-1}	Density ϱ g · cm^{-3}	Relative volume W/W_0	Relative radius r/r_0	Relative fall velocity V/V_0
98.2	35.2	1.024	1.000	1.000	1.000
98	39.2	1.026	.898	.966	.930
97	56.0	1.039	.620	.853	.739
96	73.2	1.051	.468	.777	.620
95	86.7	1.061	.392	.733	.556
94	99.3	1.070	.339	.698	.509
93	112.5	1.080	.297	.668	.469
92	124.3	1.089	.267	.645	.441
91	137	1.099	.240	.622	.414
90	147.7	1.107	.221	.605	.394
88	168.5	1.122	.191	.576	.364
86	189.5	1.140	.167	.551	.337
84	206.8	1.153	.151	.532	.319
82	225	1.168	.137	.516	.303
80	241	1.182	.1266	.502	.291
78	257	1.195	.1173	.490	.279
76	273	1.208	.1092	.478	.269
75	281 (sat)	1.215	.1057	.473	.266
75	1,000 (dry)	2.1	.01677	.256	.139

TABLE 2.3

Fall velocities of sea water droplets and of sea salt particles in equilibrium with 91.4 per cent relative humidity and time constants for changes in the fall velocity with changing relative humidity. w is weight of sea salt in particles in $\mu\mu$g; $r_{91.4}$ radius at 91.4 % RH

r_0 in μ	$r_{91.4}$ in μ	w in $\mu\mu$g	log w	V_0 cm · sec^{-1}	$V_{91.4}$ cm · sec^{-1}	τ in sec	$3\tau V_0$ cm
.872	.550	.100	— 1.00	.0091	.0038	.022	$.6 \cdot 10^{-3}$
1.058	.667	.178	— .75	.0133	.0056	.032	$1.3 \cdot 10^{-3}$
1.28	.807	.316	— .50	.0195	.0082	.047	$2.8 \cdot 10^{-3}$
1.55	.976	.563	— .25	.0287	.0121	.070	$6.0 \cdot 10^{-3}$
1.88	1.178	1.000	± .00	.0420	.0176	.102	$1.3 \cdot 10^{-2}$
2.28	1.436	1.78	.25	.0618	.0260	.150	$2.8 \cdot 10^{-2}$
2.76	1.74	3.16	.50	.0905	.0380	.22	$6.0 \cdot 10^{-2}$
3.34	2.10	5.63	.75	.133	.056	.32	$1.3 \cdot 10^{-1}$
4.05	2.55	10.00	1.00	.195	.082	.47	$2.8 \cdot 10^{-1}$
4.91	3.09	17.8	1.25	.286	.121	.70	$6.0 \cdot 10^{-1}$
5.94	3.75	31.6	1.50	.420	.176	1.02	1.3
7.20	4.53	56.3	1.75	.618	.260	1.50	2.8
8.72	5.50	100	2.00	.905	.380	2.2	6.0
10.58	6.67	178	2.25	1.33	.56	3.2	13
12.8	8.07	316	2.50	1.95	.82	4.7	28
15.5	9.76	563	2.75	2.87	1.21	7.0	60
18.8	11.78	1,000	3.00	4.20	1.76	10.2	130
22.8	14.36	1,780	3.25	6.18	2.60	15.0	280
27.6	17.4	3,160	3.50	9.05	3.80	22	600
33.4	21.0	5,630	3.75	13.3	5.60	32	1300
40.5	25.5	10,000	4.00	19.5	8.20	47	2500

The evaporation will take a certain time which is a function of the relative humidity and the original size of the droplet. The evaporation rate can be approximated to a steady state for our purpose and with this assumption

$$\frac{dW}{dt} = -4\pi r D \Delta\varrho \qquad (2.12)$$

where W is the volume and r the radius of the drop, $\Delta\varrho$ is the vapor density difference between the surface of the drop and at infinity, i.e. that of the environment while D is the molecular diffusion constant which for water vapor can be put equal to 0.3 cm$^2 \times$ sec^{-1}. As $\frac{dW}{dt} = 4\pi r^2 \frac{dr}{dt}$ we get

$$r\frac{dr}{dt} = -D\Delta\varrho \qquad (2.13)$$

which shows that the decrease in radius is a parabolic function of time at least for the initial state. An approximate treatment of the problem can be done by putting

$$\Delta\varrho = \frac{36\,\overline{S}\,\varrho_0}{58\left(1 + \frac{LD}{K}\frac{d\varrho}{dT}\right)} \cdot \frac{r^2 - r_0^2}{r_0^2} \qquad (2.14)$$

where r_0 is the equilibrium radius and ϱ_0 the equilibrium vapor density, $\overline{S}$ the average salinity in g · g^{-1} of the drop in the size interval studied, L the latent heat of evaporation, D the molecular diffusion coefficient for water vapor, K the heat conductivity of air and T the temperature. The term within brackets accounts for the effect of heat of condensation or evaporation on the vapor pressure of the droplet. Evaluation of

$$\frac{36\,\overline{S}}{58\left(1 + \frac{LD}{K}\frac{d\varrho}{dT}\right)}$$

in the range RH 91.4 to 98.2 and 25°C and $\overline{S} = 87 \cdot 10^{-3}$ gives 0.0115 so we can write

$$\frac{d(r^2)}{dt} = -0.023\varrho_0 D\frac{r^2 - r_0^2}{r_0^2} \qquad (2.15)$$

or

$$\frac{d(r^2)}{r^2 - r_0^2} = -\frac{0.023\varrho_0 D}{r_0^2} \qquad (2.16)$$

which incidentally shows that the fall velocity which is proportional to r^2 changes approximately exponentially with a time constant τ

$$\tau = \frac{r_0^2}{0.023 \varrho_0 D} \qquad (2.17)$$

Some values of τ for $\varrho_0 = 2 \cdot 10^{-5}$, $D = 0.3$ and various equilibrium radii is given in table 2.3 where also the weight of the salt in the particle is given as well as the fall velocity V_0 for a droplet in equilibrium with sea water and in equilibrium with 91.4 per cent relative humidity. In the same table also $3\ \tau V_0$ is calculated to show the magnitude of the distance travelled before the equilibrium velocity through evaporation is attained. It is seen that this distance is proportional to the forth power of the radius and is very small for small particles but appreciable for large particles. The calculations are made so that the time of evaporation for ejected sea salt droplets of different size can be estimated. It is evident that this time has some influence on the possibility of ejected sea salt droplet to be removed by turbulence into the air through the turbulence itself must be a much more important factor.

It is apparent that a selective process occurs at the sea surface whereby the smaller salt particles are favored compared to big ones. A given distribution of sea water droplets generated will be considerably modified in the layer close to the surface. A low relative humidity will favor the formation of larger sea salt particles because of a more rapid evaporation. As the main mass of salt is found in the larger particles, regions of low relative humidity like trade wind regions can be expected to be important source regions for sea salts in the atmosphere. Other areas also produce sea salt particles but production of the larger particles is impeded by the high relative humidity so that presumably smaller particles are produced in any number.

It is known that a substantial poleward transport of water vapor takes place carrying latent heat from subtropical into temperate zones. Similarly, a net transport of sea salt particles probably takes place from the subtropical regions into the temperate zones. This is strongly suggested by the fog water analyses carried out by CUNNINGHAM (1941) on the north-east coast of the U.S.A. He found much larger chloride concentrations in fog water from air masses of tropical origin than in polar air masses.

The main regions of sea salt particles generation in the temperate zones must be the cyclone tracks due to frequent high wind velocities though probably not in the warm sector of a storm. The cold air side of a cyclone has, of course, much more favorable conditions for sea salt generation as the air is being heated along its way.

Bursting bubbles in the sea can also be expected to remove organic matter in surface films that are always present on the sea surface. This mechanism for removal was discovered accidentally by WOODCOCK et al. (1953) in their experiments on bursting bubbles. It is felt that this is a geochemically important process which probably accounts for the presence of organic matter in rain and snow even when collected in places where hardly any vegetation grows and no human contamination is present.

The oceans are also sources of gaseous compounds, an aspect which has been discussed recently by ERIKSSON (1959) as mentioned earlier. There are, however, gaseous compounds that are formed in the biological cycle either in the surface layer or in shallow parts of the sea and reaches the atmosphere and are carried in over continents contributing to the circulation of these elements. An element of special interest is sulphur whose circulation is still puzzling. In order to balance the river run-off of sulphur CONWAY (1942b) hypothesized a production over the shelf areas of H_2S which reached the atmosphere and was carried in over the continents. The possible oceanic sources of sulphur will be discussed later. It may be sufficient at present to point out that intertidal flats which apparently are of a fair extent, may produce quite sizeable amounts of H_2S. It is possible that also the biological turnover in the sea produces sizeable quantities which are brought into the atmosphere.

III. Sea salt particles in the atmosphere

1. *General*

Most of the work on sea salt particles in the atmosphere over oceans has been carried out by A. H. WOODCOCK, Woods Hole Oceanographic Institution in connection with cloud physics studies. Sampling has been done from small aircrafts at different levels by the impaction method on glass slides and identification and measurements by the so-called isopiestic

method. The sampling slides are exposed to a controlled, constant humidity in which the salt particles grow to equilibrium at which their sizes are measured microscopically. The method is not specific for sea salts, as all easily soluble salts will react like sea salt particles. Over the oceans the assumption that these particles are sea salt particles is not entirely correct as will be discussed later though no serious error is introduced in most cases. Over land such a method may be more questionable unless sea salt components are identified in some other way. TWOMEY (1954) for instance used the phase transition method to establish the identity of sea salt particles samples over Australia. Chemical tests for chloride in sampled particles have been developed by SEELY (1952) and later, in a more convenient form by LODGE (1954) enabling them to identify and measure the concentration of chloride particles over continents. LODGE (l.c.) has also developed similar techniques for sulfate and magnesium—ion particles.

Considering the oceans as the main source for sodium and chloride in the atmosphere, it is clear that the data obtained by Woodcock in his sea salt particle studies are most valuable as they may be used to obtain the average sea salt load of maritime air. How far this can be transported into continents can be surmised from investigation by TWOMEY (1955), CROZIER and SEELY (l.c.) and BYERS et al. (1956) who all sampled from aircrafts. Ground sampling by impactor methods used by FOURNIER D'ALBE (l.c.) in Pakistan seems to be excellenty suited for synoptic studies on a large scale and over longer periods where aircraft sampling would be prohibitively costly.

Some characteristic features of sea salt particle distributions will be discussed in the present section followed by a discussion on the vertical mass distribution at various places in the next section.

a. *Number-size distributions of sea salt particles.* It was mentioned earlier that the formula, developed by JUNGE (1952)

$$\frac{dN}{d(\log r)} = \frac{k}{r^3} \qquad (3.1)$$

where N is the cumulative number of particles per unit volume with a radius smaller than or equal to r and k is a constant, cannot describe

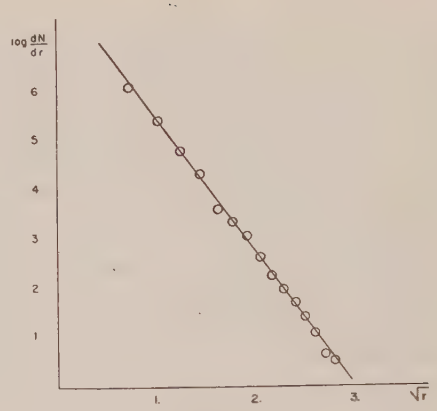

Fig. 3.1. Log $\frac{dN}{dr}$ as a function of $\sqrt{r}$.

Average of 67 samplings from Hawaii (WOODCOCK 1957). N in number · m^{-3}, r in microns (μ).

number distributions of sea salt particles properly. If (3.1) were valid then the mass of sea salt within each logaritmic size interval would be the same whereas in fact it is more like a normal distribution as pointed out earlier. From this it is apparent that the exponent of r must be a function of r.

It was found, however, from WOODCOCK's Hawaiian data (1957) that the number distribution could be expressed by a function

$$\frac{dN}{dr} = a \cdot e^{-\beta\sqrt{r}} \qquad (3.2)$$

Fig. 3.1 shows the average of all 67 samplings from Hawaii when log $\frac{dN}{dr}$ is plotted as a function of $\sqrt{r}$. It is seen that the data fit relation (3.2) very well over practically the entire size range of sea salt particles. This does not, of course, mean that eq. (3.2) gives a physical interpretation of the whole complex of phenomena that leads to this distribution; the only purpose the equation can have is to describe the nature of the number-size distribution by a simple formula.

WOODCOCK (1953) summarized earlier values in order to show how the wind strength influenced the number-size distribution, anticipated from the known mechanism of sea salt particle production. The results as presented by Woodcock are shown in fig. 3.2 where N is plotted against w on a log-log scale. The weight w is given in $\mu\mu$g (10^{-12}g). It is

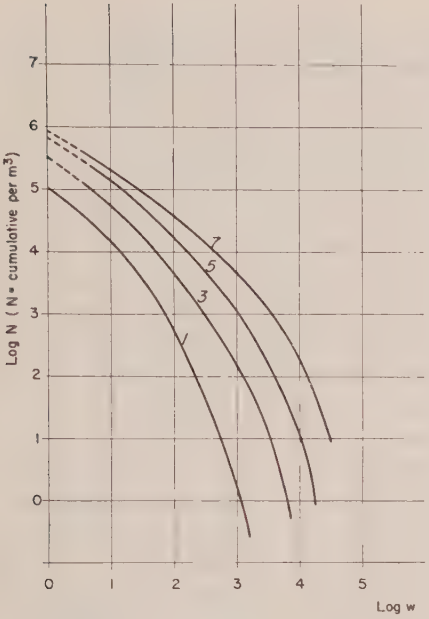

Fig. 3.2. Number-weight distributions of sea salt particles at different wind forces. Wind force in Beaufort. (From Woodcock 1953.)

found that these average curves for different wind force (in Beaufort) also seem to fit eq. (3.2) with some exceptions. A plot of the data in a way similar to fig. 3.1 is shown in fig. 3.3. Two things are, however, noted. Firstly, each wind force obeys eq. (3.2) in certain intervals. Below 2 μ the curves run nearly parallell but above that size they have different β values. It looks as if β is influenced by the wind force and actually by converting the wind forces given on the figure into corresponding wind speeds it is found that β most likely is inversely proportional to the square root of the wind velocity in this upper size range or at least inversely related to the wind velocity.

Fig. 3.3 indicates that the nature of the number-size distribution of sea salt particles as expressed by the parameter β is related to external factors at least above a certain size. Below that size β is presumably independent of wind force though the total number is still a function of wind strength.

Eq. (3.2) is not valid in all regions as will be pointed out in the next section.

b. *Mass-weight distributions of sea salt particles.* This kind of distribution is defined as

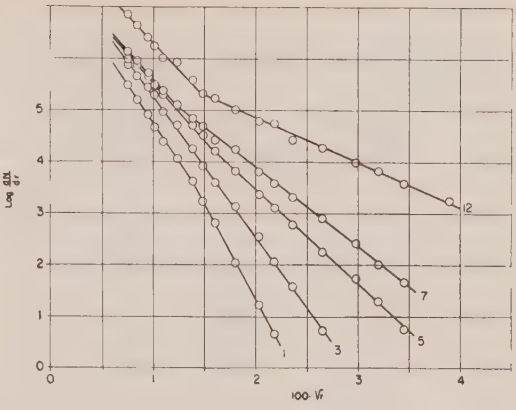

Fig. 3.3. Log $\frac{dN}{dr}$ as a function of $\sqrt{r}$ at different wind forces (in Beaufort), obtained from fig. 3.2. N in number · m^{-3}, r in cm.

the mass of sea salt per logaritmic weight interval and can be formulated

$$\frac{dm}{d(\log w)} = F(w) \qquad (3.3)$$

where m is the total mass of sea salt per unit volume and w is the weight of individual particles.

Considering that

$$dm = -wdN = -wNd(\ln N) \qquad (3.4)$$

it is apparent that the total mass m can be arrived at graphically in two ways. If wN is plotted as a function of $-\log N$ the area below the curve, which forms a kind of a statistical distribution, multiplied by 2.3 will be the total mass of sea salt per unit volume. From (3.4) we can also write

$$dm = -wN\frac{\partial(\ln N)}{\partial(\ln w)}d(\ln w) \qquad (3.5)$$

which shows that if $-wN\frac{\partial(\log N)}{\partial(\log w)}$ is plotted as a function of log w the area below this curve, multiplied by 2.3 will also be the total mass m. Both methods have been employed in the following for estimating the total concentration of sea salt.

The mass-weight distribution defined by $dm/d(\log w)$ have some interesting features. From Woodcock's number-weight distributions in fig. 3.2 the corresponding mass-

weight distributions have been constructed, and the results are seen in fig. 3.4 where for comparison also the radius is given on top of the diagram. First it can be noted that the mass-log (weight) distributions are approximately normal with well defined maxima. It can also be noted that the maximum in mass density is situated at about 6 μ for the greatest wind force and is shifted towards smaller sizes for lower wind forces. Finally it is seen that the total mass of salt is strongly dependent upon the wind force.

The type of mass-weight distributions seen in fig. 3.4 are prevalent in most regions but there are interesting exceptions which will be discussed later.

2. *Vertical variations over ocean areas*

In section II the behaviour of particulate matter in the atmosphere was discussed and it was shown that at a steady state

$$-K\frac{\partial n}{\partial z}+Vn=0 \qquad (3.6)$$

where n is the number concentrations of particles who have a fall velocity V (being negative), K is the turbulent diffusion coefficient and z the vertical coordinate. Further conditions implied in this equation are that the particles are conserved, i.e. no coalescence or disintegration of particles or removal by precipitation takes place and secondly that the horizontal gradient of n is zero.

As the fall velocity increases with the size of the particles it is obvious that the number-size distribution must vary in the vertical in such a way as to decrease the mass concentration. This is generally true too but important exceptions occur. Mordy (1959) has found that K in the eq. 3.6 can be computed from Woodcock's Hawaii data (1958) for some levels, and gives a value of K around 10^5 cm^2 $\times$ sec^{-1} in agreement with the K-value one can compute from the total evaporation in lower latitudes. At many levels, however, anomalies in the number-size distributions occur showing a far too great excess of large sea salt particles. Woodcock (personal communication) who also observed the abundance of large particles around clouds has explained this as due to coalescence of cloud droplets within a cloud and subsequent evaporation which will inevitably lead to an excess of

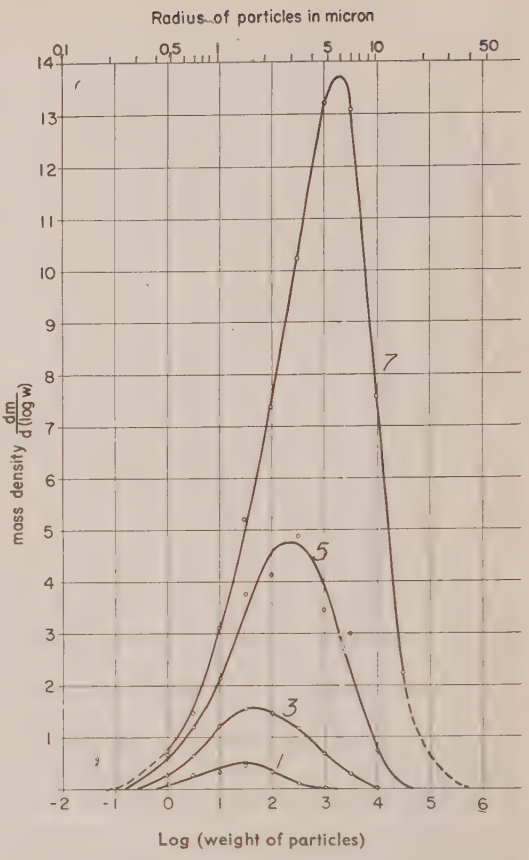

Fig. 3.4. Mass-weight distributions of sea salt particles at different wind forces. Obtained from fig. 3.2. Mass, m, in $\mu g \cdot m^{-3}$, w in $\mu\mu g$ (10^{-12} g) units.

larger particles at cloud level. These higher numbers occur as invisible clouds, often in the rear of tradewind clouds where evaporation of the cloud droplets normally occur. Another mechanism which may operate in cloud and favour large particles is visualized by Woodcock as follows. If the cloud is pictured as a ring vortex with moist, salt laden air flowing upward in the center, large salt particles will reach the largest sized cloud droplets. In the upper part of the cloud where the upward moving air diverges the velocity of the air stream decreases. Cloud droplets of the largest size will fall downward closest to the centre but on arrival at the bottom of the cloud they are evaporated and drawn into the upward moving air. Smaller droplets will be carried further out from the cloud before reaching the cloud base level and will have less chance of

being drawn into the cloud again than the larger salt particles forming the larger droplets. Such a cloud should thus tend to concentrate larger particles until it dissipates when it leaves an invisible cloud of larger salt particles.

Though these mechanisms explain the anomaly in the vertical number weight distribution of larger sea salt particles they do not explain the sometimes observed fact that the smaller particles which are hardly influenced by gravity under normal conditions, also increase upwards to some level. To understand this we must consider the nature of air flow in trade wind regions. The trades are not the uniform flow of air many times visualized though the steadiness of the winds are great. In these belts the flow of air has a wave-like nature so that winds increase and decrease more or less periodically. As these variations in wind force often are accompanied by wind shifts and weather phenomena like cloudiness and precipitation it has become customary to talk about weather disturbances in the form of waves that may move with the wind or against the wind (cf. RIEHL 1954). Such disturbances are always accompanied by higher winds than usually due to convergence and release of latent heat by precipitation in the disturbances. The disturbances may occur on different scales and the best known are those recognizable on a synoptic scale. One significant fact in this connection is that the areal extent of the synoptic disturbances is much less than of the undisturbed regions. On a much smaller scale and much less active, such disturbances may be responsible for the often remarkably regular pattern of cloud areas, i.e. areas where trade wind clouds occur more or less densely distributed. Such patterns have been described by STARR MALKUS (1957) from the Caribbean region and are sometimes even stationary, i.e. the air just passes through the cloud areas without moving the whole area.

All this indicates that wind velocities vary from time to time and from place to place and that the areal frequency of high winds is much less than of low winds. As the production of sea salt particles increases rapidly with increasing winds, one can apparently divide the whole trade wind belts into "source" areas and "sink" areas, the latter removing particles from the atmosphere.

Now, the application of eq. (3.6) is, of course, restricted. A more complete equation should read (considering only two dimensions)

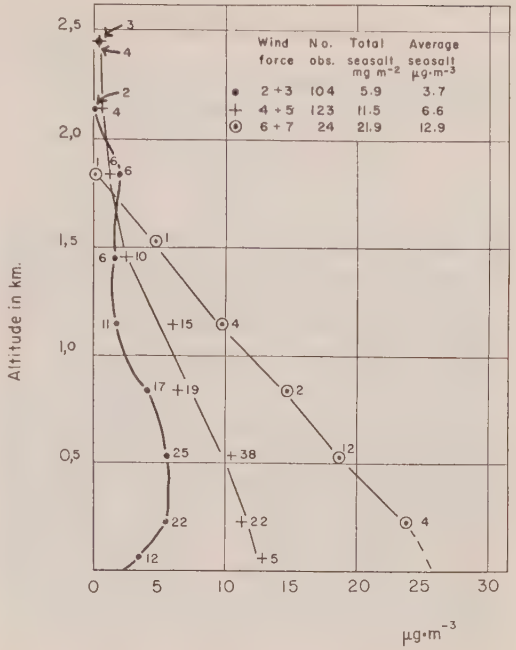

Fig. 3.5. Mass concentrations of sea salt particles as a function of altitude at different wind forces (in Beaufort). From WOODCOCK (unpublished).

$$\frac{\partial n}{\partial t} + u\frac{\partial n}{\partial x} + V\frac{\partial n}{\partial z} + \alpha n = \frac{\partial}{\partial z}\left(K\frac{\partial n}{\partial z}\right) \quad (3.7)$$

where u is the wind velocity in the horizontal x-direction and αn is the rate at which particles disappear due to removal by coagulation, coalescence and precipitation. The equation is neglecting vertical motion of air and may be applicable in a sink region where occasional cloud formation and precipitation takes place.

Consider eq. (3.7) in a steady state ($\partial n/\partial t = 0$) when air is emerging from a source region. To demonstrate what happens neglect the fallout and the dispersive term. Then

$$u\frac{\partial n}{\partial x} + \alpha n = 0 \quad (3.8)$$

which gives

$$n = n_0(z)\, e^{-\frac{\alpha}{u}x} \quad (3.9)$$

Let $n_0(z)$, the vertical distribution at the source, be exponential of the form exp. $(-z/h)$, then

$$n = n_0 e^{-\frac{z}{h} - \frac{\alpha}{u} x} \qquad (3.10)$$

Let u increase linearly with height, say by $u = u_0 z$. Then n has a maximum at

$$z = \sqrt{\frac{\alpha h}{u_0} x}$$

i.e. proportional to the square root of the distance. Thus, as we proceed from the source, a maximum in n is formed close to the surface and is shifted upwards, first rapidly, then more and more slowly.

Inclusion of the dispersive term cannot remove this maximum, only flatten it and inclusion of the fallout term would only shift its position to a lower altitude. The example above is simplified but on can expect such a maximum in the salt load to appear in a sink region whenever the wind increases with height because of more rapid advection from the source region at higher levels than at lower.

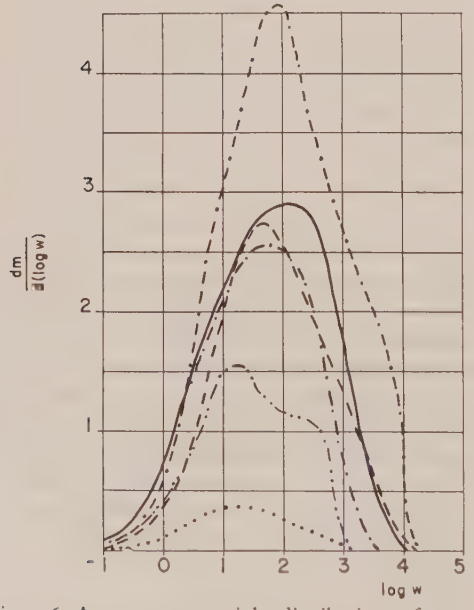

Fig. 3.6. Average mass-weight distributions of sea salts at different altitudes in Hawaii. Mass, m, in $\mu g \cdot m^{-3}$, w in $\mu\mu g$ (10^{-12} g). Data from WOODCOCK (1957).

————	500 feet altitude
— — . — — .	1,000—2,000 feet altitude
— — — — — —	2,000—3,000 " "
— . — . — . — .	3,000—4,000 " "
— . . — . . — . .	4,000—5,000 " "
. . . . .	5,000—8,000 " "

Now we can conclude that if sampling is done regularly at a certain place one would frequently find a maximum in the sea salt particle concentrations around the cloud base level in more normal wind conditions and a regular decrease with height when sampling in strong winds. This can actually be seen in fig. 3.5 (which has been received from WOODCOCK) where the average variations of mass of sea salt with height in three different groups of wind speeds are shown. It is seen that the lowest wind speeds give a clear maximum at about cloud base level. The next group of wind forces give a nearly constant mass with height up to the same level whereas the highest winds show a clear decrease all the way upwards.

Before discussing the mass-weight distributions further it should be remarked that excessive maxima may partly be due to an unfair large proportion of samples from cloud base level compared to lower levels.

Looking at mass-weight distributions at different levels, fig. 3.6 shows the distributions obtained from WOODCOCK's Project Shower data (1957). It is seen that there is a higher average mass density of sea salt in the atmosphere between 1,000 and 2,000 feet than at around 500 feet. From 2,000 feet it is fairly constant up to 4,000 feet which probably is not characteristic for Hawaii but may be influenced by the so-called Kona-storms which occurred in late November and early December in 1954. At higher levels the mass density decreases rapidly.

As to the mass-weight distributions themselves the one at the 500 feet level has a maximum around a particle weight of 100 $\mu\mu g$ which corresponds to a radius of 2.2 microns. In the next layer, 1,000—2,000 feet, the maxima in the distribution is shifted somewhat to the left but there is an appreciable mass in large sea salt particles. There is at this level more mass in the interval 1,000—10,000 $\mu\mu g$ than in the same interval at 500 feet which may depend on formation of larger particles in the clouds.

At higher levels it is seen that the mass of the larger particles is considerably reduced though the maximum in the distribution is nearly the same. In the highest layers, however, the maximum is shifted close to $w = 10$ $\mu\mu g$ which is roughly about 1 micron radius.

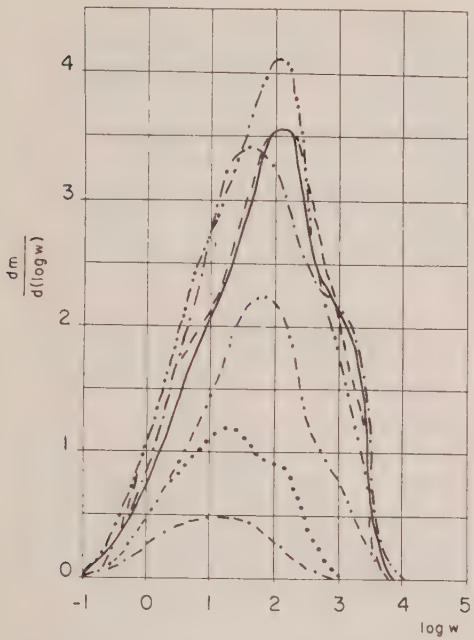

Fig. 3.7. Average mass-weight distributions of sea salts at different altitudes in the Caribbean area. Mass, m, in $\mu g \cdot m^{-3}$, w in $\mu\mu g$ (10^{-12} g). Data from WOODCOCK (unpublished).

————	100 feet altitude
— . — . — . —	500 " "
— — — —	1,000 " "
— . . — . .	1,500 " "
— — . . — — . .	2,000—2,500 feet altitude
. . . . .	3,000—3,500 " "
— — . — — .	4,000—8,000 " "

The next set of mass-weight distributions at various levels shown in fig. 3.7 are from the Caribbean area. Data have been obtained by WOODCOCK (mostly unpublished) and the sampling was done at various places in the West Indies, from Puerto Rico to Barbados. Similar features to those from Hawaii are seen. The mass of salt per unit volume is nearly constant up to 1,000 feet but shows a maximum at 1,500 feet. From thereon it decreases steadily. The maximum in the mass-weight distribution is again around $w = 100\,\mu\mu g$ except at the two highest layers where it is around 10 $\mu\mu g$ just as in the Hawaiian distributions.

Comparing figs. 3.6 and 3.7 one can conclude that there are hardly any regional differences neither in type of distributions, nor in mass of sea salts per unit volume and but small in the vertically integrated load of sea salts.

From these distributions which are obtained in oceanic areas we may proceed to the coast of Florida, a place which is close to a large continent. Woodcock's data from Pompano Beach in Florida have been worked up in a similar way as in figs. 3.6 and 3.7 and the results are shown in fig. 3.8. Here we see something entirely new, namely a bimodal distribution of mass with respect to log w at all levels. This type of distribution can apparently not fit eq. (2). The same type mass weight distribution is also found in a set of data published by BYERS et al. (l.c.) to be discussed later. On this occasion they sampled chloride particles which were identified and measured on millipore-filters using LODGE's (l.c.) technique on a flight from New Orleans to Illinois.

One thing that is clearly seen in fig. 3.8 is that the first maximum is centered at $w = 10$

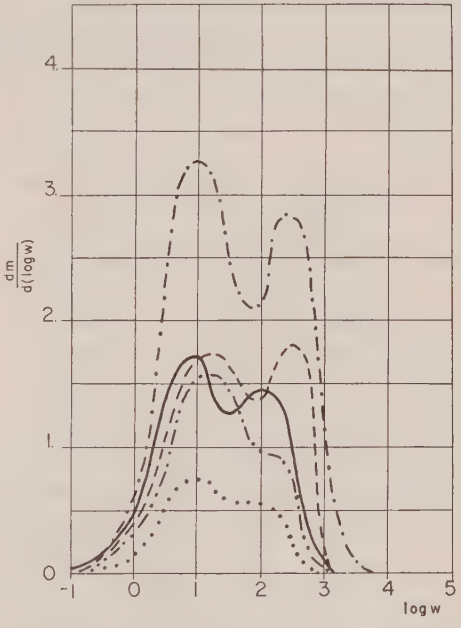

Fig. 3.8. Average mass-weight distributions of sea salts at different altitudes at Pompano Beach, Florida. Mass, m, in $\mu g \cdot m^{-3}$, w in $\mu\mu g$ (10^{-12} g). Data from WOODCOCK (unpublished).

————	100— 500 feet altitude
— — — — —	800—1,100 " "
— . — . — .	1,400—1,600 " "
— . . — . . —	3,000—3,200 " "
. . . . .	4,000—6,000 " "

$\mu\mu$g very consistently whereas the second varies from 100 $\mu\mu$g to 300 $\mu\mu$g. So even the distribution of larger particles is different from those in Hawaii and the Caribbean where the maximum was found close to $w = 100$ $\mu\mu$g or somewhat below.

It is of little use speculating on the reasons for these differences. The sea salt particles in fig. 3.8 are most probably generated on the adjacent shelf area of the Atlantic and it may be possible that the biological turnover in these comparatively shallow waters give rise to different sea surface properties than in the "deserts" of the open trade wind regions. A special study of sea surface properties would probably shed light on this problem[1].

As to the vertical distribution of mass, a maximum is again found around 1,500 feet just as in the other regions.

There are, unfortunately, no data available from more temperate regions like the North Atlantic. Woodcock (1953) has some data from South Australia but they are too few to base a similar discussion on. The same is true for a couple of vertical profiles from off the isle of Nantucket on the New England coast.

From the mass-weight distributions in figs.

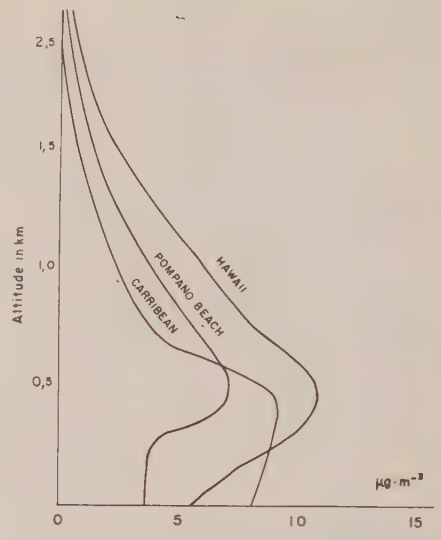

Fig. 3.9. Sea salt particle mass concentrations as a function of altitude at Hawaii, the Caribbean area and Pompano Beach, Florida. From fig. 3.6, 3.7 and 3.8.

[1] Woodcock (personal communication) suggests that the anomaly in the Florida mass-weight distribution is due to outflow from the continent at higher levels of modified maritime air. This outflow is compensating the inflow at lower levels caused by heating of the land surface.

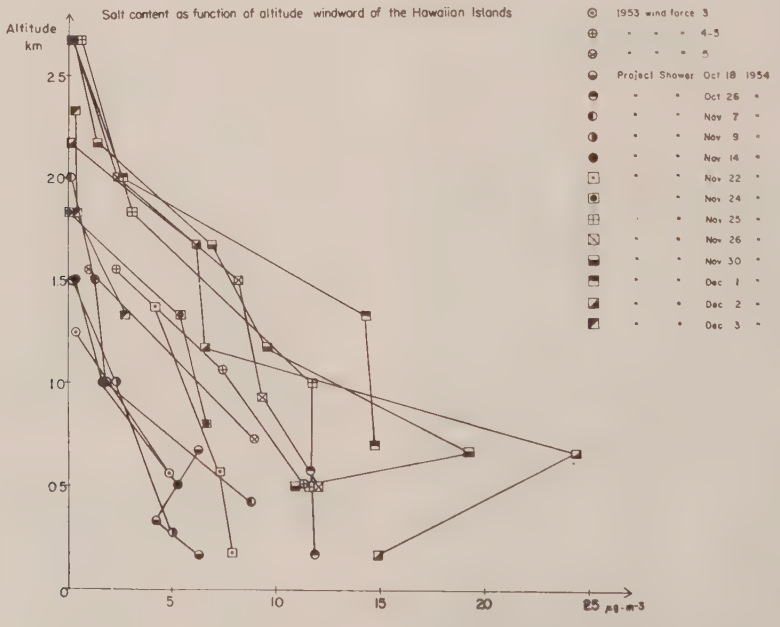

Fig. 3.10. Mass concentrations of sea salts as a function of altitude on various days in Hawaii. Data from Woodcock (1957).

3.6, 3.7 and 3.8 the mass concentration at the different levels has been obtained by measuring the corresponding surface areas. Fig. 3.9 shows the average vertical mass concentration as a function of height for Hawaii, the Caribbean area and Pompano Beach. The maximum around 500 m is quite pronounced. Integrating these vertical distributions one obtains the average salt load per unit surface area which becomes

Hawaii	11.2 mg × m^{-2}
Caribbean	7.2 mg × m^{-2}
Pompano Beach	6.8 mg × m^{-2}

It is seen that average salt load is somewhat higher in Hawaii which no doubt is due to a unfair proportion of weather disturbances. The average for all three is 8.4 mg × m^{-2}. This may be taken as a representative figure for the amount of sea salt particles in the trade wind areas under fairly normal conditions. Whether the same load is found in higher latitudes is an open question. Under normal wind conditions it can, however, hardly be higher as the conditions for formation of large sea salt particles is somewhat limited by the higher relative humidity. The frequency of storms is, however, greater and this may contribute appreciably.

Nothing has been shown so far of the variations from day to day of the salt load of the air over the oceans. One can get a fairly good idea about the variability from WOODCOCK's Project Shower measurements. Some of the occasions when sampling was done at several altitudes have been chosen and are presented in fig. 3.10 as the mass concentration versus altitude. The variability is, as seen, great and yet no severe weather disturbances occurred during the time. In a region like the Caribbean and the coast of Florida the variability would certainly be greater due to the fairly regular occurrence of hurricanes in late summer in these areas. WOODCOCK (1950b) has measured the salt concentration from a lighthouse on the Florida coast during a hurricane when the wind force was 12 (Beaufort scale) and obtained extremely large sea salt particle concentrations.

Even more moderate weather disturbances in the Caribbean can give rise to quite large sea salt concentrations. One such case can be traced in data by LODGE (1955) in which the salt concentration reached well above 100 μg × m^{-3} at about 400 m altitude and the total salt load was about 100 mg × m^{-2}.

3. *Sea salt particles over land*

As pointed out before, data over land are scanty and very seldom so systematically collected as over the oceans and the information is many times qualitative. Yet those that exist are of considerable interest as they reveal interesting differences between land and sea.

TWOMEY (1955) investigated the maritime air flow south-west over the south-east part of Australia. On three occasions he followed the air by aircraft from the south-west and studied the change in the vertical distribution of sea salt particles that took place during its passage 600 miles inland. Two significant conclusions can be drawn from his work. There was a marked change in the vertical distribution of sea salt particles as the air entered the continent due to the increased turbulence and convection over land. Sea salts were thus transported upwards so that the vertical gradient decreased. This, of course, decreased the concentration of salt near the surface as the particles became more evenly distributed. Further, as he points out, if no precipitation or convective cloud formation took place there was no appreciable reduction in the sea salt concentration of the air during its long travel. Precipitation, and even convective cloud formation without apparent precipitation was very effective in removing the salt from the air. That even cloud formation alone could reduce the number of salt particles—as he actually measured—can be understood as coalescence of cloud droplets and subsequent evaporation forms a few large particles from many small and these really large particles soon fall out of the air.

The investigations undertaken by BYERS et al. (l.c.) also furnished very important information on sea salt particles over continents. They made some vertical samplings in Illinois on a few occasions. From their data fig. 3.11 has been constructed. It should be mentioned that the estimates of mass of salt made from their data are somewhat uncertain though they may be correct within ±30 per cent. The vertical distributions in fig. 3.11 shows relatively

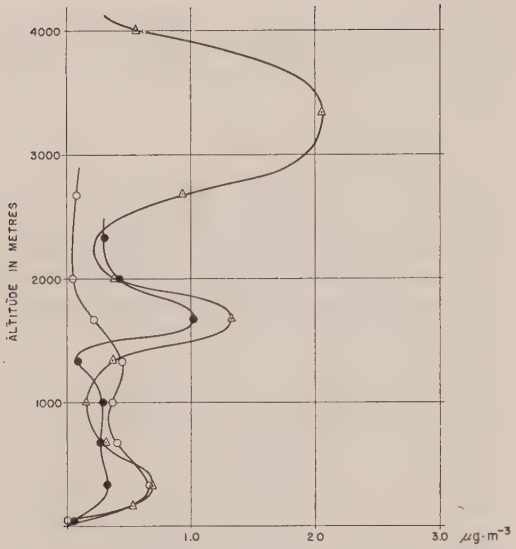

Fig. 3.11. Mass concentrations of chloride as a function of altitude in Illinois on three different occasions. Data from Byers et al. (1956).

● Nov. 10, 1954. 0.81 mg · m^{-2} up to 3,000 m
○ " 5, 1954. 1.09 " " " 3,000 m
△ June 11, 1954. 1.90 " " " 3,000 m
3.67 " " " 4,000 m

low mass concentrations but they can extend to great altitudes. In the June 11 case the air had moved from the Gulf of Mexico, but there is a marked stratification suggesting layers of somewhat different origin. In the other two cases the air flow was northerly and it may represent air from the North Pacific which has passed over the mountains to the west where a good deal of the sea salts got lost.

The most interesting is, however, the deep layer of salt at around 10,000 feet altitude. The lower part may have been washed out during the travel up to the Mississippi Valley. The Mississippi Valley is certainly important for the water vapor transport into the continent as well as for the sea salt transport as inferred earlier by Eriksson (1955a).

Byers et al. also made two horizontal sections along the Mississippi Valley sampling chloride particles. On June 6, 1954 they sampled at regular intervals at 5,000 feet elevation on the route from Illinois to the Gulf and on June 9 they returned flying at 2,500 feet altitude. Their results recalculated into μg salt × m^{-3} are shown below

	Illinois								*Gulf*
June 6									
5,000 feet	.23	.80	1.65	1.03	.85	.52	.09	.25	2.04
June 9									
2,500 feet	.11	.35	.71	.97	.90	.95	.97	5.75	1.52

There is in the first place a maximum south of Illinois and a minimum close to the Gulf. In view of the vertical variability shown in fig. 3.11 the variations in the horizontal may simply be due to varying height of a strata situated around 5,000 feet indicating some wave character in the northward flowing air current. At lower levels the vertical variation is presumably less leading to a regular decrease northwards. It should be mentioned that the vertical profile in Illinois with the large concentration at high levels was made in the same air stream only two days after the return flight.

Another interesting feature of the return flight is found in the mass-weight distribution which was definitely bimodal at all places, just as the distributions at Pompano Beach in Florida.

Finally a more qualitative but extremely interesting investigation was carried out by Crozier, Seely & Wheeler (1952) in the western part of the United States. They also sampled from aircraft and though their technique does not give more than relative data on the largest salt particles the numbers they found per m^3 are certainly proportional to the salt concentration in the air.

In their first investigation they made a cross country flight at 10,000 feet elevation. Starting from Alberquerque in New Mexico they first flew westward. During the first part of the flight they were in what they call marginal Gulf of Mexico air and the number of chloride particles observed was around 500 × m^{-3}. Over California they passed through a tongue of air which had presumably originated in a tropical disturbance off the coast of SW Mexico which had dissipated two days earlier. The chloride particle concentration rose to about 3,000—4,000 × m^{-3} in the center of this tongue. Out over the Pacific they entered into descending stable air from the Pacific High which is a nearly permanent feature in this region. This air had a chloride particle content of only 100—200 × m^{-3}. Off the coast of California they turned and flew in a northeast direction and once more they entered

the Cl-particle rich tounge of air which they followed northward and were able to trace to Utah. From there on to Iowa the particle content was low as they where entirely in descending air. In Iowa they once more encountered Gulf of Mexico air with particle concentrations up to $1{,}000 \times m^{-3}$ and this air prevailed to eastern Illinois where they entered continental polar air with practically no chloride particles. The identification of air masses was made from ordinary weather maps.

The significant feature, apart from the Gulf of Mexico air which in summer penetrates far north, is the long tongue of air from the tropical disturbance. It is known that greater disturbances like hurricanes require an outflow of warm air at higher levels in order to maintain themselves (cf. RIEHL 1954) and this is presumably true for smaller disturbances too. CROZIER & SEELY (1952) continued to look for such chloride rich strata during a two weeks study and once more encountered a tongue over the Death Valley, this time originating in a disturbance off Baja California and with particle concentrations as high as 10,000 $\times m^{-3}$.

The importance of these findings can hardly be overly stressed as it shows that chloride rich air can be transported at high levels into continents, thus passing over mountain barriers without washout of chloride. Once over continents mixing with colder air will cause precipitation of water and sea salt from such strata. The transport and subsequent accumulation of sea salt in the Bonneville Basin in Utah is thus easier to understand.

4. *Rate of production of sea salt particles*

The rate of production of sea salts in a "source" region must be equal to the rate of removal in sink regions. The removal is accomplished by two processes, removal by precipitation and removal by fallout. The rate of removal by precipitation is rather difficult to estimate directly but can perhaps be related to the rate of removal by fallout which is better suited for computations, using the average distributions presented earlier.

The fallout must be estimated at the sea surface in the so-called laminar boundary layer in which only molecular phenomena are supposed to take place, and consequently, where particles, falling into it, have no way of escape into the turbulent region again.

There are, however, a couple of problems involved in practice. In the laminar boundary layer the relative humidity is much higher than in the free air and this may influence the fall velocity of the particles. If they are small, equilibrium is probably so rapidly established that they essentially fall under equilibrium conditions. But if they are large, equilibrium is probably never attained and they fall through the laminar boundary essentially at the same rate as in the free air.

When the conditions in the boundary layer are defined, the rate of fallout can be simply computed from the concentration of particles in the boundary layer through multiplying with the appropriate fall rate. As to the concentrations of particles in the boundary layer, they are not known but a crude estimate can be done by extrapolating the vertical distributions to sea level. A check on the correctness of this procedure can be done afterwards by comparing the fallout rate with the turbulent diffusion coefficient in the free air to see if any appreciable gradient is needed for the transport down to the surface.

a. The boundary layer

The vertical transport mechanisms in the air at sea level has been thoroughly discussed by SVERDRUP (1951) on which the following discussion is mainly based. Of different assumptions made about the vertical transports the following seems to fit best the scanty observations made (cf. SVERDRUP): "Next to the surface there is a true diffusion layer of thickness $\lambda\nu/w_{*r}$ where w_{*r} applies to a rough surface. From the top of this layer the eddy diffusivity increases at the same rate as the eddy viscosity". In the formula above ν is the kinematic viscosity of air, λ is a constant and w_{*r} is the friction velocity. The rate of transport in the laminar boundary layer (= the true diffusion layer) is then

$$F = -D\frac{\partial \varrho}{\partial z} \qquad (3.11)$$

where D is the molecular diffusion coefficient. Above this layer

$$F = -K\frac{\partial \varrho}{\partial z} \qquad (3.12)$$

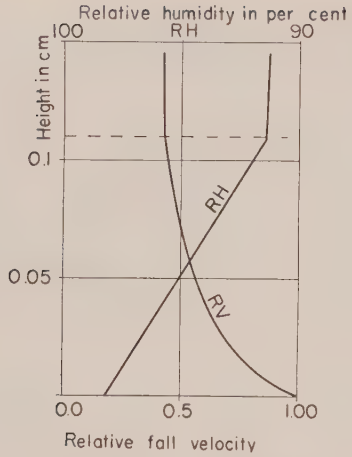

Fig. 3.12. The variation of relative humidity and fall velocity of a sea salt particle at equilibrium, in the laminar boundary layer over sea water.

where K is the turbulent diffusion coefficient. The following relations are to be used

$$K = k_0 w_{*r} (z + z_0) \tag{3.13}$$

$$w_{*r} = \gamma w \tag{3.14}$$

$$\gamma = \frac{k_0}{\ln \frac{z + z_0}{z_0}} \tag{3.15}$$

where k_0 is Karman's constant (= 0.4) and z_0 the roughness parameter (= 0.6 over a rough sea surface) and w is the wind velocity at the level z.

As to λ which determines the thickness of the boundary layer, a value of 27.5 has been suggested for a rough sea surface, while λ = 11.5 has been suggested for a smooth surface.

Using λ = 27.5 and the values for the other constants as given one can compute the vertical vapor density profile from the average rate of evaporation and surface vapor density over tradewind areas (referred to in section 11) and an average wind speed at 8 m level of 6 m $\times$ sec^{-1}. These computations give a laminar boundary layer of 1.1 mm and a relative humidity at the top of the boundary layer of 91.4 per cent. As to the rest of the profile data have been tabulated in table 3.1. It is seen that the relative humidity at z = 800

TABLE 3.1

Vertical distribution of relative humidity over sea water and of relative volumes, radii and fall velocities of sea salt particles. Salinity of sea water 35.2 per mille, wind speed 6 m/s

Height in cm	Relative humidity in per cent	Relative volume of sea salt particles	Relative fall velocity of sea salt particles at equil.	Relative radius of particle	Remarks
0.0	98.2	1.000	1.000	1.000	Laminar
0.11	91.4	.250	.424	.630	boundary
0.2	91.2	.245	.419	.726	layer
0.3	91.0	.240	.414	.622	
0.4	90.8	.236	.409	.619	
0.5	90.6	.232	.405	.615	
0.8	90.2	.224	.397	.608	
1.0	90.0	.221	.394	.605	
1.5	89.5	.212	.385	.597	
2.0	89.2	.207	.380	.593	
3.0	88.7	.200	.372	.586	
4.0	88.2	.194	.366	.579	
5.0	87.9	.190	.362	.575	
10.0	86.5	.172	.343	.557	
20	85.7	.164	.334	.547	
30	85.0	.158	.327	.541	
50	84.2	.152	.320	.534	
60	83.9	.150	.317	.531	
100	82.9	.143	.309	.523	
200	81.8	.136	.301	.516	
300	80.8	.131	.295	.507	
500	80.3	.128	.292	.504	
600	79.9	.126	.290	.501	
800	79.5	.124	.288	.499	

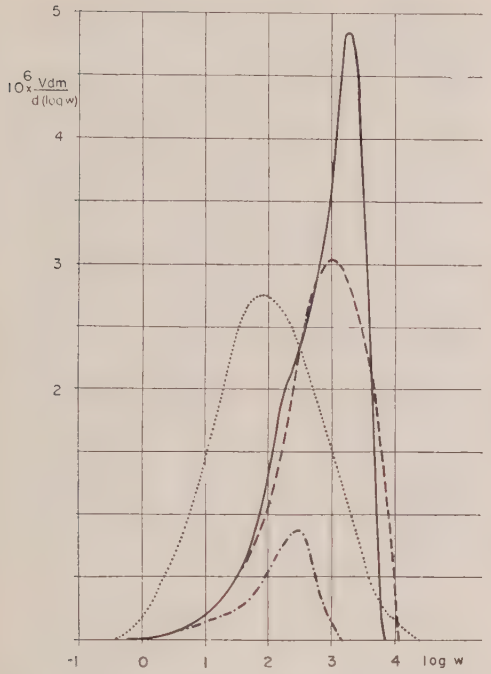

Fig. 3.13. Rate of fallout of sea salts and rate of production in breaking waves. Mass, m, in $\mu g \cdot m^{-3}$, w in $\mu\mu g$ (10^{-12} g).

———— Hawaii
— — — — Caribbean area
— . — . — . Pompano Beach, Florida
. . . . . Rate of production in breaking waves computed from data by BLANCHARD-WOODCOCK (1956). Note, original computed figures have been divided by 600.

cm is close to 80 per cent which is a good average for trade wind areas. In table 3.1 relative radii, volumes and fall rates are also shown. It is seen that above the laminar boundary layer the fall velocity is only 42 per cent of the value at saturation (98.2 per cent). The change in fall velocity further upwards is comparatively slow.

The conditions in the laminar boundary layer can be seen in fig. 3.12 where the fall velocity at equilibrium is given as a function of height. It is seen that the fall velocity changes but slowly until the surface is reached.

b. Fall rate and adjustment time to evaporation

One may thus assume that particles that arrive at the top of the boundary layer have a fall speed equal to about 40 % of that of equilibrium with sea water. Next we may try to estimate how long time they spend in the boundary layer before they fall into the water. Full saturation vapor pressure is not reached until the salt particles reach the very surface. One can compute the average fall velocity from the growth equation with some simplifying assumptions. This has been done and it is remarkable how little the average fall velocities differ from those on the top of the boundary layer. The greatest difference is in the small end of the size-spectrum but even there (at $w = 0.15$ $\mu\mu g$) the difference is less than 10 per cent. Considering that these small particles contribute very little to the fallout rate of mass one can compute the fallout with the simple assumption that the rate of removal is equal to the fall velocities of particles in equilibrium with the water vapor pressure at the top of the boundary layer.

c. The distribution of rate of fallout versus weight

The mass-weight distributions of the type discussed earlier can now be used to study the variation of the rate of fallout with size. Let ΔF be the rate of fallout of mass of particles in the interval $\Delta \log w$. Then we have

$$\frac{dF}{d(\log w)} = V\left[\frac{dm}{d(\log w)}\right]_{\text{boundary}}$$

and as boundary values we chose those at the lowest level presented in figs. 3.6, 3.7 and 3.8, while V is taken from table 2.3. It is obvious that no extensive turbulent transport need to take place in the lowest part of the atmosphere when the fall velocities of particles are only to a small extent influenced by the increasing relative humidity as we approach the surface. The assumption that the distribution of particles in the boundary layer is the same as that at say the 100 feet level or so therefore seems appropriate.

The results of the computations of rate of fallout are shown in fig. 3.13 for the three regions in question, Hawaii, the Caribbean and the coast of Florida. It is seen that this type of distribution naturally has its maximum in the large weight region, centered around $w = 10^3$ $\mu\mu g$. An exception is the Florida distribution where the maximum is centered at $w = 10^{2.5}$ $\mu\mu g$.

The total fallout can now be estimated from the area below the curves and becomes

Caribbean 6.0×10^{-6} $\mu g \times cm^{-2} \times sec^{-1}$
Hawaii 5.1×10^{-6} $\mu g \times cm^{-2} \times sec^{-1}$
Florida 1.0×10^{-6} $\mu g \times cm^{-2} \times sec^{-1}$

The very low value for Florida is perhaps not representative for the sea as a whole, the other two are appreciably higher. As an average for trade wind areas a figure of 5.5×10^{-6} $\mu g \times cm^{-2} \times sec^{-1}$ may be used.

The average weighted fallout rates may now be estimated. The salt concentrations at the lowest levels are obtained from fig. 3 and are

Caribbean 8.1 $\mu g \times m^{-3}$
Hawaii 7.2 $\mu g \times m^{-3}$
Florida 3.6 $\mu g \times m^{-3}$

so that average velocities become

Caribbean 0.74 $cm \times sec^{-1}$
Hawaii 0.71 $cm \times sec^{-1}$
Florida 0.28 $cm \times sec^{-1}$

These figures can be compared to" deposition velocities" or vertical transport rates as defined earlier where, for the sea a value of 0.87 $cm \times sec^{-1}$ was estimated from evaporation data. They are thus comparable.

The rate of removal over the entire sea surface, using a fallout rate of 5.5×10^{-6} $\mu g \times cm^{-2} \times sec^{-1}$ becomes 540 million tons $\times$ $year^{-1}$ and the corresponding chloride 300 million tons $\times$ year.

We may ask how much is removed by precipitation. We can then compare the fallout velocity over the sea with the deposition velocity over land which, as will be shown later, is about 2 $cm \times sec^{-1}$. Over land about two times as much chloride is removed by dry fallout as by precipitation. Over the sea the dry fallout should consequently be less important relative to precipitation than over land maybe by a factor of 2. Thus one may assume that at least as much sea salt is removed by precipitation as by dry fallout. This gives a figure for the total removal over sea of more than 1,000 million tons a year. The rate of run-off from land is of the order of magnitude 100 million tons $\times$ $year^{-1}$ so a figure of 1,000 million tons per year could represent the total production rate over the sea.

d. The production rate in breaking waves

Blanchard & Woodcock (1956) have made a thorough study of various mechanism for sea salt production. As to breaking waves, which presumably is the most important source for sea salt particles in the atmosphere, they made a study of the size and number of par-

TABLE 3.2

Data and computations of the rate of production of the mass of sea salt particles in a breaking wave. Data obtained from Blanchard and Woodcock (1956)

log w	v cm · sec^{-1}	$n(w)$	w^2	$\frac{dN}{dD}$	$\frac{dD}{dw}$	$dm/d(\log w)$
—.50	.0128	.0	.1	$2.51 \cdot 10^3$	20.1	0
—.25	.0217	.2	.316	$7.95 \cdot 10^2$	19.2	36
.00	.0340	.5	1.0	$2.51 \cdot 10^2$	10.0	98
.25	.054	1.2	3.16	$7.95 \cdot 10^1$	7.1	266
.50	.0852	1.7	10.0	$2.51 \cdot 10^1$	5.04	419
.75	.136	2.3	31.6	7.95	3.56	645
1.00	.214	2.8	100	2.51	2.52	871
1.25	.34	3.3	316	$7.95 \cdot 10^{-1}$	1.79	1,160
1.50	.54	3.7	1,000	$2.51 \cdot 10^{-1}$	1.27	1,465
1.75	.78	4.0	3,160	$7.95 \cdot 10^{-2}$	.90	1,620
2.00	1.1	4.0	10^4	$2.51 \cdot 10^{-2}$	.64	1,635
2.25	1.6	3.8	$3.16 \cdot 10^4$	$7.95 \cdot 10^{-3}$	.45	1,580
2.50	2.1	3.4	10^5	$2.51 \cdot 10^{-3}$	.317	1,390
2.75	3.0	3.0	$3.16 \cdot 10^5$	$7.95 \cdot 10^{-4}$	.224	1,176
3.00	4.0	2.5	10^6	$2.51 \cdot 10^{-4}$	.159	920
3.25	5.3	1.9	$3.16 \cdot 10^6$	$7.95 \cdot 10^{-5}$	.113	660
3.50	7.0	1.3	10^7	$2.51 \cdot 10^{-5}$	.080	418
3.75	9.0	.6	$3.16 \cdot 10^7$	$7.95 \cdot 10^{-6}$	.0565	177
4.00	11.0	.4	10^8	$2.51 \cdot 10^{-6}$	.0400	102

ticles produced by breaking bubbles, the ejected height, the bubble size distribution in breaking waves and the rate of rise of bubbles of different sizes. All this information is contained in tables and diagrams and has been used in the following for computing the rate of production of sea salt droplets. This result depends much on the number of ejected droplets that can be considered to be carried away by the turbulence of the air above the laminar boundary layer. For small ejected particles with small fall velocities the most important requirement is that they penetrate the laminar boundary layer and in this way the probable number of successful droplets can be estimated. For large particles, however, turbulent conditions become more and more important and very little guidance is received from the height of the ejected heights. The choise of the number of successful droplets on this side of the distribution of ejected droplet becomes therefore more arbitrary but evidently they must decrease with increasing size. By this procedure the rate of production in a breaking wave can be computed as follows.

Let N be the cumulative number of bubbles arranged according to decreasing size and $n(w)$ the number of droplets that can possibly reach equilibrium above the boundary layer. Further let w be the weight of salt in each droplet and $D = \phi(w)$ be the relation between bubble size and weight of salt in a droplet ejected from the bursting bubble. Then we get for the mass m

$$dm = v \cdot n(w)\, w\, dN = vn(w) w \frac{dN}{dD} dD =$$

$$= vn(w) w \frac{dN}{dD} \frac{d\phi}{dw} dw =$$

$$= 2.3\ vn(w) w^2 \frac{dN}{dD} \frac{d\phi}{dw} d(\log w) \quad (3.16)$$

where v is the rise velocity of the bubbles. As to $n(w)$ this can be obtained as a smoothed function of log w applying principles discussed above. The units used are the same as in the computation of rate of fallout. It should be pointed out that the relations found by BLANCHARD & WOODCOCK have been extrapolated.

The computed $dm/d(\log w)$ shown in table 3.2 have been entered in fig. 3.13 on a scale that is directly comparable to the Caribbean fallout distribution, i.e. the surface areas below these curves are the same. To achieve this the data in table 3.2 were divided by 600. Considering the removal by precipitation it looks as if the rate of production in a breaking wave is 300 times the rate of removal. This can be interpreted to mean that about 0.3 % of the ocean areas is always covered with breaking waves.

The most striking thing about the distribution is, however, its position relative to the fallout curves. This really suggests a far reaching coalescence process in the air especially for the small-sized particles, shifting their mass to bigger sizes.

It should be pointed out that the right side of the distribution is tentative in a respect. It is certainly strongly influenced by the wind force because in a strongly turbulent air a greater number of the ejected droplets will be carried away by turbulence than indicated in table 3.2 For small-sized particles this influence is much smaller. We may have a reason here for the peculiarities in the dN/dr distributions discussed earlier. The nature of the distribution of larger-sized particles will be influenced by the wind much more than that of the small particles.

TABLE 3.3

Residence times of sea salt particles calculated both from fallout (τ_1) and from rate of production (τ_2)

log w	dM/d (log w)	$V\, dm/d$ (log w)	Rate of prod. dm/d (log w)	τ_1 days	τ_2 days
.00	9.9×10^4	.014	.33	82	3.5
1.00	2.4×10^5	.17	2.90	16	1.0
2.00	3.0×10^5	1.35	5.45	2.6	0.6
3.00	1.3×10^5	3.73	3.07	0.4	0.5

e. The residence time of different sized particles

With the material available we may also compute residence times for various sizes. Defining

$$dM = \int_{z=0}^{z=\infty} dmdz \qquad (3.17)$$

the amount of salt present in the air per unit area and logarithmic interval of w is dM/d (log w) and can be arrived at by plotting dm/d (log w) as a function of height for various values of w. Then the residence time can be formulated in two ways. If the fallout was the only process that removed the particles we would have

$$\tau = \frac{dM/d\,(\log w)}{V[dm/d\,(\log w)]_{z=0}} \qquad (3.18)$$

If there are other processes like coalescence that dominate we should use the production function discussed earlier, weighted by dividing the values in table 3.2 by 300, thus accounting also for removal by precipitation. Using the Caribbean distribution the computed residence times in days for selected values of w becomes those in table 3.3 for these two alternatives.

It is seen that the residence times computed on the basis of rate of fallout becomes extremely large for the small-sized particles and this is incompatible with the observed variability of particle numbers of these particles. Therefore, the residence time based on rate of production is much more reasonable and shows that they are fairly rapidly removed, naturally by coalescence, forming larger particles. As to the large particles fallout and removal by precipitation is, perhaps, much more important and, in fact, removes also particles that are formed by coalescence. Thus, the real residence time for these large particles is most probably smaller than indicated in the table.

It should be noted, however, that following a certain mass of salt as represented by a particle its residence time in the atmosphere will be appreciably greater than the values derived from the production of sea salt because it is constantly passing through increasing sizes before it is removed.

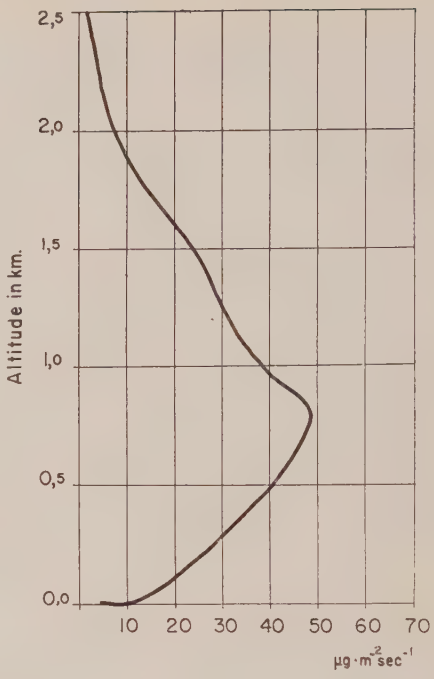

Fig. 3.14. Rate of advection of mass of sea salt from 60° at different altitudes windward of Hawaii. Computed from Project Shower data (Woodcock 1957, Amman 1957).

5. Advection of sea salt as a function of altitude

When considering the horisontal transports of the salts some information may be arrived at from the Project Shower data. Frequent rawin soundings during the operation make it possible to estimate the wind speeds and directions at various levels. The soundings were made at Hilo on the isle of Hawaii which is situated at the windward coast. Whether these soundings are representative for the trade wind areas as a whole is a question that will be left open but the influence of the land may not be too great. Anyway, the computation of the salt transport is at any rate representative for what happened at the windward side of Hawaii.

Data from the soundings have been compiled by Amman (1957).

The following days, when more complete data on the sea salt particle distribution existed were used. November 14, 22, 24, 25, 26 and 30 and December 1 and 2, 1954. As there were four soundings per day, those laying closest in time to Woodcock's sampling times were selected, plotted and the 60° components computed from the directions and wind speed.

For each of the days listed the product of the 60° wind speed and salt concentration in air were calculated at every 200 m level and from these an average of the 8 days calculated. The result is shown in fig. 3.14 where the product in $\mu g \times m^{-2} \times sec^{-1}$ is seen as a function of altitude.

The days chosen include the out of the trade wind season Kona-storm which, however, did not effect the average wind direction severely but had a considerable effect on the vertical stability. For this reason the salt transport at higher levels is probably somewhat larger than under average conditions.

There is a well marked maximum in the salt transport, namely at 800 m elevation. At that level the advection of sea salts is nearly five times larger than at sea level. The integrated transport amounts to 62 $mg \times m^{-1} \times sec^{-1}$. Thus, across each meter of the coast, perpendicular to the wind direction (60°) passes 62 mg sea salts per second as an average. This is $\sim$ 5.4 $kg \times m^{-1} \times day$ or 5.4 tons $\times km^{-1} \times day^{-1}$.

One cannot, of course, expect the advection from the ocean to the continents to follow exactly this distribution but on the coast something similar will show up. The winds generally increase with height to some level of the order of 1,000 m and, if the mass distribution with height also shows maximum at that level, the maximum transport of sea salt will occur at the same level and be magnified in relation to the mass distribution. If the mass distribution was uniform a larger transport would still take place at higher levels.

How the advection looks like over land is entirely dependent on the stability of the air. In summer with vigorous convection due to heating greater vertical wind shears will not occur but in winter stratification of air over continents is quite common which will facilitate different advection rates of sea salts at different levels.

As pointed out earlier in connection with the observations by CROZIER & SEELY (l.c.) over the western U.S. advection of sea salt at higher levels is important because mountain barriers will not cause a rainout of the salt.

To be continued in Tellus 12: 1.

The Dependence of Artificial Radioactivity in Rain on Rainfall Rate

By J. F. BLEICHRODT, JOH. BLOK, R. H. DEKKER and C. J. H. LOCK

Medical Biological Laboratory of the National Defence Research Council T. N. O., Rijswijk, Netherlands

(Manuscript received February 18, 1959)

Abstract

The artificial radioactivity in rain was measured as a function of rainfall rate. As a rule an inverse relationship was found between the specific activity and the rate of rainfall. A tentative explanation is given.

Introduction

Radioactive material released by nuclear explosions is returned to earth in several ways. If the particles are relatively large, gravity fall will be an important factor. On small particles, however, the influence of gravity will be negligible. The deposition of these particles is mainly accomplished by rain.

When no radioactive dust from recent atom bomb explosions is present in the troposphere the rain will contain only small particles of about 5 μ diameter and smaller, because bigger particles will have been deposited by gravity already. Little is known about the mechanism by which these particles are collected by rain or cloud drops.

Falling raindrops will collect radioactive dust particles by impaction. CHAMBERLAIN (1953) and GREENFIELD (1957) made some calculations on this "scrubbing" effect of raindrops. However, these calculations are based on assumptions which are difficult to justify. First the so-called "collision-efficiencies" are used as computed by LANGMUIR (1948) who incorrectly treated the particles as points. MASON (1957) published more exact values which differ appreciably from those given by Langmuir. Both Langmuir's and Mason's data refer to particles of a specific gravity of 1 g cm^{-3}.

Secondly Chamberlain and Greenfield assumed that each collision between a drop and a dust particle results in coalescence. If, however, the particle is not wetted easily it will only enter the drop when it penetrates deeply enough to be enclosed by the drop. Moreover, a nonwettable particle may not be retained for long because it will possibly be expelled as soon as it reaches the drop surface.

Finally Chamberlain and Greenfield use the size distributions of raindrops mentioned by BEST (1950). These distributions, however, apply only to raindrops at ground level. The raindrop spectrum will undoubtedly change with the altitude as the evaporation rate varies with the size of the drop and drops of different size will coalesce. Information on this subject is scarce.

Besides radioactivity collected by impaction, the rain will contain radioactivity picked up in the cloud. Radioactive particles may act as nuclei of condensation and, moreover, the

cloud droplets will collect atomic debris by diffusion. GREENFIELD (1957) also made some calculations on this pickup in the cloud.

It will be clear that the scavenging action of rain is a very complex mechanism, which will require extensive experimentation to be fully understood. Greenfield arrives at the conclusion that the fraction of airborne radioactivity scavenged by impaction is proportional to the product of rainfall rate and time. The present paper describes an investigation of the dependence of the radioactivity in rain on rainfall rate.

Experimental

Rain was collected in a galvanized tray of 5 m^2 which was placed with a slight slope on the flat roof of the laboratory. To the lowest part of the tray an outlet-pipe was attached through which the rainwater could be collected in a vessel.

Shortly before the collection of rainwater started, the tray was thoroughly cleaned with tap water in order to remove fall-out material. This method of cleaning proved to be sufficient.

A measuring cylinder was then placed under the outlet-pipe. As soon as the measuring cylinder contained about half a liter of rainwater the remaining water film in the tray was swept down as fast as possible by means of a screen wiper. The total volume collected in this way, usually amounting to about one liter, and the time in which it was obtained were noted. From these data the average rainfall rate (mm h^{-1}) was calculated. The measuring cylinder used was immediately replaced by another.

The bulk of the beta-activity in the rainwater fraction was isolated by adding about 4 g of active coal (Norit C, Norit Verkoopmaatschappij, Amsterdam) per liter, stirring it from 15 to 30 minutes and filtering off the coal. In this way less than 25 % of the beta-activity remained in the water. The filtrate was then evaporated and the residue together with the coal containing filter was ashed at 500° C. This procedure was followed to minimize loss of radioactivity.

At least three days after sampling, to allow the natural radioactivity to decay, a weighed sample of ash was put in a brass tray under an end-window Geiger-Müller tube (Philips 18506) and counted for betaactivity (standard error < 3 %).

The beta-activity per liter of rainwater could then be computed from the measured activity, the sample weight, the total ash weight and the volume of rainwater collected.

Results and conclusions

The results of the experiments lead to the conclusion that the specific activity is dependent on the rate of rainfall, in such a way that the specific activity increases when the rain intensity decreases and conversely. In Figure 1 is plotted a representative part of eleven showers which were analysed.

By means of the measured decay rates of the radioactivity in the rainwater and the approximate relation (HUNTER and BALLOU, 1951; HOLTER and GLASSCOCK, 1952)

$$A = A_1 t^{-1.2}$$

where A is the activity at time t and A_1 is the activity at unit time after fission, it was possible to demonstrate that the fission products in the collected rain were "older" than two months (once a value of 51 days was found). As mentioned earlier this implies that the presence of large particles is very improbable. Further BLOK (1957) could show by experiments using a cascade impactor that radioactive dust of such "age" contains largely particles smaller than 1.5 μ in diameter.

On the other hand it is shown by extrapolating Mason's "collision efficiencies" (MASON, 1957) that such small particles will be washed out only in minute amounts. Therefore, it is not likely that the dependence of the specific activity on rainfall rate is due to impaction effects. Moreover, experiments made in this laboratory on the hourly fluctuations in airborne activity have never shown a decrease in activity during showers. In interpreting this finding it should be kept in mind, however, that air streams continually bring fresh radioactivity into the rain zone.

If the impact mechanism plays a minor rôle there are two other processes by which the observed phenomenon may be explained. First the evaporation of raindrops will effect an increase in specific activity which is larger when the rainfall rate is lower. Observations on drop size spectra show the mean drop diameter to increase with rainfall rate (BEST,

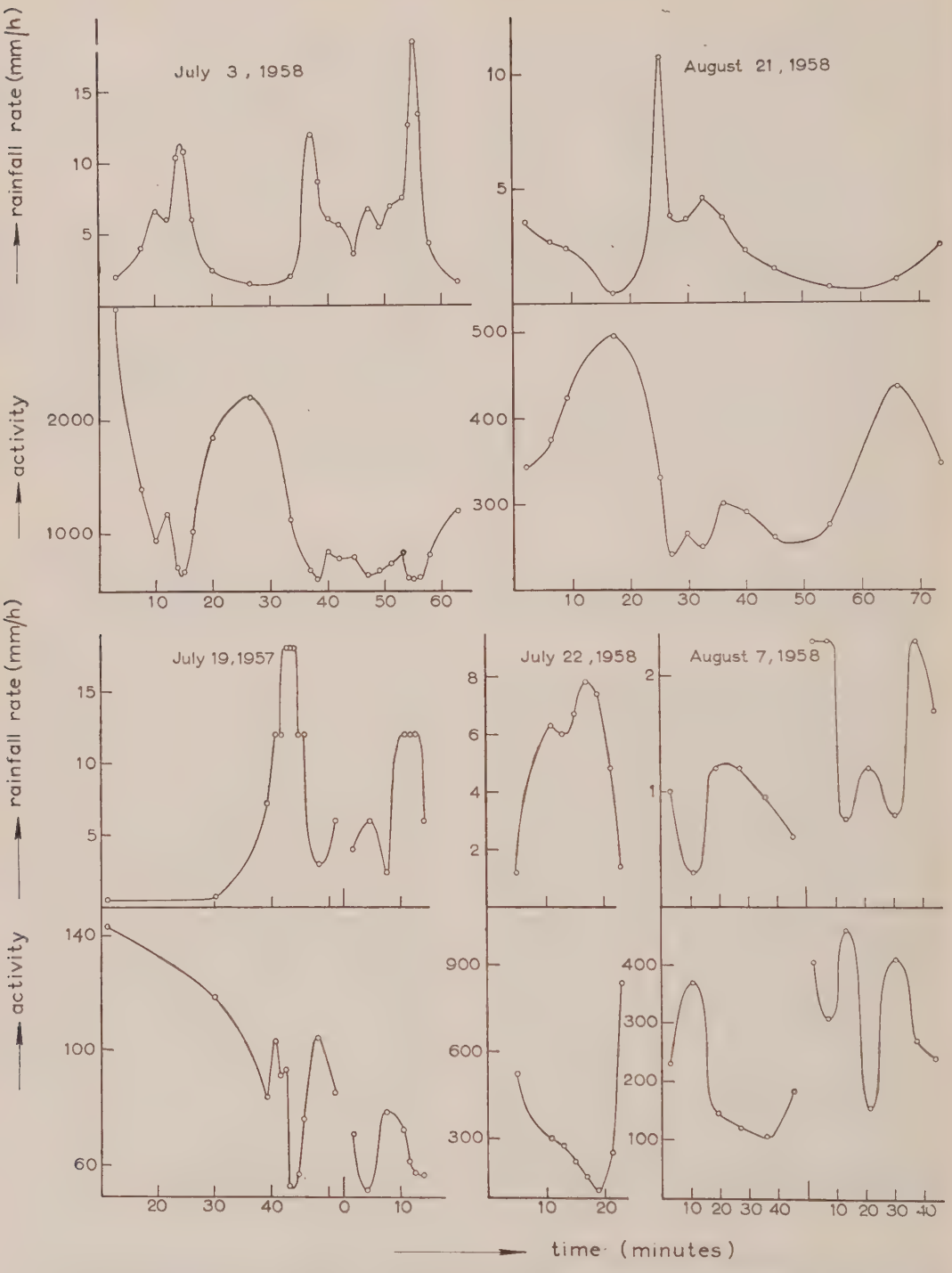

Fig. 1. Fluctuations in rainfall rate and the corresponding fluctuations in specific activity. The upper parts of the graphs show the fluctuations in rainfall rate versus time, the lower parts the specific activity (arbitrary units) versus time. The first point of a curve usually does not coincide with the beginning of the shower.

1950; MARSHALL and PALMER, 1948; MASON and RAMANADHAM, 1953). Large falling drops evaporate relatively slower than small ones (KINZER and GUNN, 1951) so that at low rainfall rates a larger percentage of rainwater will evaporate giving a higher specific activity at ground level.

Secondly the observed fluctuations may be the result of the pickup mechanism in the cloud. The physics of rain formation is not yet sufficiently understood. Therefore it is impossible at the present time to predict the dependence of the specific radioactivity of the rain on rain intensity just below the cloud base.

Recently COWAN and STEIMERS (1958) reported measurements of the fluctuations of radioactivity in rainwater. By collecting hourly samples and evaluating gross activity they could discern two types of behaviour:

1. The gross activity is usually proportional to the volume of rainwater in the sample.

2. The concentration of activity tends to vary inversely with the volume of rainwater so that high concentrations are observed during periods of low rainfall rate and low concentrations when heavy rainfall occurs.

In the light of the results reported in this article this is understandable. By taking hourly samples the fluctuations in specific radioactivity will, for the greater part, be masked. This explains the first type of behaviour. A variation of activity with rainfall rate as reported by these authors will be found only when the rainfall rate differs slightly from the mean during an hour of sampling and the mean rainfall rate varies sufficiently from hour to hour.

Acknowledgement

The authors are indebted to Prof. Dr. W. Bleeker and Dr. F. H. Schmidt of the Royal Netherlands Meteorological Institute for valuable discussions.

REFERENCES

BEST, A. C., 1950: The size distribution of raindrops, *Quart. J. R. Meteor. Soc.*, **76**, p. 16.

BLOK, JOH., 1957: *Radioactieve besmetting van de biosfeer in Nederland*, Thesis Vrije Universiteit, Amsterdam, H. A. van Bottenburg N. V.

CHAMBERLAIN, A. C., 1953: Aspects of travel and deposition of aerosol and vapour clouds, *A.E.R.E. HP/R 1261*, Harwell.

COWAN, F. P., and STEIMERS, J., 1958: The distribution of fallout activity in rainfall at Brookhaven National Laboratory, June to September 1957, *BNL 496(T-117)* Upton, N.Y.

GREENFIELD, S. M., 1957: Rain scavenging of radioactive particulate matter from the atmosphere, *J. Meteor*, **14**, p. 115.

HOLTER, N. J., and GLASSCOCK, W. R., 1952: Tracing nuclear explosions, *Nucleonics*, **10**, No. 8., p. 10.

HUNTER, H. F., and BALLOU, N. E., 1951: Fission product decay rates, *Nucleonics*, **9**, No. 5, p. C-2.

KINZER, G. D., and GUNN, R., 1951: The evaporation, temperature and thermal relaxation-time of freely falling waterdrops, *J. Meteor.*, **8**, p. 71.

LANGMUIR, I., 1948: The production of rain by a chain reaction in cumulus clouds at temperatures above freezing, *J. Meteor.*, **5**, p. 175.

MARSHALL, J. S., and PALMER, W. M., 1948: The distribution of raindrops with size., *J. Meteor.* **5**, p. 165.

MASON, B. J., 1957: *The physics of clouds*, Oxford, Clarendon Press, p. 424.

MASON, B. J., and RAMANADHAM, R., 1953: A photoelectric raindrop spectrometer, *Quart. J. R. Meteor. Soc.*, **79**, p. 490.

The Influence of Cloud Nucleus Population on the Microstructure and Stability of Convective Clouds

By S. TWOMEY and P. SQUIRES

C. S. I. RO., Division of Radiophysics, Sydney

(Manuscript received April 6, 1959)

Abstract

Measurements of the concentration of cloud droplets and of the supersaturation spectrum of the cloud nucleus population in the air below cloud base showed a strong correlation between these properties. It is concluded that variations in the cloud nucleus content of the air are primarily responsible for variations of cloud droplet concentrations and colloidal stability.

1. Introduction

Rain from clouds which do not reach the freezing level, usually called warm rain, is generally agreed to form by coalescence of cloud droplets. It is commonly observed that warm clouds differ widely in efficiency as rain producers; in maritime air, cumuli usually rain soon after reaching a depth of some 6,000 ft, whereas well inland clouds often reach much greater depths without raining. It has been suggested that this difference in behaviour is due to the fact that the droplets in a cloud should be relatively large for the coalescense process to proceed efficiently and that the supersaturation spectrum of those condensation nuclei which grow into cloud droplets ("cloud nuclei") was the chief factor determining the size of the droplets formed in cloud condensation (SQUIRES 1952). In the absence of a method of measuring the spectrum of these cloud nuclei, indirect support for this hypothesis was gained from measurements of droplet spectra in cumuli. It has been shown that the droplet concentration is systematically less in maritime than in continental cumuli (SQUIRES 1956; BATTAN and REITAN 1957), and that the average and maximum drop sizes found in maritime cumuli, are considerably greater than those found in continental cumuli (SQUIRES 1958a). Evidence has been presented to show that these differences cannot be explained by a difference in typical updraught velocity or average lifetime of cloud parcels (SQUIRES 1958b), or in the concentration of giant sea salt nuclei (SQUIRES and TWOMEY 1958).

Techniques capable of measuring the spectrum of cloud nuclei have recently been described by WIELAND (1956) and TWOMEY (1959a). Twomey (loc. cit.) has shown that the cloud nucleus spectra in maritime and continental air, sampled at ground level, were systematically different, the latter being much richer in these nuclei. Typical nucleus spectra and representative updraught speeds were used (TWOMEY 1959b) to compute the number of nuclei which would become activated and grow into cloud droplets in both maritime and continental cumuli; the results are summarized below and compared with the average concentrations observed by SQUIRES (1958a).

The discrepancy between the observed droplet concentrations and the values computed from the nucleus spectra is not very serious: at ground level, the air may have been richer in nuclei than at cloud base level; the observations of nucleus spectra and of cloud droplet concentrations were made quite independently

Table 1. Comparison between average droplet concentrations observed in maritime and continental cumuli and those computed from mean cloud nucleus spectra, for various assumed updraught velocities.

Updraught velocity assumed in computing droplet concentration (m sec^{-1})		Air Mass	
		Maritime	Continental
Computed	0.1	36	290
	1	60	520
	10	100	930
Observed	—	45	228

and not even at the same place or time; finally it is possible that processes may operate within clouds to eliminate some droplets after they have been formed. The results of Table I appear to leave little doubt that the contrast between cloud nucleus spectra in maritime and continental air is the major factor causing the contrast in cloud droplet concentrations. According to the argument presented above, differences in cloud nucleus spectra are ultimately responsible for differences in mean and maximum droplet sizes and in colloidal stability.

Measurements of cloud droplets and cloud nucleus spectra have now been carried out simultaneously, the air sample for spectrum determination being taken in the free air below cloud base.

2. Sampling

A series of flights were made near Parkes, New South Wales, during the spring of 1958. This area, some 300 km inland from Sydney, lies near the northern edge of the westerlies at that time of the year. The wind direction varies from north to north-west ahead of the cold fronts to south to south-west behind them. The prefrontal northerly air typically has had a land trajectory of some 2,000 km, having crossed the coast of Queensland as a south-east to east (trade) wind several days previously and gradually turned southward after penetrating up to 1,000 km inland. The air behind the fronts comes from the Southern Ocean, crossing the intervening 600—800 km in about a day. Thus the air masses sampled at Parkes ranged from fairly continental to slightly modified maritime. Two flights were made from Sydney later in the year, one in continental air from the west, and one in a maritime stream from the south-east.

The techniques for measuring cloud droplets and cloud nuclei both have been described elsewhere (Squires and Gillespie 1952; Squires 1958a; Twomey 1959a). During each flight droplet samples were taken in one or more non-raining cumuli, usually at several levels, with the aim of deriving an average value for the droplet concentration. Samples of air from below the cloud base were taken in plastic (P.V.C.) bags with a volume of about $^1/_4$ cubic metre; the nucleus content of the air samples was measured on the ground immediately after each flight.

In the DC-3 aircraft used, it was not feasible to circle within the updraught feeding a cumulus, so that there was no assurance that any air sample was representative of the air in which the cloud formed; it is well known that the updraught may differ considerably from the surrounding air in humidity mixing ratio, and hence the cloud nucleus content may also have been different. The following procedure was therefore adopted; during the climb to cloud levels, temperature and humidity measurements were made, plotted on an aerological diagram and the adiabatic condensation levels computed. Usually the air near ground level was found to have an adiabatic condensation level below the observed height of cloud base, while air near cloud base level had a condensation level above cloud base. At some intermediate height the computed condensation level coincided with the observed cloud base; the air sample was taken at this height, on the grounds that the mean properties of this air were most likely to correspond with those of the updraught when it reached cloud base.

3. Determination of Cloud Nucleus Spectra

The production of continuous small supersaturations by diffusion between surfaces of pure water and dilute aqueous HCl, and the measurement by a photographic technique of the droplet concentration in the cloud produced when an air sample is admitted to a water-HCl diffusion chamber, has been discussed in detail elsewhere (Twomey 1959a). During the observations under discussion, cloud nucleus measurements were made by passing a portion of an air sample into each of a set of five diffusion

chambers containing HCl solutions selected to give a range of supersaturation from 0.08 % to 8 %. Each chamber was thoroughly flushed with filtered nucleus-free air before accepting the sample air; the procedure used was known to permit no pollution of the diffusion chambers by room air. Following the introduction of sample air, clouds formed in the diffusion chamber and several photographs were taken of each cloud. From the photographs, the number of droplets formed per unit volume in each chamber was determined and plotted as a function of supersaturation. A curve was then drawn through the representative points; this curve was taken as the nucleus spectrum. A small correction (usually of order +10 %) was made to allow for the decrease in number of nuclei during the period for which they had been stored. This correction was only a minor one and the final results would be little changed by its omission.

4. Computation of Cloud Droplet Concentration from Cloud Nucleus Spectra

Given the nucleus spectrum, it would be possible to predict directly the concentration of cloud droplets, if the maximum supersaturation attained in the cloud was known. Since it is not possible to measure the supersaturation, it is necessary to compute its maximum value.

This value is influenced not only by the rate of cooling of the air but also by the number and nature (critical supersaturations) of the nuclei present. It has been shown (TWOMEY 1959b) that the expression

$$S_m{}^{k+2} = \frac{1.6 \times 10^{-3}\, V^{3/2}}{c k\, B^{3/2},\, k/_2} \qquad (1)$$

gives, with fair accuracy, the maximum supersaturation S_m(°C) attained when air at 800 mb, 10° C, containing nuclei distributed logarithmically so that there are cS^k nuclei per cm³ active at supersaturations up to and including S, ascends at V cm sec⁻¹. The computed cloud droplet concentration is then found from the nucleus spectrum; it is simply the number of nuclei active at supersaturation S_m.

When the observed nucleus spectra were approximately linear when plotted on a logarithmic scale, the straight line log N= log c+k log S furnishing the best approximation was drawn, and the corresponding values of c and k were inserted in equation (1) to obtain the maximum supersaturation; the computed number of cloud droplets was then obtained by reference to the nucleus spectrum.

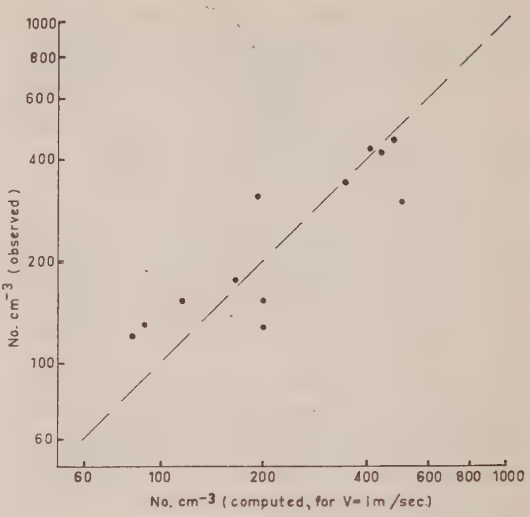

Fig. 1. Measured cloud droplet concentrations (cm⁻³) plotted against those computed from the observed cloud nucleus spectra, assuming a value of 1 m sec⁻¹ for the updraught velocity in the critical region near cloud base where the supersaturation passes through its maximum value. The dashed line represents exact agreement between observed and computed values.

Some of the samples gave spectra which deviated considerably from the logarithmic; S-shaped curves (designated type B curves in an earlier paper) were found on several occasions. In such cases, the number of nuclei may increase by a factor of ten over a relatively small range of supersaturation, and the computation of cloud droplet concentration may not be reliable, since small errors in the maximum supersaturation could entail large errors in computed cloud droplet concentration. Observations from which spectra of this kind resulted (three out of a total of fifteen) were not included in the final analysis.

5. Comparison between Observed and Computed Droplet Concentration

In Figure 1 the mean of observed cloud droplet concentrations are plotted against the droplet concentration computed from the nucleus spectrum (assuming an updraught of 1 m/sec). It is apparent that the agreement between the observed and computed values is excellent. This supports the contention that the systematic differences observed with respect

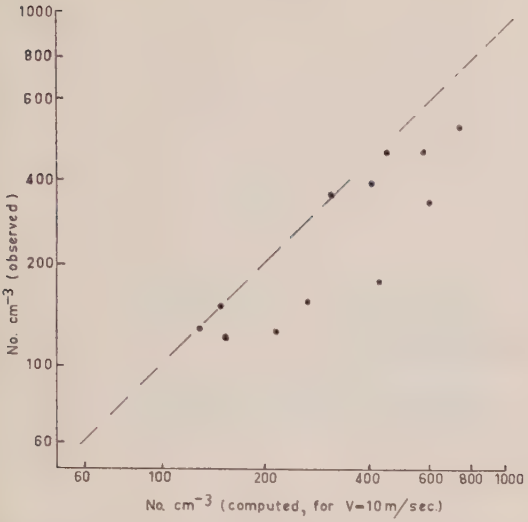

Fig. 2. Measured versus computed droplet concentrations for an assumed updraught velocity of 10 m/sec. The dashed line represents exact agreement between observed and computed values.

to cloud droplet concentration and spectra are primarily caused by variations in cloud nucleus population.

The use of a value other than 1 m/sec for the updraught velocity would give a set of different values for S_m and hence for the computed droplet concentration. However, the computed droplet concentration, being proportional to $V^{3k/2k+4}$ (where k was usually about $^1/_5$ and never exceeded $^4/_5$), was not strongly influenced by updraught velocity. Thus the good agreement shown in Figure 1 was not critically dependent on the choice of 1 m/sec for the updraught velocity. When the data was computed for an updraught of 10 m/sec, all but one of the computed droplet concentrations were now greater than the corresponding observed values, and the correlation between the observed and computed values was not as good (Fig. 2).

6. Conclusions

The degree of agreement shown in Figure 1 between the observed cloud droplet concentrations and those predicted from the measured cloud nucleus spectra seem satisfactory in view of the uncertainties involved. There is no assurance that the nucleus populations of the free air samples were strictly representative of those in the updraught in which the cloud formed. If the samples had been taken within the updraught at cloud base level, and if the updraught velocity could have been measured in each case, it seems probable that the agreement between observed and computed values would have been even better.

It may be concluded that the observed variations of droplet concentration in cumuli can be explained by variations in the cloud nucleus population. Continental clouds exhibit large droplet concentrations because continents are major sources of cloud nuclei. As a result of the greater numbers, the droplets are smaller than in maritime clouds, and it seems likely that this, in turn, explains why continental clouds are much less efficient in producing warm rain.

7. Acknowledgements.

The measurements described in this paper were made from aircraft provided and flown by the Aircraft Research & Development Unit of the Royal Australian Air Force.

REFERENCES

Battan, L. J., and Reitan, C. H., 1957: Droplet size measurements in convective clouds. *Artificial Stimulation of Rain*, Pergamon Press, pp. 184—191.

Squires, P., 1952: The growth of cloud drops by condensation, Part II: the formation of large cloud drops. *Aust. J. Sci. Res.* A **5** (3) pp. 473—499.

Squires, P., and Gillespie, C. A., 1952: A cloud droplet sampler for use on aircraft. *Q. J. R. M. S.* **78** (337) pp. 387—393.

Squires, P., 1956: The microstructure of cumuli in maritime and continental air. *Tellus* **8** pp. 443—444.

— 1958 a: The microstructure and colloidal stability of warm clouds, Part I: The relation between structure and stability. *Tellus* **10** pp. 256—261.

— 1958 b: The microstructure and colloidal stability of warm clouds, Part II: The causes of the variations in microstructure. *Tellus* **10**, pp. 262—271.

Squires, P., and Twomey, S., 1958: Some observations relating to the stability of warm cumuli. *Tellus* **10**, pp. 272—274.

Twomey, S., 1959 a: The nuclei of natural cloud formation, Part I: The chemical diffusion method and its application to atmospheric nuclei. *Geofisica pura e applicata*, **43**, pp. 227—242.

— 1959 b: The nuclei of natural cloud formation, Part II: The supersaturation in natural clouds and the variation of cloud droplet concentration. *Geofisica pura e applicata*, **43**, pp. 243—249.

Wieland, W., 1956: Die Wasserdampfkondensation an naturlichem Aerosol bei geringen Ubersattigungen. *E. T. H. Zurich, Promotionsarbeit Nr. 2577.*

Integration of Four-Level Prognostic Equations over the Hemisphere

By H. L. KUO and JACK NORDÖ, Massachusetts Institute of Technology

(Manuscript received September 11, 1958)

Abstract

The three-dimensional quasi-nondivergent prognostic equation derived previously by Kuo is integrated over the hemisphere, the vertical distribution being represented by four levels. The effects of the mean radiational heating, friction and heating from the ground, and that of the turbulent diffusion have been included in this investigation. The initial disturbance considered is a random combination of ten wave components in x and seven wave components in y. The result of the integration is that at the end of the fourth day at 850 mb, three closed lows have been formed, all around latitude 60°, while the pole is occupied by a high. These lows have the dimensions of the semi-permanent lows in winter.

1. Introduction

This investigation is an attempt to integrate the quasi-nondivergent equations developed by Kuo (1956, hereafter referred to as I) over the entire hemisphere by Green's method, so as to eliminate the errors introduced by placing arbitrary side boundaries. In this computation, the effects of the average radiational heating and cooling, the heat exchange between the atmosphere and its lower boundary (continent and ocean) and turbulent heat transfer, are all included.

The vertical distributions of the various quantities are represented by values at four levels, at 850 mb, 550 mb, 250 mb, and 50 mb. The 250 mb surface is taken as the mean level of the tropopause, so that the stratosphere is represented by one additional layer.

Because of the limitations of the electronic computer, it is impossible to include both hemispheres conveniently. Therefore we were compelled to take the vertical plane along the equator as a plane of symmetry and consider one hemisphere only. Furthermore, the nonlinear potential vorticity equation demands the stream function to be an odd function of y, which implies the vanishing of the north-south velocity along the equator. Thus any communication between the two hemispheres is excluded in the present computation. Such a condition would be a severe limitation for actual forecasting in low latitudes, and therefore only arbitrary artificial initial disturbances are considered in this investigation. Since a larger computer will be available in the near future, it will be possible to include both hemispheres in the computation and this limitation be removed.

2. Fundamental equations

As is well known, any horizontal velocity vector $\vec{v}$ can be separated into a nondivergent part $\vec{v}_1$ and an irrotational part $\vec{v}_2$ so that

$$\vec{v} = \vec{v}_1 + \vec{v}_2$$

$$\vec{v}_1 = \vec{k} \times \nabla \psi, \qquad \vec{v}_2 = \nabla X,$$

where ψ is the stream function for $\vec{v}_1$ and χ the potential function for $\vec{v}_2$, and $\vec{k}$ is the unit vector along the vertical. In I, Kuo discussed the class of motions in which $|\vec{v}_2|$ remains much less than $|\vec{v}_1|$ at all times, so that we have $|\vec{v}_1| \gg |\vec{v}_2|$ and $\left|\frac{\partial \vec{v}_1}{\partial t}\right| \gg \left|\frac{\partial \vec{v}_2}{\partial t}\right|$. This class of motions is called the "quasi-nondivergent" flow, and is considered to be representative of the large scale atmospheric motions. Since the vertical velocity is small and the horizontal dimension is large, the hydrostatic approximation holds at all times and the horizontal equation of motion may be written as

$$\left(\frac{\partial}{\partial t} + \omega \frac{\partial}{\partial p}\right)\vec{v}_1 + (f+\zeta)\,\vec{k} \times \vec{v} = -$$
$$- \nabla\left(\phi + \frac{1}{2} v_1^2\right) + \vec{F} \qquad (1)$$

where the (λ, φ, p) system is used, $\phi = gz$ is the geopotential and $\omega = \frac{dp}{dt}$. Thus the dynamic equations do not contain $\frac{\partial \vec{v}^2}{\partial t}$ and $\frac{dw}{dt}$; these quantities can only be obtained indirectly from the $\vec{v}_1$ field.

Since $\vec{v}_1$ is determined completely by the stream function ψ, it is convenient to apply the curl operator to (1) and obtain the equation for the vorticity $\zeta = \nabla^2\psi$, given by

$$\frac{\partial \zeta}{\partial t} + \tau(\psi, \zeta + f) - (f+\zeta)^2 \frac{\partial}{\partial p}\left(\frac{\omega}{\zeta + f}\right) +$$
$$+ \vec{k} \cdot \nabla\omega \times \frac{\partial \vec{v}_1}{\partial p} + \vec{v}_2 \cdot \nabla(\zeta + f)$$
$$- \vec{k} \cdot \nabla \times \vec{F} = 0 \qquad (2)$$

where $\tau(a, b) = \partial(a, b)/\partial(\lambda, \varphi)$.

In addition, we have the thermodynamic equation

$$\left\{\frac{\partial}{\partial t} + \left(\vec{v}_1 + \vec{v}_2\right) \cdot \nabla\right\}\left\{\frac{\partial \phi}{\partial p} - \frac{R\Gamma}{p}\omega\right\} = -\frac{R}{c_p}\frac{Q}{p} \qquad (3)$$

where $\Gamma = \frac{T}{\Theta}\frac{\partial \Theta}{\partial p}$, Θ being the potential temperature, and Q is the rate of the nonadiabatic addition of heat per unit mass. Thus (2) and (3) are the two fundamental equations. In these equations, the transport of heat and vorticity by $\vec{v}_2$ is of minor importance; therefore we may replace $\vec{v}_2$ by its first approximation.

Assuming that the motion $\vec{v}_1$ and the pressure distribution are always in a nearly balanced state, represented by the relation

$$(f+\zeta) \nabla \psi = \nabla\left(\phi + \frac{1}{2} v_1^2\right) \qquad (4)$$

we may then obtain the distribution of ψ or ϕ when one of the two is given, by integrating this equation. Furthermore, we may also obtain a rough approximation of $\vec{v}_2$ by substituting this relation in the equation of motion (1), to give

$$-\bar{f}\,\vec{v}_2 = \left(\frac{\partial}{\partial t} + \omega\frac{\partial}{\partial p} - \frac{\partial}{\partial x_j} A_j \frac{\partial}{\partial x_j}\right) \nabla \psi$$
$$\approx \left(\frac{\partial}{\partial t} - A_j \cdot \frac{\partial^2}{\partial x_j^2}\right) \nabla \psi \qquad (5)$$

where $\bar{f}$ is a mean value of f which will be defined below, and A_j is the eddy viscosity coefficient in the direction of x_j and the summation convention over the repeated index j is being used. In this approximation, the first term represents the isallobaric wind while the second term represents the frictional wind, respectively. We note that in this form, both terms are expressed in terms of ψ alone. These quantities can be simplified further. For example, in the first term, we may replace $\partial\psi/\partial t$ by the past tendency, and in the second term, replace the sum $A_j \frac{\partial^2 \nabla \psi}{\partial x_j^2}$ by $A \frac{\partial^2 \nabla \psi}{\partial^2 z}$, or even by $-k_1 \nabla \psi$. It seems that this simple way of including the effect of $\vec{v}_2$ is a reasonable procedure and does not require much extra computation. On the other hand, we could also solve the equation (I 15) for ω and then obtain χ from the continuity equation $\nabla^2\chi = -\frac{\partial \omega}{\partial p}$. The divergence velocity $\vec{v}_2 = \nabla\chi$ can

then be obtained. Since this procedure will increase the computation time enormously we shall not follow it in this computation.

We separate the temperature into two parts, a normal temperature T_0, taken as a function of p alone, and a departure T'. In this way, we may replace $\partial\phi/\partial p$ in equation (3) by $\frac{\partial\phi'}{\partial p} = -RT'/p$, which is assumed to be related to ψ by the integrated thermal wind relation

$$\frac{\partial\phi'}{\partial p} = \bar{f}\frac{\partial\psi}{\partial p} \tag{6}$$

where $\bar{f}$ is a certain mean value of f. By making use of the approximations (4), (5) and (6), the two equations (2) and (3) reduce to two equations in ψ and ω. Eliminating ω from these equations and neglecting some of the less important terms we then obtain

$$\left\{\frac{\partial^2}{dx^2}+\frac{\partial^2}{\partial y^2}-\frac{a^2 f\bar{f}\cos^2\varphi}{R}\frac{\partial}{\partial p}\frac{p}{\Gamma}\frac{\partial}{\partial p}\right\}\frac{\partial\psi}{\partial t} = \\ = -H_e(x, y, p) \tag{7}$$

where

$$H_e(x,y,p)\approx\tau_e(\psi,\zeta+f)-\frac{f}{R}\tau_e\left(\psi,\bar{f}\frac{\partial}{\partial p}\frac{p}{\Gamma}\frac{\partial\psi}{\partial p}\right)- \\ -\frac{fa^2\cos^2\varphi}{c_p}\frac{\partial}{\partial p}\left(\frac{Q}{\Gamma}\right)-a\cos\varphi\,\vec{k}\cdot\nabla\times\vec{F}-M_e \tag{8}$$

and $\tau_e(a, b)=\dfrac{\partial(a, b)}{\partial(x, y)}$ and $x=\lambda$, $y=\displaystyle\int_0^{\varphi}\frac{d\alpha}{\cos\alpha}$

are the horizontal coordinates in the Mercator projection. This projection is used in order to transform the Laplacian operator to the simple form so as to facilitate the finding of the Green's function, and also to facilitate the enumeration of the grid points in the coding. The subscript e in H and in the two Jacobians denotes that the horizontal differentiations are with respect to x and y. We note that the two Jacobians in H_e represent the effects of the transports of vorticity and heat by $\vec{v}_1$, and the last term M_e denotes the effect of transports by $\vec{v}_2$ and is given by

$$M_e\approx-\frac{2\bar{f}}{R\Gamma}\nabla_e\frac{\partial\psi}{\partial p}\cdot\nabla_e\frac{\partial}{\partial p}\left(\frac{\partial\psi}{\partial t}+k_1\psi\right) \tag{8a}$$

where k_1 is the coefficient of friction. For more details of the function H_e, see I.

The boundary conditions at earth's surface $p=p_0$, $\phi=\phi^*$ is

$$\frac{\partial^2\psi}{\partial t\partial p}+s\frac{\partial\psi}{\partial t}+\tau\left(\psi,\frac{\partial\psi}{\partial p}\right)-\frac{s}{\bar{f}}\tau(\psi,\phi^*)+ \\ +\frac{RQ}{c_p p_0 \bar{f}}=0 \tag{9a}$$

where $s=-\dfrac{1}{\Theta}\dfrac{\partial\Theta}{\partial p}$. For the top of the atmosphere $p=0$ we have $\omega=0$, we will also assume that the kinetic energy per unit volume vanishes there. A deduction hereof is

$$\lim_{p\to 0}\rho^{1/2}\frac{\partial\psi}{\partial t}=0 \tag{9b}$$

which provides us with the upper boundary condition, ρ being the density.

3. Green's Function for the Multi-layer System

In I the integration of the system (7) and (9a, b) by Green's method was discussed. To simplify the Green's function, a normal static stability is assumed and is given by

$$\Gamma_0\equiv\frac{\partial T_0}{\partial p}-\frac{R}{c_p}\frac{T_0}{p}=-\frac{Cp}{(p+\alpha p_0)^2} \tag{10}$$

The value of C is taken to be 110° C and the value of α is $\alpha=0.5$ for the troposphere and $\alpha=0$ for the stratosphere, which corresponds to a nearly constant Γ_0 in the troposphere and an isothermal stratification in the stratosphere. The latter assumption is necessary in order to satisfy the upper boundary condition $\omega=0$ at $p=0$ if we assume T, V and Q to remain finite at the top of the atmosphere, as can be seen from the thermal energy equation (3). A very small but yet finite α may also be used for the stratosphere, representing a nearly isothermal condition in the lower stratosphere and $T\to 0$ as $p\to 0$.

Writing $\dfrac{\partial\psi}{\partial t}$ as the sum of two functions, $\dfrac{\partial\psi_1}{\partial t}$ and $\dfrac{\partial\psi_2}{\partial t}$ we then have

$$\frac{\partial \psi_1}{\partial t} = (p + \alpha p_0)^{-1/2} \iiint K(P, Q)\, H_s(Q) \frac{dp'}{(p' + \alpha p_0)^{1/2}} dA'_s \qquad (11)$$

where $dA'_s = a^2 \cos\varphi d\varphi d\lambda = a^2 \cos^2\varphi\, dx dy$, $H_s(Q) = H_e/a^2 \cos^2\varphi$, and $K(P, Q)$ is the Kern function and is given by

$$K(P, Q) = \frac{1}{4\pi l}\left\{\frac{e^{-\frac{lr}{2}}}{r} + \frac{e^{-\frac{lr'}{2}}}{r'} + 2hIe^{-h(q+q')}\right\}, \qquad (12)$$

$$r, r' = \left\{(x - x')^2 + (y - y')^2 + \frac{1}{l^2}(q \mp q')^2\right\}^{1/2},$$

$$r'(\beta) = \left\{(x - x')^2 + (y - y')^2 + \frac{1}{l^2}(q + \beta')^2\right\}^{1/2}$$

$$q = \ln\left[\frac{1 + \alpha}{p/p_0 + \alpha}\right], \quad l = a\bar{f}\cos\varphi/\sqrt{RC}, \qquad (12a)$$

$$h = \frac{1}{2} + (1 + \alpha)p_0 \frac{\partial \ln \Theta}{\partial p},$$

$$I = \int_{q'}^{\infty} \mathrm{Exp}\left\{h(q + \beta) - \frac{lr'(\beta)}{2}\right\} \frac{d\beta}{r'(\beta)}.$$

Details of the K function are given in I. Since $K(P, Q)$ depends only upon the relative positions of the source point Q and the field point P under consideration, the integral in (11) may be evaluated in any coordinate system. However, both the derivation of K and the evaluation of ζ are greatly simplified by the use of the Mercator projection because of the simplification of the Laplacian operator ∇^2.

The second part of the solution $\frac{\partial \psi_2}{\partial t}$ which comes from the nonhomogeneous terms of the boundary condition (9a), is given by

$$\frac{\partial \psi_2}{\partial t} = (p/p_0 + \alpha)^{-\frac{1}{2}} \sum_{m=-\infty}^{\infty} \sum_{n=-\infty}^{\infty} \frac{A_{mn}}{h - \lambda_{mn}} \cdot e^{-\lambda_{mn} q}\, e^{i(mx + ny)} \qquad (13)$$

where

$$\lambda^2_{mn} = \frac{1}{4} + \frac{m^2 + n^2}{l^2}$$

$$A_{mn} = \frac{1}{4\pi^2} \iint B^\star(\xi, \eta) e^{-i(m\xi + n\eta)}\, d\xi d\eta$$

and

$$B^\star = (1 + \alpha)^{3/2}\left\{\tau_s\left(\psi, p\frac{\partial \psi}{\partial p}\right) - \frac{s_0 p_0}{\bar{f}}\tau_s(\psi, \phi^\star) + \frac{RQ}{c_p \bar{f}}\right\}_{p = p_0}$$

The subscript s in the Jacobians indicates that the differentiations refer to spherical coordinates. Thus $B^\star$ represents the effects of heat transfer and nonadiabatic heating at the ground level and the effect of topography.

To facilitate the computation, we shall also put $\frac{\partial \psi_2}{\partial t}$ into an integral form and try to combine it with $\frac{\partial \psi_1}{\partial t}$. Thus substituting A_{mn} into (13) we obtain

$$\frac{\partial \psi_2}{\partial t} =$$

$$= -\frac{1}{4\pi^2}(p/p_0 + \alpha)^{-\frac{1}{2}} \iint \sum_m \sum_n \frac{e^{-\lambda_{mn} q}}{\lambda_{mn} - h} \cdot B^\star(\xi, \eta) e^{im(x - \xi) + in(y - \eta)} d\xi d\eta = -$$

$$- \left(\frac{p}{p_0} + \alpha\right)^{-\frac{1}{2}} \iint K_2(x, y, q; \xi, \eta, 0) \cdot B^\star(\xi, \eta)\, d\xi\, d\eta \qquad (14)$$

where K_2 is another Green's function for the surface disturbance, and is given by

$$K_2 = \frac{1}{4\pi^2} \sum \sum \frac{1}{\lambda_{mn} - h} \mathrm{Exp}\left\{-\lambda_{mn} q + im(x - \xi) + in(y - \eta)\right\} \qquad (14a)$$

To evaluate K_2, let us put $m = k\cos\alpha$, $n = k\sin\alpha$, $-\pi < \alpha \leq \pi$; $x - \xi = \varrho\cos\Theta$, $y - \eta = \varrho\sin\Theta$; we then have $\lambda^2_{mn} = \frac{1}{4} + \frac{k^2}{l^2}$ and

$$K_2(\varrho, q; \varrho', 0) = \frac{1}{4\pi^2} \sum \sum \frac{e^{-\lambda_k q}}{\lambda_k - h} \cdot e^{ik\varrho\cos(\alpha - \Theta)} \qquad (14b)$$

The limits of k and α are now $o \leq k \leq \infty$ and $-\pi < \alpha \leq \pi$. Changing the sums into integrals we then obtain

$$K_2 = \frac{1}{4\pi^2}\int_0^{\infty}\int_{\alpha_0}^{\alpha_1} \frac{e^{-\lambda_k q}}{\lambda_k - h} e^{ik\varrho\cos(\alpha-\Theta)}\, k\,dk\,d\alpha \quad (14c)$$

Putting $w = \alpha - \Theta$, we have

$$I_1 = \int_{\alpha_0}^{\alpha_1} e^{ik\varrho\cos(\alpha-\Theta)}d\alpha = \int_{\omega_0}^{\omega_1} e^{ik\varrho\cos\omega}d\omega = 2\pi J_0(k\varrho)$$

where $J_0(k\varrho)$ is the normalized Bessel function of order zero. This integral is made to be independent of Θ by allowing the imaginary part of w to go to infinity. Thus the Green's function K_2 is given by

$$K_2 = \frac{1}{2\pi}\int_0^{\infty} \frac{e^{-\lambda_k q}}{\lambda_k - h} J_0(k\varrho)\, k\,dk \quad (15)$$

Note that both for large and for small values of k/l, we have

$$\lambda_k = \left(\frac{1}{4} + \frac{k^2}{l^2}\right)^{1/2} \approx \frac{k}{l} + \frac{1}{2} \approx \frac{k}{l} + h.$$

Therefore the integral above is given by

$$K_2 = \frac{e^{-q/2}}{2\pi} l \int_0^{\infty} e^{-kq/l} J_0(k\varrho)\,dk = \frac{l}{2\pi}\left(\frac{p/p_0 + \alpha}{1+\alpha}\right)^{1/2}\frac{1}{r_0} \quad (16)$$

where $r_0 = (\varrho^2 + q^2/l^2)^{1/2}$ is the effective distance from the source point Q_0 $(\xi, \eta, 0)$ on the earth's surface to the field point $P(x, y, q)$.

The complete solution $\frac{\partial\psi}{\partial t}$ is thus given by

$$\frac{\partial\psi}{\partial t} = \iiint G_1(P, Q) H_s(Q) d\zeta' dA_s' + \iint G_2(P, Q_0)\, E_0 dA_s' \quad (17)$$

where $dA_s' = a^2\cos^2\varphi d\xi d\eta$ is the spherical area element and

$$G_1 = K_1(P, Q)/\sqrt{(\zeta+\alpha)(\zeta'+\alpha)}$$

$$G_2 = \frac{1}{(1+\alpha)}\cdot\frac{1}{2\pi l r_0} \quad (18)$$

and

$$E_0 = -(1+\alpha)^{1/2}\frac{\bar{f}^2}{RC}B^{\star} = (1+\alpha)^2\left\{\tau_s\left(\psi, \frac{\bar{f}^2}{RC}\frac{\partial\psi}{\partial\zeta}\right) + \frac{\bar{f}Q}{c_p C}\right\}_{\zeta=1}$$

for a plane earth, and $\zeta = p/p_0$.

The Green's function G_2 for the surface effect is nearly equal to the value of $(G_1)_{\zeta'=1}$ for the near-by points, but decreases at a much slower rate with increasing distance, and becomes more than twice as large as $(G_1)_{\zeta'=1}$ at greater distances from the source point.

We note that the heating factor appears in the forcing function H_s in the differentiated form

$$H_2 = -\frac{\partial}{\partial\zeta}\frac{1}{p_0\Gamma}\left\{\tau_s\left(\psi, \frac{\bar{f}^2}{R}\zeta\frac{\partial\psi}{\partial\zeta}\right) + \frac{\bar{f}Q}{c_p}\right\},$$

and in undifferentiated form in the surface forcing function E_0. Putting $H_s = H_1 + H_2$, where H_1 denotes the other part of H_s given by (8), we may write the solution (17) in the following form

$$\frac{\partial\psi}{\partial t} = \iiint\left\{G_1 H_1 + \frac{\partial G_1}{\partial\zeta'}E\right\}d\zeta' dA_s' + \iint (G_2 - G_{1s})\, E_0 dA_s' \quad (17a)$$

where G_{1s} is the value of G_1 for $\zeta' = 1$ and

$$E = (\zeta+\alpha')^2\left\{\tau\left(\psi, \frac{\bar{f}^2}{RC}\frac{\partial\psi}{\partial\zeta'}\right) + \frac{\bar{f}}{c_p C}\frac{Q}{\zeta'}\right\} \quad (18a)$$

Here the heating effect appears in undifferentiated form in every integral. However, although equation (17a) gives a better physical insight into the heating effect, equation (17) is more convenient for computation since only one volume integral is involved.

In actual application, the atmosphere is divided into n layers of depth Δp. Similarly, the horizontal coordinates are replaced by the grid points $x=i\Delta x$, $y=j\Delta y$. The integrals in (17) are then replaced by summations of the products of the Green's function and the forcing function at the grid point, each result representing the mean value in the volume element $\Delta\zeta'\Delta\xi\Delta\eta$. For convenience sake, we shall put the thickness factor $\Delta\zeta'$ into the Green's function and obtain

$$\overline{G}_1(P, Q) = \frac{1}{(\zeta+\alpha)^{1/2}} \int_{\zeta_Q-\frac{1}{2}\Delta\zeta'}^{\zeta_Q+\frac{1}{2}\Delta\zeta'} \cdot \int_{\xi_Q-\frac{1}{2}\Delta\xi}^{\xi_Q+\frac{1}{2}\Delta\xi} \int_{\eta_Q-\frac{1}{2}s\eta}^{\eta_Q+\frac{1}{2}\Delta\eta} \frac{K_1(P, Q)}{(\zeta'+\alpha)^{1/2}} \frac{d\zeta' d\xi d\eta}{\Delta\xi\Delta\eta} \quad (19)$$

Average values of the function G_2 may be obtained in a similar manner. Replacing the integrations by summations the solution (17) may then be written in the form

$$\frac{\partial\psi}{\partial t} = \sum_i \sum_j \sum_k \overline{G}_1(P, Q_k)\left\{H_s(Q_k) + \frac{bE_0}{\Delta\zeta'_1}\right\} dA' \quad (20)$$

where $b=\overline{G}_2\Delta\zeta'/\overline{G}_1$, which is nearly equal to 1 for the near-by points and is larger than 1 for far away points. Since the surface effect is not very important, this ratio is replaced by 1 in the present preliminary study to avoid the use of two different Green's functions.

In the computation, the surface forcing function $E_0(Q_0)$ is calculated from an interpolation formula and the lower boundary condition. It is considered to be distributed in the lowest layer, and that $E_k=0$ for all the other layers. Thus the object of the computation is simply to find the sum of the function H_s and E_0 at each "source point" Q, then to multiply by the influence function $\overline{G}_1(P, Q)$ and to add the resulting products together for all source points Q to obtain the rate of change of the stream function $\partial\psi/\partial t$ at the field point P. The value of ψ at time $t+\Delta t$ is then obtained by extrapolation, using a centered time difference to avoid computational instability.

It may be remarked that the value of the influence function $G_1(P, Q)$ decreases rapidly with the distance between P and Q, so that the contribution from the far away points is relatively small. We may therefore use a larger area element for the far away regions and a mean value of the influence function for this larger area element. In this way the computation time can be reduced greatly. It may be remarked that in the numerical form (19) in which the integrations have been replaced by summations, the function $\overline{G}_1(P, Q)$ is finite at every point, including the field point P itself. This is because $\overline{G}_1$ now represents the average value of G_1 for the whole volume element $\Delta\xi\Delta\eta\Delta\zeta'$ centered at P.

4. The Side Boundary Conditions

In the above only the boundary conditions at earth's surface ($p=p_0$) and at the top ($p=0$) have been considered, and no side boundary has been assumed, and therefore the region of integration in (17) and (19) must include the whole atmosphere. Since in the actual atmosphere there is actually no side boundary, such an approach is really necessary in order to make forecasts for an extended time and area. Such a study has actually been attempted; the purpose was to take into consideration all the interactions between different parts of the atmosphere and to get away from the artificial restrictions implied by imposing side boundary conditions.

However, since we approximate the vertical structure of the atmosphere by dividing it into four layers, the inclusion of the entire atmosphere requires too many grid points and was difficult to handle in the computing machine available at the time. Therefore only one hemisphere will be included at the moment. This is physically possible if we consider the two hemispheres as being exactly similar, and taking the equator as a line of symmetry. Now the terms in the Jacobian $\tau(\psi, \nabla^2\psi)$ of eq. (2) always introduce odd y-functions because of the nonlinearity. We must therefore assume ψ to be an odd function of y if symmetry at the equator is supposed, implying that the north-south velocity is zero at the equator, so that there will be no communication between the two hemispheres. Since the rate of change of the vorticity ζ is then

equal to zero, $\partial\psi/\partial t$ will also vanish at the equator. We shall therefore require

$$\frac{\partial \psi}{\partial t} = 0 \text{ at } y = 0. \tag{21}$$

Since eq. (7) is an elliptic equation in $\partial\psi/\partial t$, this condition together with the conditions (9a) and (9b) at $p = p_0$ and $p = 0$ are sufficient for the determination of $\partial\psi/\partial t$ for the hemisphere.

The condition (21) is satisfied if we assume that for every disturbance H_s at the point $Q(x, y, p)$ there is a disturbance equal to $-H_s$ at the point $Q'(x, -y, p)$ which is the image of Q with respect to the equator. Denoting the Green's function for the points P and Q' by $\overline{G}_1'$, which is obtained from $\overline{G}_1$, by replacing $y-\eta$ by $y+\eta$ in the distance $r = \{(x-\xi)^2 + (y-\eta)^2 + (q-q')^2/l^2\}^{1/2}$ and putting $\overline{F} = \overline{G}_1 - \overline{G}_1'$, the solution that satisfies the boundary conditions (9a, b) and (21) is then given by

$$\frac{\partial \psi}{\partial t} = \sum\sum\sum \overline{F}(P, Q) \left\{ H_s(Q_k) + \frac{E_0(Q_0)}{\Delta\zeta'} \right\} dA_s' \tag{22}$$

We note that in formula (22), both the quantities H_s and E_0 and the area element dA_s' refer to the spherical earth, and therefore it is possible to evaluate the integration in spherical coordinates.

It may be remarked that even though we have assumed that ψ does not change at the equator, the mean zonal velocity at the equator may still change with time, because of the turbulent friction and vertical motion, according to the equation:

$$\frac{\partial \bar{u}}{\partial t} = -\bar{\omega}\frac{\partial \bar{u}}{\partial p} - \left(\overline{\omega' \frac{\partial u'}{\partial p}}\right) + A_p \frac{\partial^2 u}{\partial p^2} + A_v \frac{\partial^2 \bar{u}}{\partial y^2} \tag{23}$$

However, such changes must be exceedingly small because of the lack of disturbances in lower latitudes as a consequence of the side boundary condition (21).

5. Effect of friction

Frictional effects appear directly in the non-homogeneous term H_e of (8) in the form of $\vec{k} \cdot \nabla \times \vec{F}$, and indirectly in the form of the frictionally driven cross isobar and isallobaric flows in the transport terms. We shall analyze the former first.

Since the atmospheric motion is always turbulent, the frictional effect in the dynamic equation may be written as

$$\vec{F} = A_v \nabla^2 \vec{v}_1 + \frac{1}{\varrho}\frac{\partial \vec{\tau}_z}{\partial z} \tag{24}$$

where A_v is the horizontal turbulent viscosity and $\vec{\tau}_z$ is the turbulent stress in the vertical planes, due to disturbances smaller than those under consideration. Since $\vec{\tau}_z = -g\varrho\mu\frac{\partial \vec{v}_1}{\partial p}$, we have

$$\frac{1}{\varrho}\frac{\partial \vec{\tau}_z}{\partial z} = -g\frac{\partial \vec{\tau}_z}{\partial p} = g^2 \frac{\partial}{\partial p}\left(\mu\varrho \frac{\partial \vec{v}_1}{\partial p}\right)$$

Setting $\mu = K\varrho$, $K = K_0\left(\frac{T}{T_0}\right)^2$, and applying the operator $\vec{k} \cdot \nabla \times$ we obtain

$$\frac{1}{\varrho}\frac{\partial}{\partial z}\vec{k} \cdot \nabla \times \vec{\tau}_z = K_v \frac{\partial}{\partial p}\left(p^2 \frac{\partial \zeta}{\partial p}\right) \tag{25}$$

where ζ is the relative vorticity, and

where $K_v = \frac{g^2 K_0}{R^2 T_0^2} \approx 1.6 \times 10^{-7}\,\text{sec}^{-1}$ if we choose $K_0 = 10^5$ cm^2 sec^{-1}. This corresponds to $\mu = 100$ gm cm^{-1} sec^{-1}. The value of A_v is taken to be 10^5 m^2 sec^{-1}, after PHILLIPS (1956).

In addition, there exists the ground friction. For simplicity this frictional effect is assumed to be proportional to the wind speed at the ground level, instead of proportional to the kinetic energy. Thus we shall assume the surface stress is given by

$$\vec{\tau}_0 = \varkappa\varrho\,|\vec{v}_0|\,\vec{v}_0 \approx k_g\varrho\,\vec{v}_0 \tag{26}$$

and take $k_g = 3.0$ cm sec^{-1}. In the numerical integration the lowest level is taken at $p = p_0 - \frac{1}{2}\Delta p$. Assuming that this frictional effect is

uniformly distributed in this lowest layer, we obtain the coefficient of ground friction $k_0 = k_g/\Delta z$. For $\Delta p = 300$ mb, this gives $k_0 = 1.0 \times 10^{-5}$ sec^{-1}.

It may be remarked that if these frictional terms are evaluated at the centered time $t = n\Delta t$, they will produce computational instability; therefore we shall evaluate them at the previous time step $t = (n-1)\,\Delta t$ (personal communication from Dr. N. A. Phillips).

6. Nonadiabatic Heating

The nonadiabatic rate of heating Q occurs in the nonhomogeneous term H_s in the form $\frac{\partial}{\partial p}\left(\frac{Q}{\Gamma}\right)$, and in the boundary effect E_0 in the form of Q. The important physical processes determining Q are radiation, evaporation and condensation and conductive heat transfer, including that due to turbulent heat transfer produced by the disturbances which are smaller in scale than those under consideration. The heat transfer produced by ordinary thermal convection will also be included in this turbulence effect.

The atmosphere receives only a fraction of its heat supply through direct absorption of the solar radiation; the rest is received from the earth through long wave radiation and through evaporation and condensation. Since the atmosphere emits and absorbs the long wave radiation mainly through its water vapor content, and since the presence of clouds has a very large effect on the distribution of the radiative heat transfer, both the long wave radiation and the release of latent heat depend very much on the water vapor distribution and on vertical motion. Thus in order to take into consideration these processes it is necessary to add new dependent variables and new equations to our system. Such a system will become extremely complex. Since we are still at the very preliminary stage of the investigation, we shall include only the statistical effects of the radiational and evaporation-condensation processes so as to furnish the system with a thermal energy supply which is roughly comparable with that in the atmosphere.

Taking the total depth of the atmosphere as a whole, the air is gaining heat in lower latitudes and losing heat in higher latitudes through the processes of radiation and evaporation-condensation. This total gain or loss is measured by the difference between the effective incoming solar radiation E and the outgoing long wave radiation A. When the quantity $E - A$ is integrated over the area from the equator to the latitude φ we obtain the accumulation of heat T through radiation in this area. This also represents the amount of heat that must be transported across the corresponding latitude circles in order to maintain a steady mean temperature distribution.

Fig. 1 summarizes several computations of the required latitudinal energy transport T. The values represented by the circles are those of HOUGHTON (1954) and the crosses are those of ALBRECHT (1931). Values obtained by others all lie between these two limits.

In eq. (22), what is needed is not the total heating $E - A$ for the whole air column but the vertical distribution. At present no such vertical distribution has been computed. Therefore we must make a plausible assumption. It is assumed that the zonally averaged rate of heating Q, produced by the combined effect of radiation and evaporation-condensation decreases upward, and is directly proportional to the pressure p. The latitudinal variation is also represented by a simple function of φ, and is given by

$$Q_1 = 2\,B\,{}^{p}/_{p_0}\,(\cos^2\varphi - {}^{2}/_{3}) \qquad (27)$$

This represents a heating from the equator to 35° 15′ and a cooling from 35° 15′ to the pole, while the total heating over the hemisphere is zero. The constant B is determined by the mean rate of heating at the equator. Supposing this is equal to 0.05 cal cm^{-2} min^{-1}, which corresponds to a heating of 0.3° C per day at the equator, we then obtain $B = 2.4 \times \times 10^{-6}$ cal gm^{-1} sec^{-1}.

Integrating (27) over the total pressure depth of the atmosphere and over the area from the equator to latitude φ we obtain the total gain of heat T per unit time. This is given by

$$T = \frac{\pi a^2}{3}\frac{p_0}{g} B \sin 2\varphi \cos\varphi \qquad (28)$$

where a is the radius of the earth. This function is represented in Fig. 1 by the curves T_a and

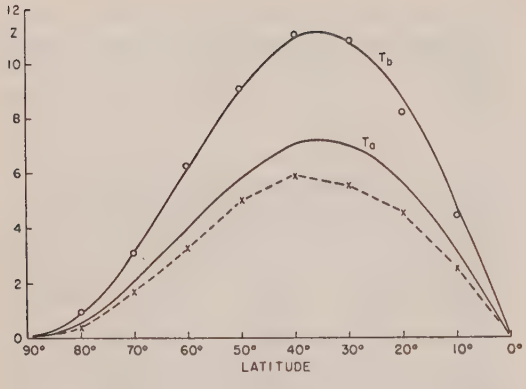

Fig. 1. Required poleward transport of heat across latitude circles to balance radiational excesses in the annual mean. Units are 10^{19} cal day^{-1}. Circles and crosses are values obtained by Houghton and Albrecht, respectively. Curves T_a and T_b are values computed from eq. (28).

T_b, corresponding to $B = 2.4 \times 10^{-6}$ cal gm^{-1} sec^{-1} and $B = 3.7 \times 10^{-6}$ cal gm^{-1} sec^{-1}, respectively. It is seen that the curve T_b fits the values of T obtained by Houghton very closely, while the curve T_a lies between Houghton's and Albrecht's values.

In the actual atmosphere, a large portion of the poleward transport of energy takes the form of latent heat. Since we are disregarding the water vapor content of the air, we may take a somewhat smaller value for the constant B so that less sensible heat need be transported poleward by the motion. The value of B used in the present computation is $B = 2.4 \times 10^{-6}$ cal gm^{-1} sec^{-1}, corresponding to the curve T_a in fig. 1.

The effect of lateral turbulent heat transfer on Q is given by

$$Q_2 = c_p A_T \nabla^2 T = -\frac{c_p}{R} \bar{f} A_T p \frac{\partial \zeta}{\partial p} \qquad (29)$$

Assuming A_T is given by

$$A_T = A_0 \frac{p^2 (1+\alpha)^2}{(p+\alpha p_0)^2}, \qquad (30)$$

we then have

$$\frac{\bar{f}}{c_p} \frac{\partial}{\partial p} \left(\frac{Q_2}{\Gamma} \right) = \frac{\bar{f}^2 A_0}{RC} (1+\alpha)^2 \frac{\partial}{\partial p} \left(p^2 \frac{\partial \zeta}{\partial p} \right) =$$

$$= K_T \frac{\partial}{\partial p} p^2 \frac{\partial \zeta}{\partial p} \qquad (31)$$

This is of the same form as the vertical turbulent diffusion of vorticity given by eq. (25), and therefore, we may combine them into a single term. Taking $A_0 = 10^5$ m^2 sec$^{-1} = A_v$, $C = 110°$ A, $\bar{f} = 10^{-4}$ sec^{-1}, $\alpha = 0.5$ we obtain $K_T = 0.7 \times 10^{-7}$ sec^{-1}. This is about one half of the value of K_v in (25). Thus if we are to include the effect of the lateral diffusion of heat, we should also include the vertical diffusion of vorticity.

Another effect of the smaller scale turbulence is the vertical transfer of heat. Since the potential temperature is more conserved than the actual temperature, this heat transfer is expected to be proportional to the vertical gradient of the potential temperature. Since the mean potential temperature increases upward, the heat diffusion equation expressed in terms of the potential temperature will give a downward heat transfer. However, if the small scale turbulence is thermally driven, the heat transfer should be directed upward. Because of this uncertainty about its direction, we shall disregard this effect at the moment.

Still another heating factor is the heat exchange between the air and the ground. This effect can be represented by

$$Q_3 = c_p k_{0T} (T_g - T_0) \qquad (32)$$

where T_g is the temperature of the ground and T_0 is the temperature of the air at ground level. This heating appears as a surface effect in the function E_0 in (22). The value of the coefficient k_{0T} may be assumed to be the same as the frictional coefficient k_0, which is taken as 10^{-5} sec^{-1}.

In considering the surface heating, we may assume T_g to be a known function of x and y at all times. On the other hand, the air temperature T_0 is unknown and is determined by the motion. Using the approximate relation (6), this effect is expressed in terms of the vertical gradient of ψ at the ground and Q_3 is given by

$$Q_3 = c_p k_{0T} \left(T_g + \frac{\bar{f}}{R} p_0 \left(\frac{\partial \psi}{\partial p} \right)_0 \right), \qquad (33)$$

In this study, the ground temperature T_g is assumed to be given by

$$T_g = 245° + 48° \cos^2 \varphi + 14° \sin \frac{3\varphi}{2} \sin 2\lambda \qquad (34)$$

in absolute degrees. The first two terms represent the zonal average and the third term the temperature departures due to two land and two ocean sectors, each 90° in extent.

7. The Grid Points

The size of the electronic computer and the available time determine the maximum number of grid points we can use to describe the motion of our atmosphere. The Computer used was the I.B.M. 704 at the General Electric Computation Laboratory, Lynn, Mass. It had an internal rapid-access memory of 8,192 36-binary digit words, together with 10 tape units and no drum. In order to make the time of computation for each time step of extrapolation not too long, and yet to have the vertical structure of the atmosphere described somewhat more accurately than by a two level model, we represented the atmosphere by four levels, namely 850, 550, 250, and 50 mb. Each of the first three levels represents the conditions in a layer of 300-mb thickness, while the 50 mb level represents the layer from zero to 100 mb. The reason for this division is that it was desired to have one level to represent the conditions in the more stable stratosphere, and another one for the tropopause level. These are assumed to be represented by the 50 mb level and the 250 mb level respectively, while the two levels at 850 and 550 mb represent the lower and middle tropospheric conditions.

Since one purpose of this study was to investigate the character of motion without introducing artificial boundaries, the spherical shape of the earth must be taken into consideration. We shall therefore use the conformal Mercator projection $x=\lambda$, $y=\int_0^{\varphi}\frac{d\alpha}{\cos\alpha}$. The advantage of this transformation is that it reduces the Laplacian operator to the simple form $(a\cos\varphi)^{-2}\left(\frac{\partial^2}{\partial x^2}+\frac{\partial^2}{\partial y^2}\right)$ and renders the finding of the Green's function more easy. However, it also has the disadvantage that by taking $\delta x\delta y$ constant the corresponding area on the earth becomes smaller and smaller as the latitude φ increases, and it requires too many grid points to represent the motion in higher latitudes. To avoid this difficulty we use one constant value for Δy in lower latitudes, from the equator to latitude 60°, and increase the values of Δx and Δy as φ increases. For the region between the equator and $\varphi=60°$, we take $\Delta x=\Delta y=0.1309$, so that there are 48 grid points around the latitude circle, the distance between two grid points being 7.5°. For middle latitudes this corresponds to a linear distance of about 500 km. For simplicity the value of Δx $(=\Delta y)$ is doubled at $j=11$ $(\varphi=60°)$, doubled again at $j=14$ and $j=15$, so that we have 48 points along the latitude circles for $0\leq j\leq 10$, 24 points for $j=11$, 12, 13, 12 points for $j=14$ and 6 points for $j=15$ $(\varphi=88.5°)$. Because of the cyclic requirement along the latitude circle, two auxiliary points are added for every j, one on each end, to facilitate the computation.

In order to compute the vorticity and the Jacobians for $j=15$, we need another row of six points at $j=16$. These points are very close to the pole indeed, although the pole itself is at infinity on the Mercator projection and therefore cannot be reached. Since we only want to use these six points along $j=16$ as auxiliary points, and since they are so close together on the actual map, we may take the average values of the stream function ψ and the temperature T of the six points along $j=15$ for the values at every one of these points. These mean values are also supposed to represent the values of the ψ and T at the pole. Thus we have 656 grid points for each level and 2,624 points altogether for the system.

8. The Initial State

For the study of the development of the general circulation of the atmosphere it may be desirable to take the atmosphere as being at relative rest and having a uniform temperature at the initial moment, and then begin the heating and investigate the development of the motion. However, such an approach is too time consuming and was beyond the monetary facilities of the project, we shall therefore start from a somewhat idealized state.

In this idealized initial state we assume that there already exists an average temperature gradient from north to south comparable to the mean state of the atmosphere, but no temperature contrast from west to east. The air temperature in contact with the ground is the same as the mean temperature of the ground and is

represented by the first two terms of (34). The temperature decreases upwards with a lapse-rate given by (10). There also exists a mean zonal wind $\bar{u}$ at all levels. The vertical variation of $\bar{u}$ is in accordance with the thermal geostrophic wind relation in the troposphere, but with no vertical shear in the stratosphere (omb $< p <$ 250 mb). The variation of $\bar{u}$ with y is very small initially. The maximum zonal wind at the 250 mb level is 30 m sec^{-1}. Superimposed on this mean zonal flow is a somewhat random disturbance, represented by the stream function ψ^1. This ψ^1 is composed of nine wave components in the x-

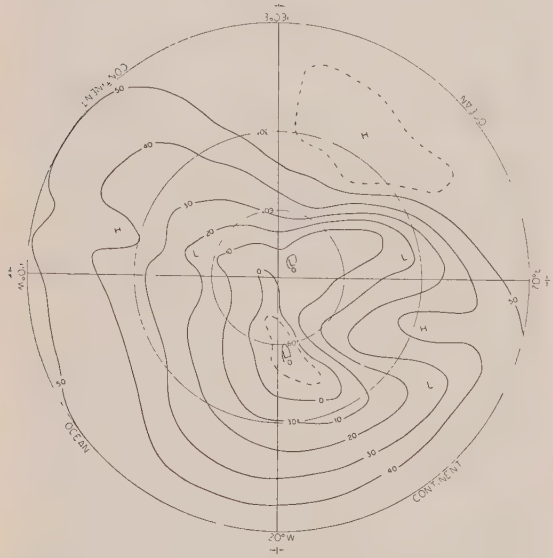

Fig. 2. Distribution of 850 mb stream function at time $t = 0$ at 10^6 m^2 sec^{-1} intervals.

Fig. 3. 850 mb stream function distribution at $t = 24$ hours.

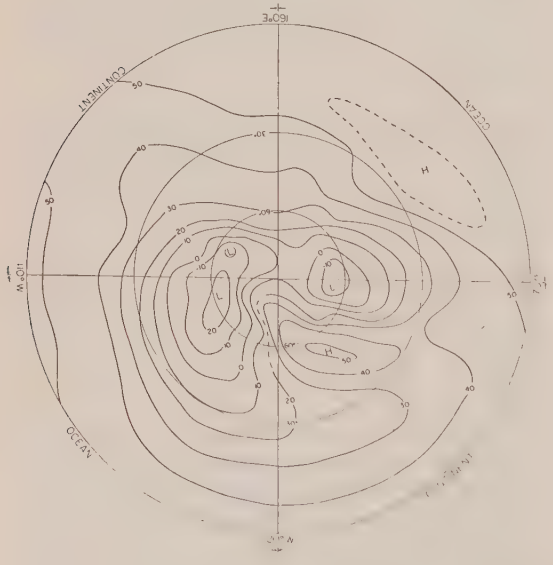

Fig. 4. 850 mb stream function distribution at $t = 48$ hours.

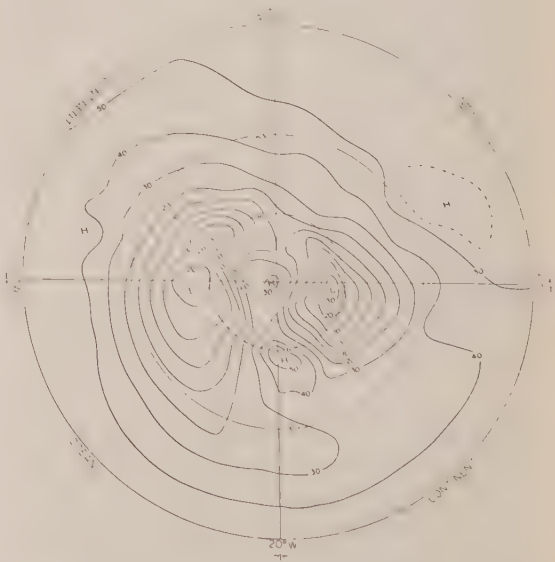

Fig. 5. 850 mb stream function distribution at $t = 72$ hours.

Fig. 6. 850 mb stream function distribution at $t = 96$ hours.

direction, the wave number m ranging from 1 to 9. The variation of ψ^1 with y is represented by sine and cosine function in y, the wave number ranging from 1 to 7. The amplitudes of the various wave components are determined so as to give the same amount of kinetic energy per unit mass for each wave component in x. The total kinetic energy of this disturbance corresponds to a mean perturbation velocity of 20 m sec^{-1}. The zero points of the various wave-components are shifted so as to give it a more random distribution. However, the disturbance so obtained is not very random, or shapeless, as we might like to assume. There is still large scale features present, as is indicated in figure 2 which gives the initial distribution of the total ψ at 850 mb. The prominent feature of this map are the two large troughs along the meridions 15° E and 75° E.

The disturbance represented by ψ^1 is assumed to be the same at all levels, so that the total ψ becomes more zonal at upper levels.

9. Development of the Flow

The rate of change of the composite stream function ψ is forecasted by eq. (22) through numerical integration. The time interval used in the integration is one hour and a half. The integration has been carried out for six days. The 850 mb flow pattern at 24, 48, 72, and 96 hours are represented in Figures 2—6. The following features of the developments may be noted:

a) The situation represented by Fig. 2, where the most prominent features are the two troughs situated along the longitudes 15° E

Fig. 7. 550 mb stream function distribution at $t = 48$ hours.

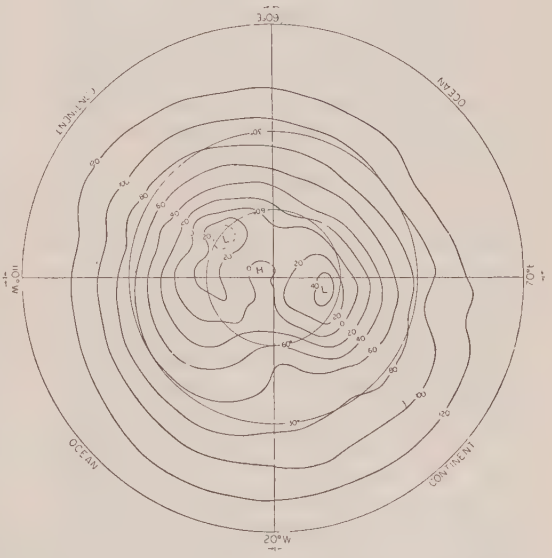

Fig. 8. 550 mb stream function distribution at $t = 96$ hours.

and 75° E[1], must be highly unbalanced because of the very short distance between them in one direction and very large distance in the other direction. Therefore it must undergo a readjustment of the distances. This adjustment takes the form of a rapid regression of the western trough.

b) The narrow ridge between the two troughs expanded into a fullsized high and moved toward the pole.

c) The two troughs developed very rapidly into two large centers, look more like the semi-permanent lows rather than the ordinary cyclones. Their latitudinal positions also correspond to the normal latitudinal position of the semi-permanent lows in winter.

d) On the third day (72 hours) the high has split up into two. The northern one moved over to the pole and stayed there.

e) Another closed low center is formed at the northern end of the weak trough along 155° W. Thus at the end of the fourth day there is a definite tendency to have three separate large lows developed.

[1] The longitudes are for reference only and bears no fixed relation to the real earth.

Because of the much stronger zonal flow at the upper levels the changes of the flow patterns are not so pronounced as at 850 mb level. Figs. 7 and 8 represent the flow patterns at 550 mb after 48 and 96 hours, respectively. The general features of the developments are the same as that at the 850 mb level but become obscured because of the stronger zonal flow. The changes at 50 mb level are small during this period.

At the end of the 5th day, a certain computational instability has developed and it becomes not possible to carry the computation to a much longer period. Apparently this is connected with the change of grid distances at $j=11$ and $j=14$. It is hoped that this difficulty can be removed in the near future and we shall be able to extend this work further.

REFERENCES

Albrecht, F., 1931: Über die "Glashauswirkung" der Erdatmosphäre und das Zustandekommen der Troposphäre. *Met. Zeit* **48**, pp. 57—68.

Houghton, H., 1954: On the annual heat balance of the northern hemisphere. *J. Meteor.* **11**, pp. 1—9.

Kuo, H. L., 1956: On quasi-nondivergent prognostic equations and their integration. *Tellus* **8**, pp. 373—383.

Phillips, N. A., 1956: The general circulation of the atmosphere: a numerical experiment. *Quart. J.R., Met. Soc.* **82**, pp. 123—164.

On the Maintenance of the Large-Scale Quasi-Permanent Disturbances in the Atmosphere

By BARRY SALTZMAN, Massachusetts Institute of Technology[1]

(Manuscript received January 17, 1959; revised version March 5, 1959)

Abstract

It is proposed that large-scale quasi-permanent flow systems are maintained against dissipative effects by a transfer of kinetic energy from smaller, cyclone-scale, disturbances which have baroclinic energy sources, the processes involved being non-linear and barotropic. To illustrate how such processes can operate, an example is given based on an idealized flow consisting of a limited number of double-Fourier components.

1. Introduction

In Fig. 1 a 500 mb synoptic map for a region covering the North American Continent and the North Atlantic Ocean is presented. The most prominent features of this map—namely, the large cyclonic area to the north sloping from northwest to southeast and the large, more diffuse, anticyclonic area to the south sloping from northeast to southwest—are typical of the quasi-steady winter conditions observed in this region. The largest scale systems shown on this map correspond roughly to disturbances of wave number three around the hemisphere and are so oriented that they transfer their kinetic energy to the zonally-averaged mean current which has its maximum velocity somewhere between the two main pressure centers. As such, these large systems constitute a representative example of those disturbances which, in the winter average, are most effective in maintaining the mean zonal current (see SALTZMAN 1957, 1958; SALTZMAN and FLEISHER 1960).

In viewing the persistence of flow patterns of this type over long time intervals (see, e.g., monthly mean maps presented by LAHEY, et al, 1958) one is led to pose the following question: How is the kinetic energy of these large-scale systems maintained in the face of a steady drain of their energy through viscous effects and through transfer to the zonal current? There are two possible answers to this question: Either the kinetic energy of the large disturbances is supplied by a direct *conversion* of potential and internal energy (i.e., by risings of warm air and sinkings of cold air on this large scale) or the kinetic energy is supplied by *transfer* from disturbances of other scales which themselves grow at the expense of potential and internal energy (e.g., from the smaller transient cyclone waves which tend to develop in the baroclinic zone south of the large quasi-stationary cyclonic vortex, such as the shorter wave length disturbances clearly evident in Fig. 1).

If, as presently indicated in studies by REED and TANK (1956), and WHITE and SALTZMAN (1956), for example, the indirect circulations in mid-latitudes, whose upward branches are

[1] This research has been sponsored by the Geophysics Research Directorate of the Air Force Cambridge Research Center under Contract No. AF 19(604)-2242.

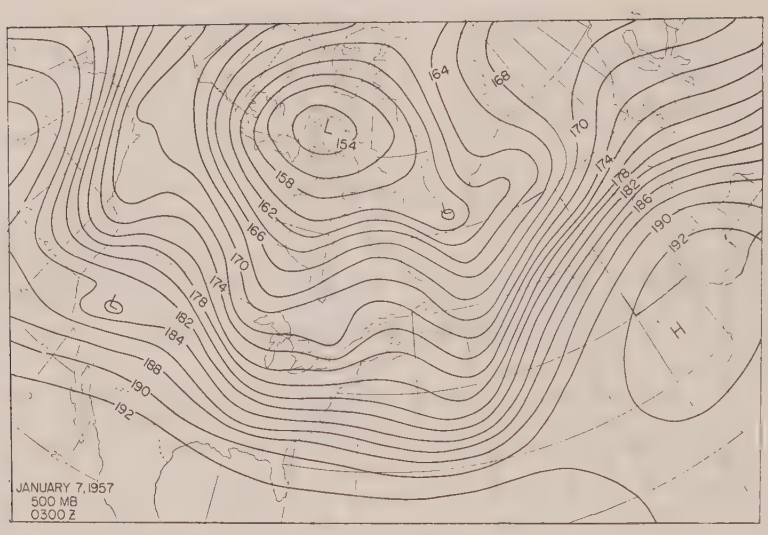

Fig. 1. Contour map of the 500 mb pressure surface for 7 Jan. 1957.

represented by rising motion in the large cold vortices to the north and whose downward branches are represented by sinking motion in the large warm highs to the south, are predominant over direct circulations on this scale, then one is forced to conclude that the large-scale features such as those shown in Fig. 1 are, in fact, steadily damped rather than amplified by direct conversion processes. In this event the maintenance of the kinetic energy of these features must rest entirely on the transfer processes mentioned above as the second alternative. In any event, however, it will be of interest to illustrate the operation of this transfer process,—by nature, a *non-linear* process—with a simple theoretical case. It is to this end that the present discussion is directed.

2. Governing equations

We assume that the transfer processes important for the maintenance of the large-scale disturbances are, as in the case of the maintenance of the zonal westerlies, of an essentially horizontal character and are governed by the barotropic vorticity equation. For simplicity, we shall apply this equation to a plane rather than a spherical surface, in which case the equation takes the form

$$\frac{\partial}{\partial t}\nabla^2\psi = -\frac{\partial\psi}{\partial x}\frac{\partial}{\partial y}\nabla^2\psi + \frac{\partial\psi}{\partial y}\frac{\partial}{\partial x}\nabla^2\psi - \beta\frac{\partial\psi}{\partial x} \quad (1)$$

where x and y are Cartesian coordinates pointing eastward and northward respectively, t is time, ψ is a stream function proportional to the contour height of a pressure surface, $\nabla^2 \equiv \partial^2/\partial x^2 + \partial^2/\partial y^2$, and β is the derivative with respect to y of the Coriolis parameter. Following procedures similar to those employed by Kampé de Fériet (1948), Gambo, et al (1955), Wippermann (1956) and Lorenz (1957), we express ψ over a fundamental region whose dimensions in x and y are K and L, respectively, in terms of a double Fourier expansion of the form

$$\psi(x, y, t) = \sum_{m=-\infty}^{\infty} \sum_{n=-\infty}^{\infty} \Psi(m, n, t)\, e^{i(kmx + lny)}, \quad (2)$$

where $k = 2\pi/K$, $l = 2\pi/L$, m and n denote the wave number in the x and y directions respectively, and the complex Fourier coefficients, $\Psi(m, n, t)$, are given by the relation

$$\Psi(m, n, t) = \frac{1}{KL}\int_0^K \int_0^L \psi(x, y, t)\, e^{-i(kmx + lny)}\, dx\, dy \quad (3)$$

To simplify the boundary conditions we take ψ to be periodic of wave lengths K and L in x and y, respectively.

By multiplying both sides of (1) by $(KL)^{-1}$ $exp\,[-i(kmx + lny)]$, integrating over the fundamental region, and applying (3) we obtain the

transformed vorticity equation governing the Fourier coefficients of the stream function. This equation has the form

$$\frac{d}{dt}\Psi(m,n) =$$

$$= \frac{kl}{(k^2m^2+l^2n^2)} \sum_{p=-\infty}^{\infty} \sum_{q=-\infty}^{\infty}$$

$$[(mq-np)(p^2k^2+q^2l^2)\Psi(p,q)\Psi(m-p,n-q)]$$

$$- \frac{\beta ikm}{(m^2k^2+n^2l^2)}\Psi(m,n) \qquad (4)$$

The total kinetic energy integrated over the fundamental region

$$\bar{E} = \frac{1}{KL}\int_0^K\int_0^L \frac{1}{2}\left[\left(\frac{\partial\psi}{\partial x}\right)^2+\left(\frac{\partial\psi}{\partial y}\right)^2\right]dx\,dy \qquad (5)$$

may be expanded in terms of a Fourier spectrum of the form

$$\bar{E} = \sum_{m=-\infty}^{\infty}\sum_{n=-\infty}^{\infty}\frac{1}{2}K(m,n) \qquad (6)$$

$$= \sum_{n=1}^{\infty}K(o,n) +$$

$$+ \sum_{m=1}^{\infty}\Big\{K(m,o) +$$

$$+ \sum_{n=1}^{\infty}[K(m,n)+K(m,-n)]\Big\} \qquad (7)$$

where $K(m,n)=(k^2m^2+l^2n^2)\,|\Psi(m,n,)|^2$. The first term on the right of (7) gives the kinetic energy of the mean zonal wind, while the term in curled brackets represents the spectral function for the mean disturbance kinetic energy superimposed on the mean zonal field. For the purpose of this study we are interested in obtaining an equation for the rate of change of kinetic energy of a given double Fourier component as a function of the transfer of kinetic energy to or from the other double Fourier components which comprise the complete stream field. Such an equation is obtained by multiplying both sides of (4) by $\Psi(-m,-n)$ and using the fact that $\Psi(-a,-b)$ is the complex conjugate of $\Psi(a,b)$. Thus we find,

$$\frac{d}{dt}K(m,n) = kl\sum_{p=-\infty}^{\infty}\sum_{q=-\infty}^{\infty}(p^2k^2+q^2l^2)(mq-np)$$

$$[\Psi(-m,-n)\Psi(p,q)\Psi(m-p,n-q) -$$

$$-\Psi(m,n)\Psi(p,q)\Psi(-m-p,-n-q)] \qquad (8)$$

By means of this last relation we are now able to calculate the instantaneous barotropic energy transfers due to the non-linear interactions among the Fourier components which comprise a field of flow in the fundamental region. It may be verified from (6) and (8) that the total kinetic energy is conserved (i.e., $d\bar{E}/dt=0$), as is implicit in the barotropic system treated.

3. An example

In this section we shall discuss the energetical properties of a simple flow system having the general features of the actual case shown in Fig. 1. This flow system will be composed of a few selected double Fourier components, grouped to represent, respectively, the mean zonal current, the long-wave disturbance, and the smaller-scale disturbance. We shall see that in such a system kinetic energy is transferred from the small-scale disturbance (which may be viewed as baroclinically-generated) to the long-wave component and, simultaneously, from the long-wave component to the mean zonal current.

For this example we take the fundamental region to be a square so that $l=k$. The stream function, ψ, is taken to be of the form

$$\psi(x,y,t) = Z(y,t) + L(x,y,t) + S(x,y,t) \qquad (9)$$

where

$$Z(y,t) = A(t)\sin ky \qquad (10)$$

represents the zonal current (wave number zero in x),

$$L(x,y,t) = B(t)[\cos k(x+y) +$$

$$+ \cos k(x-y)] + C(t)\sin kx \qquad (11)$$

represents the long-wave component (wave number one in x), and

$$S(x,y,t) = D(t)\cos k(2x-y) +$$

$$+ E(t)\cos 3kx \qquad (12)$$

represents the short-wave component (a combination of wave numbers two and three in x). Here $A = 2Im\,\Psi(0,1)$, $B = 2Re\,\Psi(1,1) = 2Re\,\Psi(1,-1)$, $C = 2Im\,\Psi(1,0)$, $D = 2Re\,\Psi(2,-1)$ and $E = 2Re\,\Psi(3,0)$. The dynamical properties of a system consisting of Z and L alone has already been studied in some detail by LORENZ (1957).

The components Z, L, and S are shown in figures 2, 3, and 4 with the following values of the Fourier coefficients:

$$\begin{aligned} A &= +3.00 \\ B &= -0.75 \\ C &= -1.50 \\ D &= +1.00 \\ E &= +1.00 \end{aligned} \qquad (13)$$

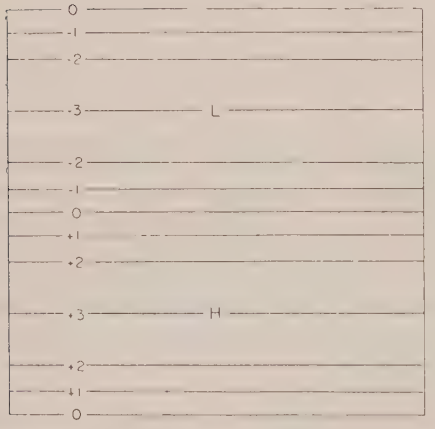

Fig 2. Stream function pattern, Z, representing the zonal motion: $Z(y) = 3.00 \sin ky$.

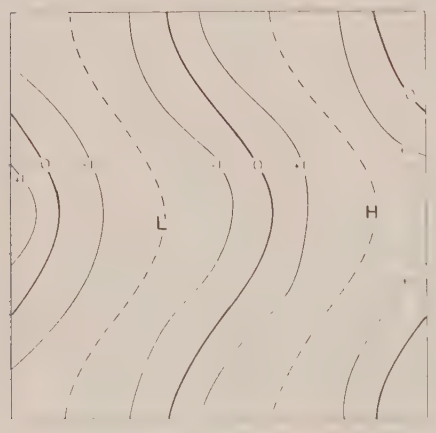

Fig. 3. Stream function pattern, L, representing the large-scale disturbances: $L(x, y) = -.75\,[\cos k\,(x + y) + \cos k\,(x - y)] - 1.50 \sin kx$.

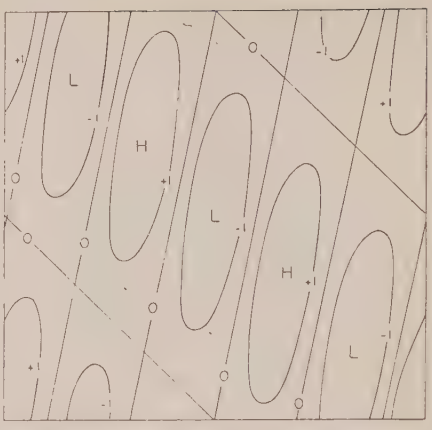

Fig. 4. Stream function pattern, S, representing the small-scale disturbances: $S(x, y) = \cos k\,(2x - y) + \cos 3\,kx$.

In Fig. 5 the sum of Z and L, representing a composite of the largest scales of motion, is

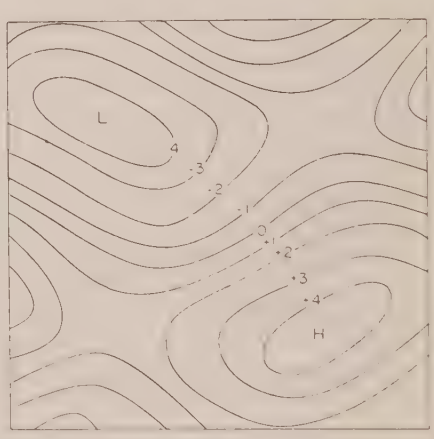

Fig. 5. Composite stream function pattern, $(Z + L)$, representing the largest scales of flow.

shown. In Fig. 6 the complete stream field, $(Z + L + S)$, obtained by superimposing the small-scale disturbance field, S, on $(Z + L)$, is shown. This stream field has many of the characteristics of the actual case shown in Fig. 1, the most obvious differences being the intensity of the large high pressure region and the strength of the easterlies.

The kinetic energy in each of these components is

$$\bar{E}_Z = .25\,k^2A^2 \qquad (14)$$

$$\bar{E}_L = .25\,k^2(4B^2 + C^2) \qquad (15)$$

Fig. 6. Composite stream function pattern, $(Z + L + S)$, representing the complete field of flow.

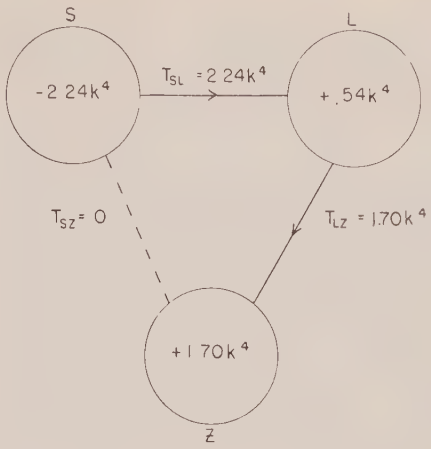

Fig. 7. Kinetic energy flow diagram for the example treated. Numbers within circles indicate the instantaneous rate of energy loss or gain due to the barotropic transfer.

$$\overline{E}_S = .25\, k^2(5D^2 + 9E^2) \qquad (16)$$

and, given the values listed in (13), $\overline{E}_Z = 2.25\, k^2$, $\overline{E}_L = 1.14\, k^2$, and $\overline{E}_S = 3.50\, k^2$.

By applying (8) we obtain the following expressions for the rate of change of $\overline{E}_Z$, $\overline{E}_L$ and $\overline{E}_S$:

$$\frac{d}{dt}\overline{E}_Z = T_{LZ} \qquad (17)$$

$$\frac{d}{dt}\overline{E}_L = -T_{LZ} + T_{SL} \qquad (18)$$

$$\frac{d}{dt}\overline{E}_S = -T_{SL} \qquad (19)$$

where

$$T_{LZ} = .50\, k^4 ABC \qquad (20)$$

measures the transfer of kinetic energy between the long wave and the mean zonal motion (i.e., between L and Z), and

$$T_{SL} = -3.00\, k^4 BDE \qquad (21)$$

measures the transfer between the short and long waves (i.e., between S and L). For this system there can be no kinetic energy exchange between the short waves and the mean flow, (i.e., $T_{SZ} = 0$). With the numbers given in (13) these energy transfer functions have the values $T_{LZ} = +1.70\, k^4$ and $T_{SL} = +2.24\, k^4$, implying an instantaneous kinetic energy flow simultaneously from the smallest scale component, S, to the larger scale component L, and to a lesser degree, from the component L to the mean zonal component Z (see Fig. 7). If we take $K = 10^9$ cm (corresponding to the dimensions of a comparable region of the atmosphere) and let the units of ψ be 10^{11} cm^2/sec (corresponding to a maximum mean zonal westerly velocity of 19 m/sec at $y = K/2$), the energy transfers are of sufficient strength to regenerate the existing kinetic energy of L in six days and that of Z in four days. These figures are of the order required by estimates of atmospheric frictional dissipation. Thus we have constructed one example in which the energy of the larger synoptic features is being maintained against dissipative effects by a transfer of energy from the smaller scale features. The latter may be presumed to grow baroclinically and hence have an independent energy source.

It will be recalled (see eq. 12) that $S(x, y)$ consists of two double-Fourier components, one of wave numbers $(2, -1)$ and the other of wave numbers $(3, 0)$. In agreement with the results of FJØRTOFT (1953), the loss of energy by the component, $(2, -1)$, is balanced by a small gain of energy by the shortest wavelength component, $(3, 0)$, and a larger gain of energy by the long-wave component, $L(x, y)$, the net effect being the transfer from S to L described above. It may be remarked, also, that kinetic energy of disturbances of higher

wave numbers than are included initially in our example would tend to be generated as *second-order* effects. Since we have been concerned here with the problem of the maintenance of quasi-steady features we have restricted attention only to the first order transfers. If potential energy conversions are not adequate to maintain the large-scale disturbances directly, these first-order transfers must, in the long-time average, be predominantly of the sign illustrated here. On specific days, however, first-order energy transfers of opposite sign (i.e., transfers from the larger to smaller scale components) may also occur and perhaps are of great actual importance in the sudden deepening of individual intermediate-scale waves observed on weather charts. An example of this reverse transfer may be obtained simply by changing the sign of either B, D or E. Clearly, many other examples illustrating transfers in either direction may be constructed using different Fourier components. It has been our purpose here to demonstrate at least one case which has the energetical properties mentioned in the introductory discussion, and, at the same time, is somewhat realistic in its correspondence with observed phenomena.

In connection with the above remarks it is pertinent to note that for our case the sign of the kinetic energy transfer between S and L, or between S and $(L + Z)$, is independent of the phase of the small-scale disturbances along the diagonal from northwest to southeast in Fig. 4. Thus the small-scale disturbances will continue to feed energy into the larger features at the same rate even if the highs and lows in Fig. 4 were interchanged, as might result from the motions of the small systems relative to the larger ones.

4. Further remarks

a) The view concerning the role of the smaller scale disturbances expressed here undoubtedly has certain connections with the experience of synoptic forecasters who regard the large features, particularly the large cold vortex to the north, as a sort of 'graveyard' for the smaller scale disturbances. The process of energy transfer from the smaller to larger waves is probably related to the familiar 'occlusion' process.

b) According to this discussion, the large scale features of the mean pressure map (i.e., of the average of the ensemble of many maps of the type shown in Fig. 1) are decisively influenced by transient smaller scale phenomena which are entirely absent from mean maps. If this view is correct, it is suggested that a linear, steady-state, theory will not be completely adequate in explaining the large-scale mean features. It would appear that a primary influence of land-sea thermal differences is to create favored areas for the baroclinic development of small-scale disturbances which, in turn, damp by non-linear barotropic processes, to maintain the larger systems. The discussion by SUTCLIFFE (1951) is of pertinence in this connection.

c) Computations from actual atmospheric data of the energy transfers occurring in the wave number domain can be performed feasibly with the use of the high speed computer. Such computations, based on equations presented by the writer (1957), are now under way at M.I.T.

Acknowledgement

The writer wishes to express his thanks to Professor V. P. Starr for his interest in this work.

REFERENCES

Fjørtoft, R., 1953: On the changes in the spectral distribution of kinetic energy for two-dimensional, non-divergent flow. *Tellus*, **5**, pp. 225—230.

Gambo, K., Katow, K., Manabe, S. and Aihara, M., 1955: Numerical forecasting over the Far East by the double Fourier series method. *J. Met. Soc. Japan*, **33**, pp. 133—139.

Kampé de Fériet, J., 1948: Harmonic analysis of the two-dimensional flow of an incompressible viscous fluid. *Quart. Appl. Math.*, **6**, pp. 1—13.

Lahey, J. F., Bryson, R. A., Wahl, E. W., Horn, L. H. and Henderson V. D., 1958: *Atlas of 500 mb wind characteristics for the northern hemisphere.* U. of Wisconsin Press, Madison.

Lorenz, E. N., 1957: Maximum simplification of the dynamic equations. *Final Report, M.I.T. Gen. Circ. Proj., AF 19(604)-1000*, pp. 491—517.

Reed, R. J. and Tank, W. G., 1956: Miscellaneous studies of polar vortices. *Sci. Rep. No. 1, AF 19(604)-1298*, U. of Wash., 21 pp.

Saltzman, B, 1957a: The energetics of the larger scales of atmospheric turbulence. *Ph. D. Thesis, M.I.T.*, 100 pp.

— 1957b: Equations governing the energetics of the larger scales of atmospheric turbulence in the domain of wave number. *J. Meteor.*, **14**, pp. 513—523.

— 1958: Some hemispheric spectral statistics. *J. Meteor.*, **15**, pp. 259—263.

—, and Fleisher, A., 1960: Spectrum of kinetic energy transfer due to large-scale horizontal Reynolds stresses. To be printed in Tellus 12.

Sutcliffe, R. C., 1951: Mean upper contour patterns of the northern hemisphere—the thermal-synoptic viewpoint, *Quart. J. Roy. Met. Soc.*, **77**, pp. 435—440.

White, R. M. and Saltzman, B., 1956: On conversions between potential and kinetic energy in the atmosphere. *Tellus*, **8**, pp. 357—363.

Wippermann, F., 1956: Numerische Untersuchungen zur zeitlichen Änderung der Spektralverteilung kinetischer Energie für eine zweidimensionale, dviergenz- und reibungsfreie Strömung. *Arch. Met. Geoph. Biokl. A. Bd.* **9**, *H. 1*, pp. 1—18.

On a Graphical Method for an Approximate Determination of the Vertical Velocity in the Mid-Troposphere

By A. WIIN-NIELSEN, Air Weather Service, Joint Numerical Weather Prediction Unit Suitland, Md.[1]

(Manuscript received April 20, 1959)

Abstract

A simple graphical method for determining the vertical velocity from a simplified, but consistent form of a diagnostic equation for this quantity is developed. It is shown that the main term in the equation is the advection of temperature in the vorticity field. Section 2 contains simple rules from which the sign of the vertical velocity may be determined.

An approximate solution to the equation is found in section 3, while section 4 contains an investigation of the accuracy of this solution as function of the scale of the motion. Different types of approximate solutions are investigated.

Section 5 contains an example of the use of the method.

1. Introduction

The vertical velocity is one of the most important quantities in the atmosphere and one of the most difficult to determine. It is hardly necessary to stress the desirability of methods for its computation. The role of the vertical velocity in large-scale conversion of potential energy into kinetic energy is well-known. In predictions of large-scale precipitation patterns (SMEBYE, 1958) we need methods for a determination of this quantity.

By a numerical integration of the equations for two or multiparameter models designed for physical weather prediction we obtain the vertical velocity as a by-product at one or several levels in the troposphere. There seems, however, to be some time to go before these maps are available almost immediately to every meteorologist in the weather services. It seems therefore worth while to consider methods which allow us to compute an instantaneous value of the vertical velocity by simple graphical methods.

The methods which so far have been available for research work have been based upon an evaluation of all terms except those containing the vertical velocity in the vorticity equation or the adiabatic equation. The other possibility, to compute the ascent or descent directly from the continuity equation, has usually been avoided because of the great sensitivity of this method to error in the observed winds. The former methods can at best give a mean value for the time-period between observations and give therefore not instantaneous values. A method which can give a good first approximation is therefore needed. The method reported here is believed to fulfil this requirement.

In the solution of equations for the vertical velocity in two or multilevel models we need usually a good first guess in order to decrease

[1] Most of the work in this study was done while attached to the International Meteorological Institute in Stockholm.

the number of relaxations to solve the equation accurately. The approximate solution given here can be used with advantages in such problems.

2. The method for determination of the vertical velocity

The following procedure for determination of the vertical velocity, $\omega = dp/dt$, consists in finding an approximate solution to the so-called ω-equation, which is obtained by an elimination of the local time derivative between the quasi-geostrophic vorticity equation and the adiabatic equation. The ω-equation has earlier been considered, first by FJØRTOFT (1955) and later by ELIASSEN (1956). Although it is possible to derive this equation from a very general form of the vorticity equation we shall here restrict ourselves to the most simple consistent form of the equation, which is

$$\frac{\partial \zeta}{\partial t} + \mathbf{v} \cdot \nabla (\zeta + f) = f_0 \frac{\partial \omega}{\partial p} \qquad (2.1)$$

where f_0 is a standard value of the Corioli's parameter. The different consistent forms of the vorticity equation has earlier been considered by the author (1959).

The adiabatic equation will be written:

$$\left.\begin{aligned} \frac{\partial}{\partial t}\left(\frac{\partial \phi}{\partial p}\right) + \mathbf{v} \cdot \nabla \left(\frac{\partial \phi}{\partial p}\right) + \sigma\omega = 0, \\ \sigma = -\alpha \frac{\partial \ln \Theta}{\partial p} \end{aligned}\right\} \qquad (2.2)$$

We shall in the following assume that the static stability, σ, is constant in any isobaric surface, i.e., $\sigma = \sigma(p)$ and shall further compute the relative vorticity by the formula:

$$\zeta = \frac{1}{f_0} \nabla^2 \phi \qquad (2.3)$$

Using (2.1), (2.2) and (2.3) we obtain the ω-equation in the form:

$$\sigma \nabla^2 \omega + f_0^2 \frac{\partial^2 \omega}{\partial p^2} = f_0 \frac{\partial}{\partial p} (\mathbf{v} \cdot \nabla \eta) -$$

$$- \nabla^2 \left(\mathbf{v} \cdot \nabla \frac{\partial \phi}{\partial p} \right) = F(x, y, p) \qquad (2.4)$$

The forcing function $F(x, y, p)$ may be expressed in a number of different ways. We shall here choose to express $F(x, y, p)$ with the aid of the height and temperature in an isobaric surface. We will further neglect variations in the Corioli's parameter in the evaluation of F, because this simplifies the procedure to a great extent. By doing so we naturally restrict the latitudional extent of the field. Using the approximations stated above we can write the forcing function in the following form

$$F(x, y, p) = \frac{2Rg}{f_0 p} \{ J(\nabla^2 z, T) + A(z, T) \} \qquad (2.5)$$

$J(\nabla^2 z, T)$ represents the usual Jacobian, while $A(\alpha, \beta)$ is a notation for the operator

$$A(\alpha, \beta) = -\left(\frac{\partial^2 \alpha}{\partial x \partial y}\right)\left(\frac{\partial^2 \beta}{\partial x^2} - \frac{\partial^2 \beta}{\partial y^2}\right) + \\ + \left(\frac{\partial^2 \alpha}{\partial x^2} - \frac{\partial^2 \alpha}{\partial y^2}\right)\left(\frac{\partial^2 \beta}{\partial x \partial y}\right) \qquad (2.6)$$

It is seen that $A(\alpha, \beta)$ is related to the deformation properties of the two fields α and β. It will consequently be called the deformation function. The deformation function obviously vanishes, if α is proportional to β. There is a general tendency for the isoterms in the midtroposphere to be parallel to the contour lines. At most places $A(z, T)$ will therefore be small compared to $J(\nabla^2 z, T)$

A direct computation of $A(z, T)$, using finite differences at 500 mb, shows the following characteristics:

1. The deformation function is locally of a smaller magnitude than the Jacobian in (2.5). A mean value of the absolute values of A turned out to be less than half of the corresponding mean value of $J(\nabla^2 z, T)$.

2. The deformation function is generally on a smaller scale than the Jacobian.

In view of the two statements above it is suggested that the deformation function can be neglected in comparison with the Jacobian, if we are interested in a fast method to obtain a first estimate of the vertical velocity. The statements 1. and 2. do not hold in general for levels above or below the 500 mb level, where we find a greater baroclinicity in the atmosphere.

We may derive a "geostrophic" expression for $A(z, T)$ which clearly show how it is depending upon the deformation properties

of the fluid. Introducing the expressions for the geostrophic wind and the geostrophic thermal wind in the form:

$$\frac{\partial u}{\partial p} = \frac{R}{f_0 p}\frac{\partial T}{\partial y}, \quad \frac{\partial v}{\partial p} = -\frac{R}{f_0 p}\frac{\partial T}{\partial x} \tag{2.7}$$

in the expression for A we can, after some manipulations, arrive at the expression

$$A(z,T) = \frac{p f_0^2}{2gR}\left\{A\frac{\partial B}{\partial p} - B\frac{\partial A}{\partial p}\right\} \tag{2.8}$$

where

$$A = \frac{\partial v}{\partial x} + \frac{\partial u}{\partial y}, \quad B = \frac{\partial u}{\partial x} - \frac{\partial v}{\partial y} \tag{2.9}$$

are the two deformation expressions for the wind. (2.8) shows first of all how the geostrophic estimate of the deformation function depends on the deformation expressions for the wind. It shows further that the deformation function will be small if A and B do not vary greatly with pressure.

In the following we shall approximate the forcing function by

$$F(x, y, p) = \frac{2Rg}{f_0 p} J(\nabla^2 z, T) \tag{2.10}$$

Let us next in order to get a first crude idea about the solution to the ω-equation consider a single component of the ω-field, say

$$\omega = A \sin kx \sin ly \sin mp \tag{2.11}$$

where k, l and m are wave numbers in the x, y and p direction, respectively. We have then

$$L(\omega) = \nabla^2 \omega + \frac{f_0^2}{\sigma}\frac{\partial^2 \omega}{\partial p^2} = -s^2\omega = \\ = \frac{2Rg}{f_0 p \sigma} J(\nabla^2 z, T) \tag{2.12}$$

where $s^2 = k^2 + l^2 + f_0^2 m^2/\sigma$ is a measure of scale. Approximating the Laplacian of Z in the usual way:

$$\nabla^2 z = -\frac{4}{d^2}(z - \bar{z}) \tag{2.13}$$

we get the following solution:

$$\omega = \frac{2Rg}{s^2 f_0 p \sigma} \cdot \frac{4}{d^2} J(z - \bar{z}), T) \tag{2.14}$$

which also may be written in the form:

$$\omega = a\mathbf{v}_\zeta \cdot \nabla T \tag{2.15}$$

where a is a positive quantity and

$$\mathbf{v}_\zeta = -\frac{g}{f_0}\nabla(z - \bar{z}) \times \mathbf{k} \tag{2.16}$$

The solution (2.15), which of course only may be considered as a first approximation, shows that $\omega < o$ *(upward motion) if we have warm air advection by the "wind" in the vorticity field, while* $\omega > o$ *(downward motion), if cold air is advected by* $\mathbf{v}_\zeta$.

The above rule may be used to locate the regions of upward and downward motion directly on a weather map, where an isotherm analysis is made, and when the vorticity field is represented by isolines for $(z - \bar{z})$. It should be mentioned that the reversed rule applies if the vorticity field is represented by $\nabla^2 z = 4/d^2 (\bar{z} - z)$, which is the usual finite difference approximation.

Although the above rule may be good enough to determine the sign of the vertical velocity, we need something better if we want to go beyond this. We are here mainly interested in the horizontal distribution of ω, and shall therefore represent the vertical distribution as simple is possible. The representation.

$$\omega(x, y, p, t) = (p - p_s)(p - p_\star)^{M(x,y)} \tag{2.17}$$

where $p_s = 100$ cb represents the surface of the earth and $p_\star = 20$ cb a level in the lower stratosphere, where $\omega = 0$, is the simplest representation which gives a reasonable distribution of convergence and divergence in the vertical direction. From (2.17) it follows that

$$\frac{\partial^2 \omega}{\partial p^2} = \frac{\omega}{\frac{1}{2}(p - p_s)(p - p_\star)} \tag{2.18}$$

and (2.4) can be written

$$\nabla^2 \omega - b\omega = h(x, y) \tag{2.19}$$

where

$$b = \frac{2f_0^2}{\sigma(p_s - p)(p - p_\star)} > 0 \tag{2.20}$$

and

$$h(x, y) = \frac{2Rg}{f_0 \sigma p} J(\nabla^2 z, T) \qquad (2.21)$$

The equation (2.19) is of the Helmholz type and is similar to equations used in numerical prediction of two parameter models. It is further of the same type as the equation used by SMEBYE (1958) in his investigation of large scale precipitation forecasting. In his solution of the equation he approximated

$$\nabla^2 \omega = -\frac{4}{d^2}(\omega - \overline{\omega}) \qquad (2.22)$$

and got the equation in the form

$$\omega - B\overline{\omega} = hd^2 \qquad (2.23)$$

where however the term containing $\overline{\omega}$ was neglected. This procedure corresponds to the solution given in (2.15) and may in many cases lead to an underestimate of ω as shown in the next section. It actually only gives an accurate solution for one particular scale, while the accuracy rapidly falls off, when we remove ourselves from this scale. We shall return to the form (2.19) and in the next section discuss a procedure for an approximate solution and its accuracy.

3. Solution of the Helmholz equation

FJØRTOFT (1952) has discussed approximate solutions to Poisson and Helmholz equations. It is shown by Fjørtoft that the speed of convergence of the series solution increases rapidly in the Poisson case, if an increasing gridsize is used in the smoothing operators used for evaluation of the terms in the formal solution. Further, it is pointed out that the convergence of the solution in the Helmholz case may be speeded up in the same way, but that this is not necessary, because already applying the same gridsize in all terms leads to a fairly accurate solution including only a few terms in the series. Although this is true it may still be desirable to investigate whether a varying gridsize will increase the accuracy to such a degree that still fewer terms give the same accuracy.

The method depends upon the use of a varying gridsize. Let $d_1, d_2 \ldots d_p \ldots$ denote a steadily increasing series of gridsizes. The finite difference form of the Helmholz equation can now be written in any of the forms

$$\nabla_p \omega - bd_p^2 \omega = d_p^2 h \qquad (3.1)$$

where

$$\nabla^2 \omega \simeq \frac{1}{d_p^2} \nabla_p^2 \omega$$

It is convenient for the following computations to define a smoothing operator:

$$\omega^{[p]} = \omega + \frac{\nabla_p^2 \omega - bd_p^2 \omega}{\alpha_p + bd_p^2} \qquad (3.2)$$

where α_p so far is an arbitrary constant. We shall later relate this smoothing to the well-known operator.

$$\omega^{(p)} = \omega + \frac{\nabla_p^2 \omega}{\alpha_p} \qquad (3.3)$$

which for $\alpha_p = 4$ is identical with the Fjørtoft-operator. By formal computations we get by repeated use of (3.2) for different values of the gridsizes:

$$\omega = -\frac{\nabla_1^2 \omega - bd_1^2 \omega}{\alpha_1 + bd_1^2} - \frac{(\nabla_2^2 \omega - bd_2^2 \omega)^{[1]}}{\alpha_2 + bd_2^2} - \ldots - \frac{(\nabla_p^2 \omega - bd_p^2 \omega)^{[1]\ldots[p-1]}}{\alpha_p + bd_p^2} + \omega^{[1]\ldots[p]} \qquad (3.4)$$

where the last term is the rest term.

Substituting from (3.1) we obtain:

$$\omega = -\frac{d_1^2 h}{\alpha_1 + bd_1^2} - \frac{d_2^2 h^{[1]}}{\alpha^2 + bd_2^2} - \ldots - \frac{d_p^2 h^{[1]\ldots[p-1]}}{\alpha_p + bd_p^2} + \omega^{[1]\ldots[p]} \qquad (3.5)$$

The next problem is to bring the solution (3.5) into a form which is easier to handle in practice. This is done by relating the two smoothing operators (3.2) and (3.3) to each other. Eliminating $\nabla_p^2 \omega$ between (3.2) and (3.3) we obtain

$$\omega^{[p]} = \frac{\alpha_p}{\alpha_p + bd_p^2} \omega^{(p)} \qquad (3.6)$$

(3.6) shows that $\omega^{[p]}$ act in principally the same way as $\omega^{(p)}$. The only difference is a further reduction of the amplitude of the different Fourier-components by the propor-

tionality factor. When finally (3.6) is inserted in (3.5) we obtain:

$$\omega = -\frac{d_1^2}{\alpha_1 + bd_1^2} h - \frac{d_2^2}{\alpha_2 + bd_2^2} \cdot \frac{\alpha_1}{\alpha_1 + bd_1^2} h^{(1)} - \ldots$$

$$\ldots - \frac{d_p^2}{\alpha_p + bd_p^2} \left\{ \prod_{\nu=1}^{\nu=p-1} \frac{\alpha_\nu}{\alpha_\nu + bd_\nu^2} \right\} h^{(1)\ldots(p-1)} +$$

$$+ \left\{ \prod_{\nu=1}^{\nu=p} \frac{\alpha_\nu}{d_\nu + bd_\nu^2} \right\} \omega^{(1)\ldots(p)} \qquad (3.7)$$

A truncated form of (3.7) may be used as an approximative solution, when we have decided which values we will ascribe to the series d_ν and α_ν. Many possibilities exist in this respect depending on what we want to obtain. If we for instance want to use the approximate solution as a first guess for a relaxation procedure it may be convenient to choose the values α_ν in such a way that a fairly accurate solution is obtained over a large interval of wave-numbers. It is not the purpose here to give any complete discussion of the solution (3.7). We shall be satisfied by showing that for the specific choice

$$\alpha_1 = \alpha_2 = \ldots = \alpha_p = 4$$

and

$$d_1^2 = \frac{1}{2} d_2^2 = \ldots = \frac{1}{2^{p-1}} d_p^2$$

we can obtain a rather accurate solution to the special form of the ω-equation discussed here.

The accuracy of the solution is of course also depending on the particular value of the constant b, which appears in the Helmholz equation. Generally speaking we obtain a more accurate solution with the same number of terms the larger b is.

4. Accuracy of the approximate solution

This section will contain an evaluation of the accuracy of the approximate solution. In order to be able to compute numerical values we shall decide upon the units to be used. A convenient unit for ω is mb per 12 hours. We shall further use a value for $d_1 = 6 \times 10^5$ m. Les us finally assume that the right hand side $h(x, y)$ has been computed with a usual finite difference procedure, i.e.

$$h = \frac{2Rg}{f_0 \sigma p} J(\nabla^2 z, T) =$$

$$= \frac{2Rg}{f_0 \sigma p} \frac{1}{4d_1^4} \mathbf{J}(\nabla^2 z, T) = \frac{c}{4d_1^4} H \qquad (4.1)$$

where

$$c = \frac{2Rg}{f_0 \sigma p}, \quad H = \mathbf{J}(\nabla^2 z, T) \qquad (4.2)$$

Using MTS-units and the above unit for ω we obtain for the 500 mb surface

$$bd_1^2 \simeq \frac{5}{2}, \quad c \simeq \frac{1}{5} \qquad (4.3)$$

The finite difference equation to which we want to find an approximate solution is

$$\nabla_1^2 \omega - bd_1^2 \omega = \frac{c}{4d_1^2} H(x, y) \qquad (4.4)$$

We shall investigate the accuracy of the solution by assuming that ω can be written in the form

$$\omega = \text{const.} + \Sigma A_{mn} e^{2\pi i \left(\frac{x}{\lambda_m} + \frac{y}{\nu_m}\right)} \qquad (4.5)$$

In this problem we shall assume that $\omega \to 0$ for $(x, y) \to \infty$. This means that we are allowed to put the constant in (4.5) equal to zero. From the expression (4.5) we may easily find the Fourier expansion for H by inserting in (4.4).

$$H = -\frac{4d_1^2}{c} \Sigma B_{mn} e^{2\pi i \left(\frac{x}{\lambda_m} + \frac{y}{\nu_n}\right)} \qquad (4.6)$$

with

$$B_{mn} = \left(4 - 2\cos\frac{2\pi}{\lambda_m} d_1 - 2\cos\frac{2\pi}{\nu_n} d_1 + bd_1^2\right) A_{mn} \qquad (4.7)$$

When we now insert the series (4.6) in the approximate solution (3.7) we can investigate with which accuracy it is possible to reproduce the series (4.5) with a truncated form of (3.7)

We note then first that for any quantity

$$\delta = \Sigma \delta_{mn} e^{2\pi i \left(\frac{x}{\lambda_m} + \frac{y}{\nu_n}\right)} \qquad (4.8)$$

we have

$$\delta^{(p)} = \Sigma R_{mn}^{(p)} \delta_{mn} e^{2\pi i \left(\frac{x}{\lambda_m} + \frac{y}{\nu_n}\right)} \qquad (4.9)$$

with

$$R_{mn}^{(p)} = \left(1 - \frac{4}{\alpha_p}\right) + \frac{2}{\alpha_p}\left(\cos\frac{2\pi}{\lambda_m} d_p + \cos\frac{2\pi}{\nu_n} d_p\right) \tag{4.10}$$

With these notations we can derive an expression for the ratio between ω_{mn}^*, which is the amplitude of the general component in the series, and ω_{mn}, which is the corresponding amplitude in the complete development of ω. The ratio $\omega_{mn}^*/\omega_{mn}$, will be used as a measure of the accuracy of the approximate solution. In order to have the possibility to express the accuracy in numbers for a rather general case, we shall select the case, where $\lambda_m = \nu_n$ and where α_p and d_p have the values stated above. We arrive at the following expression for the accuracy:

$$\frac{\omega_{mn}^*}{\omega_{mn}} = \left[4\left(1 - \cos 2\pi\frac{d_1}{\lambda_m}\right) + bd_1^2\right] \cdot \left\{\frac{1}{\alpha_1 + bd_1^2} + \left(\frac{d_2}{d_1}\right)^2 \frac{\alpha_1}{\alpha_1 + bd_1^2} \frac{R_{mn}^{(1)}}{\alpha_2 + bd_2^2} + \ldots + \left(\frac{d_p}{d_1}\right)^2 \cdot \left[\prod_{\nu=1}^{p-1} \frac{\alpha_\nu}{\alpha_\nu + bd_\nu^2}\right] \cdot \frac{R_{mn}^{(1)} \ldots R_{mn}^{(p)}}{\alpha_p + bd_p^2}\right\} \tag{4.11}$$

With our special selection of the parameters ($\lambda_m = \nu_n$, d_p, α_p) we have

$$R_{mn}^{(p)} = \cos 2\pi\frac{d_p}{\lambda_m} \tag{4.12}$$

If $\lambda_m = 4d_1$, we see immediately that $R_m = 0$. Consequently we will have complete accuracy, i.e. $\{\omega_m^*/\omega_m\}_{\lambda = 4d_1} = 1$ for this wave length, independent of the number of terms. Next we want to investigate the accuracy of the solution for other wave lengths, when we incorporate a certain number of terms in the approximate solution. The number of terms is characterized by the index p. $p = 1$ means that we include two terms etc. The accuracy of the solution for $p = 1$ and $p = 2$ is given in table 1, which shows that $p = 2$ will give an accuracy which is sufficient for most diagnostic purposes, especially when we consider the other approximations in the formulation of the problem. Also, it is worth while mentioning that $p = 1$ gives a solution with an error less than 10 % up to a wavelength close to 6,000 km.

Table 1.

λ_m	4 d	5 d	6 d	8 d	10 d	12 d	14 d	16 d
ω_m^*/ω_m, $p=1$	1.00	1.03	1.00	0.93	0.86	0.83	0.80	0.79
ω_m^*/ω_m, $p=2$	1.00	1.00	1.02	1.03	1.01	1.00	0.99	0.98

We shall next compare the accuracy of the solution given above with the one obtained without varying the gridsize in the Helmholz case. The derivation is made in a completely similar fashion as before. The approximate solution takes now the form:

$$\omega^* = -\frac{c}{4d_1^2} \cdot \frac{1}{\alpha_1 + bd_1^2}\left[H + \frac{\alpha_1}{\alpha_1 + bd_1^2} H^{(1)} + \ldots + \left(\frac{\alpha_1}{\alpha_1 + bd_1^2}\right)^{p-1} \cdot H^{\overbrace{(1)(1),..(1)}^{(p-1)}}\right] \tag{4.13}$$

The accuracy, measured in the same way as before, is now given by the formula:

$$\frac{\omega_m^*}{\omega_m} = \frac{4\left(1 - \cos 2\pi\frac{d_1}{z_m}\right) + bd_1^2}{\alpha_1 + bd_1^2} \cdot \left\{1 + \frac{\alpha_1}{\alpha_1 + bd_1^2} R_m^{(1)} + \ldots + \left(\frac{\alpha_1}{\alpha_1 + bd_1^2} R_m^{(1)}\right)^{p-1}\right\} \tag{4.14}$$

Table 2 gives the accuracy for different values of the wave length for $p = 1$ and $p = 2$.

A comparison between table 1 and 2 shows clearly that the former method is an advantage. This is particularly so, because it is not followed by any extra work, if the computations are made graphically. It should further be pointed out that the two formulas are different for $p = 1$. Only for $p = 0$ are they identical.

The reason that we obtain such a high accuracy already for $p = 1$ and 2 is due to

Table 2.

λ_m	4 d	5 d	6 d	8 d	10 d	12 d	14 d	16 d
ω_m^*/ω_m, $p=1$	1.00	0.96	0.91	0.83	0.76	0.72	0.69	0.68
ω_m^*/ω_m, $p=2$	1.00	0.99	0.97	0.94	0.87	0.85	0.83	0.82

the fact that the coefficient to ω in the Helmholz equation in this particular case is as great as 2.5.

It is at this point worth while to mention that Helmholz equations which with advantage may be solved graphically appear in other problems. The prognostic equation for the thickness field, derived by FJØRTOFT (1955) and tested by SIGGTRYGGSSON and the author (1957), also leads to a Helmholz-equation. Denoting the thickness field between 1,000 mb and 500 mb by ϕ_T we can write the prognostic equation in the form

$$\nabla_1^2 \phi_T - e d_1^2 \phi_T = d_1^2 h \qquad (4.15)$$

The value of ed_1^2, to be used in (4.15) turns out to be about 4. The accuracy of the solution with varying gridsize is shown in table 3 for this case. Again the value for $p=1$ and 2 are given. p=1 gives a good accuracy, while $p=2$ is remarkably good due to the large value of the coefficient.

Table 3.

λ_m	4 d	5 d	6 d	8 d	10 d	12 d	14 d	16 d
ω_m^*/ω_m, $p=1$	1.00	1.02	1.00	0.95	0.92	0.90	0.88	0.87
ω_m^*/ω_m, $p=2$	1.00	1.01	1.01	1.00	1.00	1.00	0.99	0.98

We shall finally comment a little on the numerical values used in the practical application of the ω-equation. When we introduce the numerical values of bd_1^2, and $c/4d_1^2$ and measure ω in mb/12h as before we obtain:

$$\omega = q + 0.88\, q^{(1)} + 0.50\, q^{(1)\,(2)} + \\ + 0.21\, q^{(1)\,(2)\,(3)} + \ldots \qquad (4.16)$$

where $q = -2/65\, H$.

In graphical work it is extremely convenient if the coefficients are simple numbers. It will do no harm, if we replace (4.16) by

Fig. 1. Horizontal distribution of vertical motion in cm sec^{-1} computed from heights and temperatures for the 500 mb surfaces by approximate formula. January 2, 1956, 0300Z.

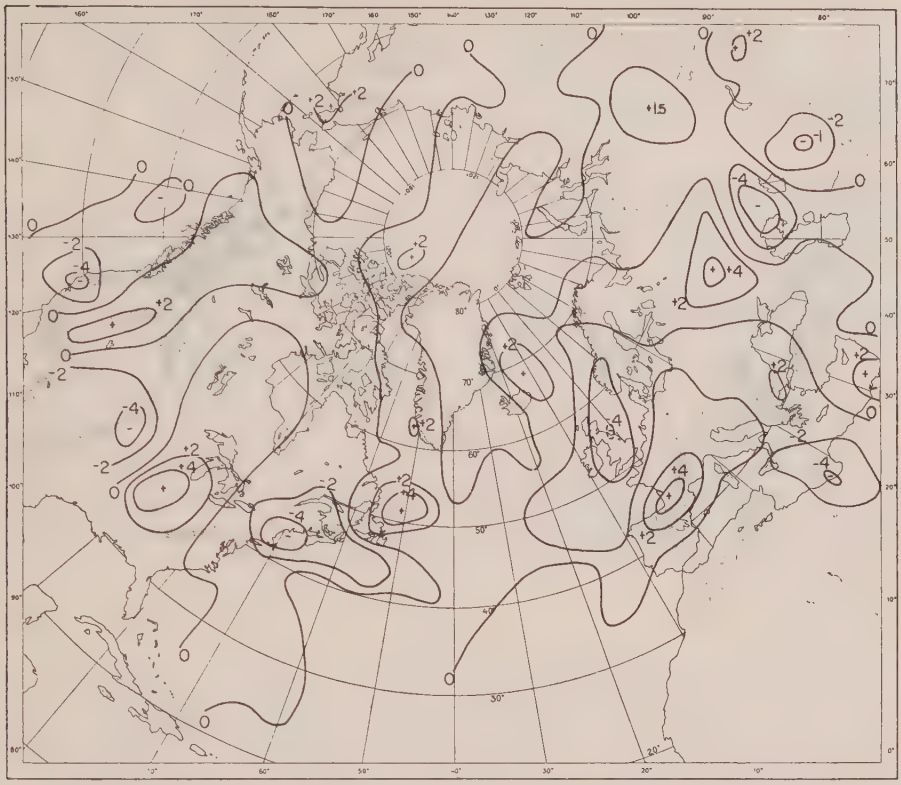

Fig. 2. Horizontal distribution of vertical motion in cm sec^{-1} computed 850, 500, and 300 mb heights using a two-parameter baroclinic model. Time as in figure 1.

$$\omega = q + q^{(1)} + \frac{1}{2} q^{(1)\,(2)} + \frac{1}{5} q^{(1)\,(2)\,(3)} \quad (4.17)$$

and compute q by the approximate relation

$$q = -\frac{2}{65} \mathbf{J}(\nabla^2 z, T) \simeq \frac{5}{4} \mathbf{J}(z - \bar{z}, T) \quad (4.18)$$

where it is understood that $(z - \bar{z})$ in the last expression is measured in decameters.

5. An example of horizontal distribution of ω

A test of the formula developed in the preceding section was made by computing ω using the method and compare the obtained distribution with the corresponding distribution obtained from a baroclinic model.

The two data fields used for the approximate solution were the height and temperature fields for the 500 mb surface for January 2, 1956, 0300Z.

The baroclinic vertical velocity was obtained from a model using the height fields for 850, 500 and 300 mb as initial data.

Fig. 1 and 2 give the two distributions, where fig. 1 is the approximate solution. It is seen that all maxima and minima which appear on one of the figures can be found on the other. There are some differences in the configurations, but the agreement is in general good, when it is realized that the two fields are computed from different, although not independent, data.

It should finally be mentioned that the graphical method naturally also can be formulated in such a way that the two fields used in the computation are a height field and a thickness fields.

6. Summary and conclusions

A simple, but consistent form of an equation for the vertical velocity is analyzed in section 2.

It is found that the dominating term in the forcing function is the advection of temperature in the field of isolines for relative vorticity. A simple rule from which the sign of the vertical velocity may be determined is formulated.

Section 3 contains a method for solving a Helmholz-equation similar to the one developed by Fjørtoft for a Poisson-equation and using a variable gridsize.

The accuracy of the solution is computed in section 4, which also contains a comparison between the solution and one obtained without varying the gridsize.

An example is shown in section 5.

The method developed in this paper to obtain the horizontal distribution of the vertical velocity will be of use in cases, where the distribution is not available from integration of a baroclinic model of the atmosphere. The main advantage of the method is that it can give instantaneous values of the vertical velocity. Local values of the vertical velocity can easily be obtained without laborious graphical manipulations.

REFERENCES

Eliassen, A., 1956: Lectures on Physical Weather Prediction, University of California, Los Angeles.

Fjørtoft, R., 1952: On a Numerical Method of Integrating the Barotropic Vorticity Equation, *Tellus*, **4**, pp. 179—194.

— 1955: On the Use of Space-Smoothing in Physical Weather Forecasting, *Tellus*, **7**, pp. 462—480.

Siggtryggsson, H., and Wiin-Nielsen, A., 1957: Experiments in Numerical Forecasting Using Space-Smoothed Fields, *Tellus*, **9**, pp. 296—312.

Smebye, S. F., 1958: Computation of Precipitation from Large-Scale Vertical Motion, *Journal of Meteorology*, **15**, pp. 547—560.

Wiin-Nielsen, A., 1959: On Certain Integral Constraints for the Time-Integration of Baroclinic Models, *Tellus*, **11**, pp. 45—59.

The Horizontal and Vertical Wind Profiles of the Subtropical and Polar Jet for January 1—7, 1956 and the Variation of the Equivalent Barotropic Level

By HESSAM TABA

International Meteorological Institute, University of Stockholm[1]

(Manuscript received May 30, 1959)

Abstract

All the available wind information over central, west and north Europe, the Atlantic Ocean, the United States and Canada has been studied for a period of seven days, January 1—7, 1956 0300 Z. The axis of the subtropical and the polar jets have been chosen as reference coordinates. Mean horizontal and vertical wind profiles have been computed at 100 km intervals from the axis of both jets and are discussed. Based on these profiles, the average wind and the equivalent barotropic level is computed. It is shown that the height of the equivalent barotropic level changes as the distance from the axis of the jet varies. The equivalent barotropic level is shown to have a maximum height of 432 mb at the axis of the subtropical jet and a minimum height of 560 at a distance of 1,000 km north of the polar jet. Finally, an average E.B.L. is computed and is shown to have a height of 505 mb.

Part I

Introduction

In a series of recent articles DEFANT and TABA (1957—1958) have studied changes in the type of general circulation by means of tropopause maps. It was shown that hemispheric tropopause maps were most suitable for depicting changes in the three dimensional structure of the atmosphere. The authors had also emphasized the close relation between the breaks of the tropopause height and the main wind belts. It has also been demonstrated that the vertical structure of the atmosphere is quite different on either sides of the two jets and that the subtropical and polar jet divided the atmosphere into three distinct parts with different characteristics. The conservative properties of the atmosphere on either side of the jets suggest that in statistical studies of the large scale atmospheric motion the most suitable reference coordinate would be the axis of the jets. In the first part of this paper the horizontal and vertical wind profiles north and south of the two jets are presented. It should be stressed since all the wind information used in this study is what was available for the part of the hemisphere mentioned, one can say for sure that the average values obtained are at least a good representation of the mean motion of the atmosphere for this period of the year.

[1] This report is part of investigation on the General Circulation of the Atmosphere, with special emphasis on upper atmospheric layers, sponsored by Air Research and Development Command USAF, under Contract AF 61 (514)—963, through the European Office, ARDC in Brussels.

Preparation of the material

All available wind information for a period ofs even days, January 1—7, 1956 0300 GMT has been plotted. This covers the area of the United States, Canada, the Atlantic Ocean, North, West, and Central Europe and North Africa. A total number of 950 stations have been studied which means about 132 stations per day. The following procedure has been followed:

1) With the help of pressure maps of 850, 500, 300, 200 and 100 mb and tropopause maps, the position of the axis of both the polar and the subtropical jet has been located.

2) These jets are used as coordinates of reference. The horizontal distance of every station from the axis of the jet has been measured. Here the map factor is $m = \frac{1+\sin 50}{1+\sin \varphi_m}$ where φ_m is the latitude of the half of the distance from the station to the jet axis.

3) For each isobaric level the wind speed of each station has been plotted on a diagram with the distance from the jet axis as one coordinate and the speed as the other coordinate. In this way a point cloud distribution has been obtained. For the sake of presentation one of these levels, namely the 250 mb (subtropical jet), is presented in Fig. 1. As one can see, the number of points are quite different within each 100 km horizontal distance. This means that the value of the mean speed computed is based on different number of observations.

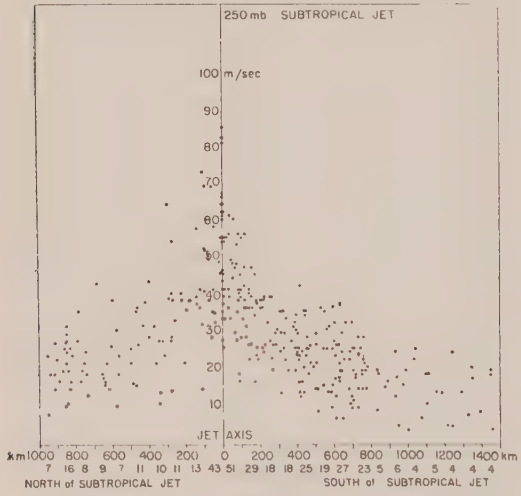

Fig. 1.

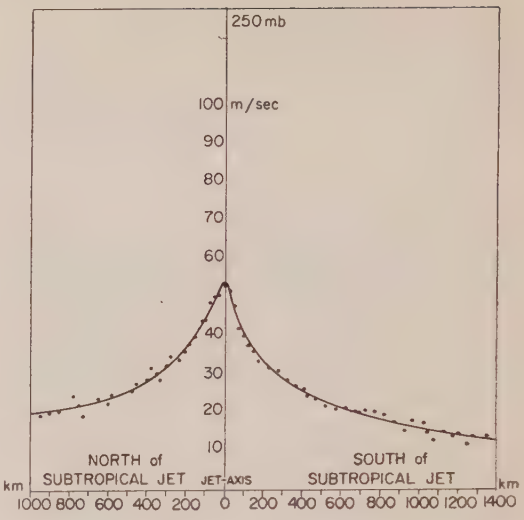

Fig. 2. The mean wind at 250 mb as a function of distance from the axis of the subtropical jet. The horizontal axis shows distances in km and the vertical axis the speed in m/sec.

It is quite clear from the figure that for example within a certain horizontal distance, say 100 km, on either side of the jet, one finds quite a different range of speeds. This is an indication of the fact that in this case the subtropical jet has been more intense in some regions of the northern hemisphere and relatively weaker in other regions and at other times.

Fig. 2 represents the mean wind as a function of distance from the jet. Within every 50 km horizontal distance the average wind speed has been computed. To obtain a more smooth profile, a further average is computed covering a horizontal distance of 100 km. It should be mentioned that as there were not enough wind observations at heights above 50 mb, it was decided not to continue above this level.

Horizontal wind profiles

1. *The subtropical jet*

Figs. 3 and 4 show the horizontal wind profiles for the subtropical jet for different isobaric levels. The following are important points which deserve considerations.

a) The strongest wind to be observed in these two figures is about 55 meter per second

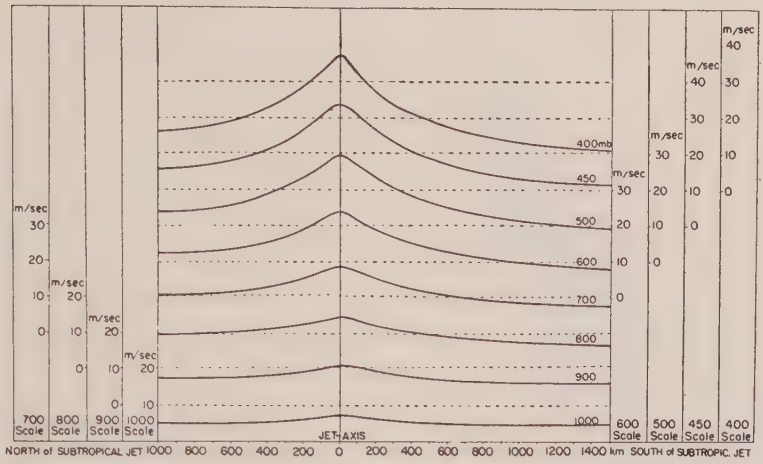

Fig. 3. The horizontal wind profile of the subtropical jet 1000—400 mb.

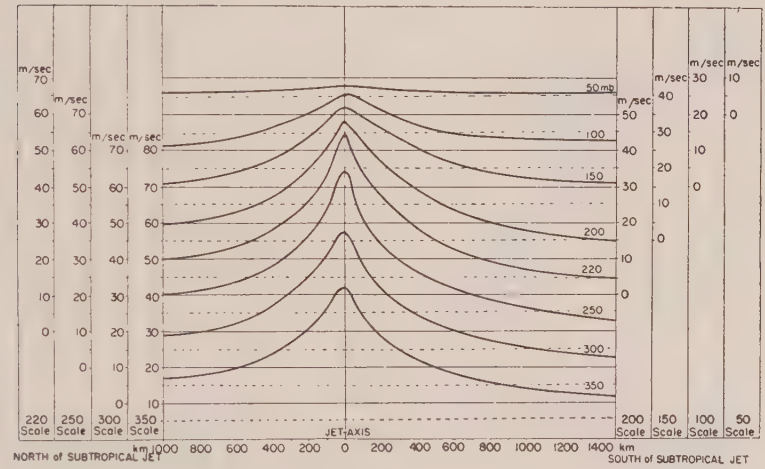

Fig. 4. The horizontal wind profile of the subtropical jet 350—50 mb.

and at the level of 220 mb. However, this is not the level of maximum wind. The level of maximum wind is at about 228 mb with a speed of 58—60 m/sec.

b) At each level the shear is strongest near the axis of the jet and decreases away from it. The strongest shear is found on the southern side of the subtropical jet.

c) As seen from the figures, towards south the wind profiles reach a horizontal distance of 1,500 km while towards north it does not exceed 1,000 km. The reason for this difference is that the space north of the subtropical jet was occupied partly by the polar jet as well. This means that the intermediate area between the two jets was covered by stations some of which belonged to north of the subtropical jet and the rest to south of the polar jet.

2. *The polar jet*

Figs. 5 and 6 show the horizontal wind profiles for the polar jet for different isobaric levels. Here are some noteworthy points:

a) The strongest wind to be observed in these two figures is about 50 m/sec at the 300 mb level. This is not really the level of maximum wind. The maximum wind is about

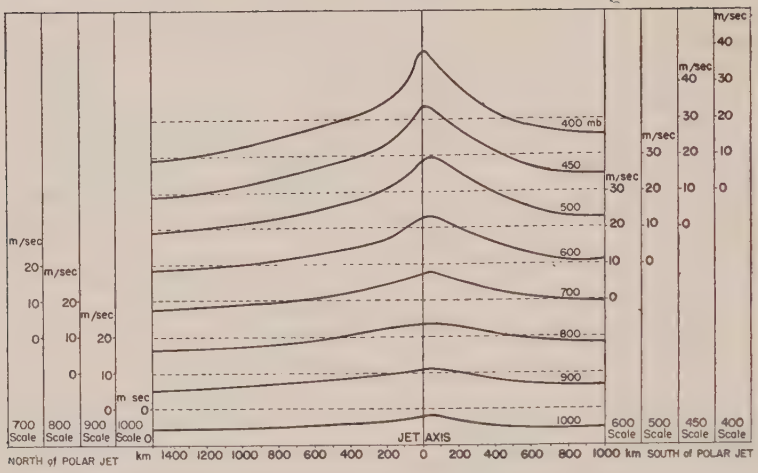

Fig. 5. The horizontal wind profile of the polar jet 1000—400 mb.

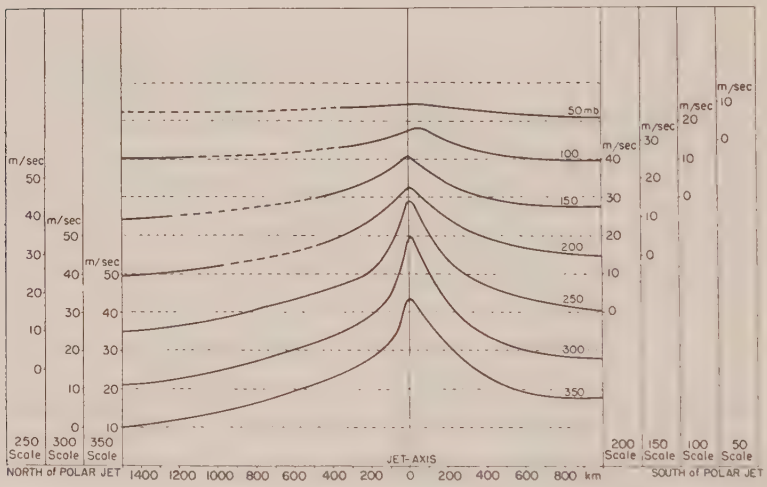

Fig. 6. The horizontal wind profile of the polar jet 350—50 mb.

53 m/sec and the height at which it is observed is at about 295 mb.

b) Near the axis of the polar jet the horizontal shear is much more pronounced than at distances further away from the jet. Observe the relatively much stronger shear on the *northern* side of the jet.

c) In the case of the polar jet, the wind profile to the north extends to a horizontal distance of 1,500 km while towards the south it reaches only to 1,000 km. The reason for this is exactly what was mentioned for the subtropical jet.

d) The profiles of 200, 150, 100, 50 mb have some dashed parts towards the north. This is to show that at these levels the data studied was not quite enough and reliable.

e) Notice the displacement of the strongest wind towards the south at the levels 400, 500, 600 and 700 mb. Fig. 5.

Vertical wind profiles

1. *South of the subtropical jet*

Fig. 7 shows the vertical wind profiles of south of the subtropical jet. The numbers

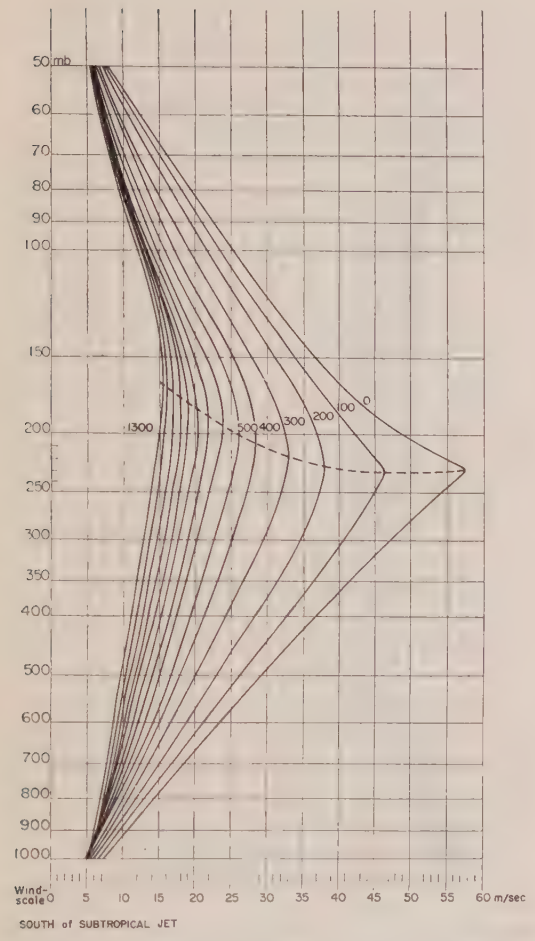

Fig. 7. The vertical wind profiles south of the subtropical jet. The number on each profile indicates the distance from the jet axis. Observe the increase of the height of maximum wind towards south.

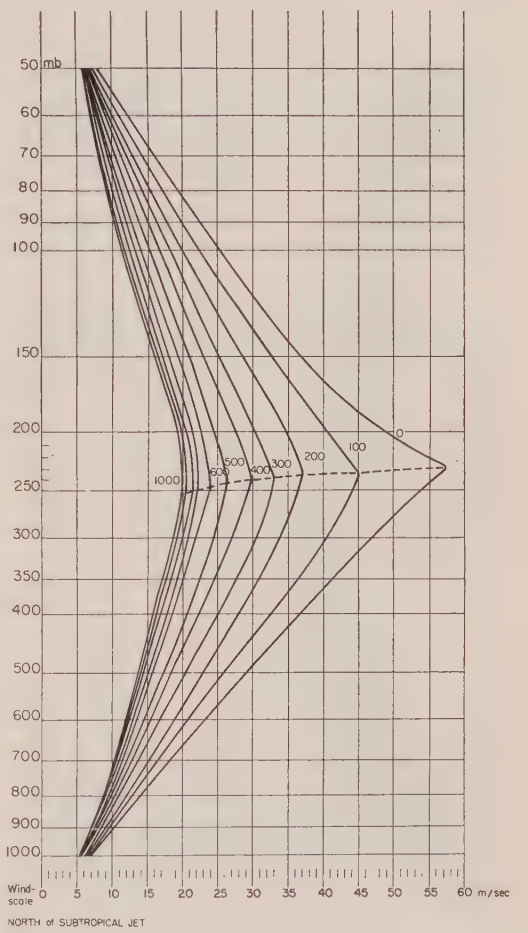

Fig. 8. The vertical wind profile north of the subtropical jet. Observe the decrease of the height of maximum wind towards north.

on each profile indicate the distance from the axis of the jet. Here are some interesting features:

a) As mentioned before, the strongest wind observed is about 58 m/sec at the level of 228 mb and at the axis of the jet.

b) The decrease of the wind with the distance from the axis of the jet is much more pronounced in the middle troposphere than at lower and higher levels.

c) Notice the increase of the height of maximum wind as one goes further towards the south. This is indicated by the dashed line.

2. *North of the subtropical jet*

Fig. *8* shows the vertical wind profiles north of the subtropical jet. There is a difference between this profile and the one to the south. This is the decrease of the height of maximum wind as one goes from the center of the jet towards the north as indicated by dashed lines.

3. *South and north of the polar jet*

Figs. *9* and *10* show the vertical wind profiles south and north of the polar jet.

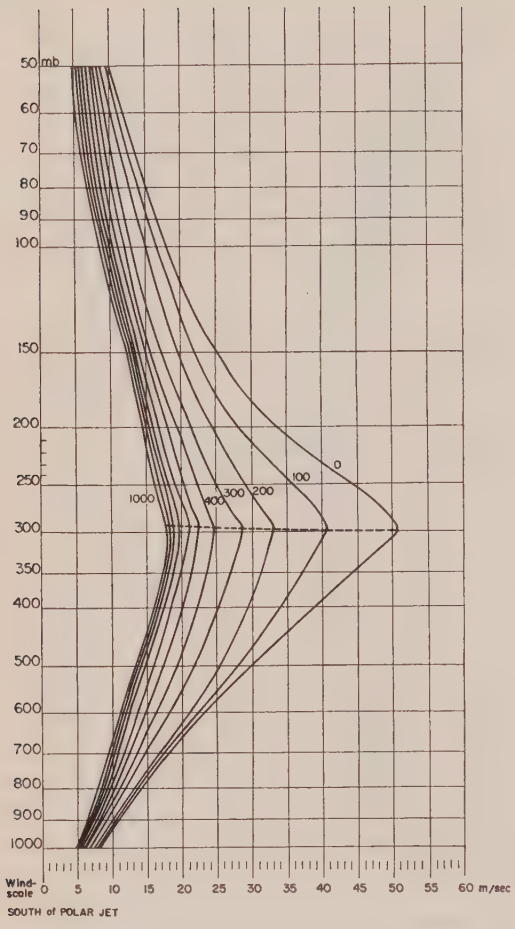

Fig. 9. The vertical wind profile south of the polar jet. The height of the maximum wind increases towards south.

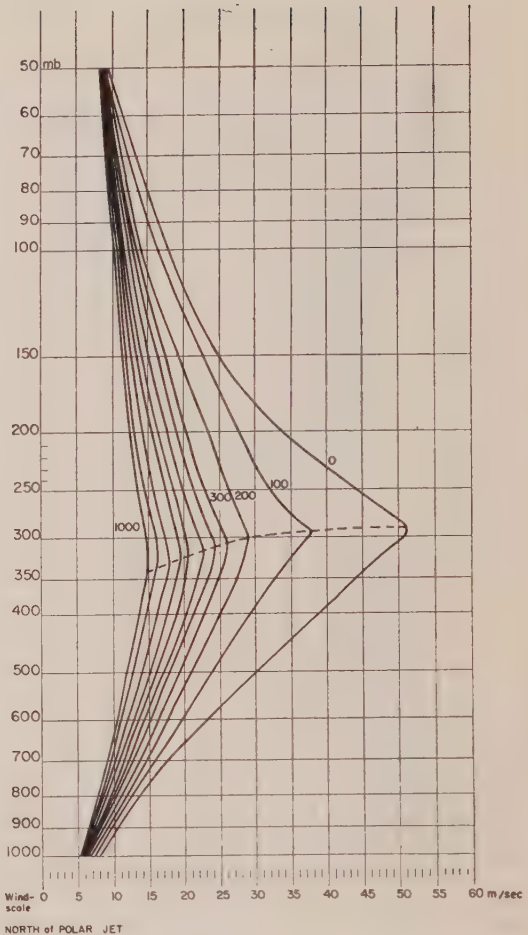

Fig. 10. The vertical wind profile north of the polar jet. The height of the maximum wind drops with the distance from the axis of the jet.

a) The strongest wind is about 52 m/sec and at a height of 295 mb.

b) The horizontal shear is strongest near the jet axis, the difference becomes less the further the distance increases. This is even noticed in the middle of the troposphere.

c) The height of the maximum wind increases towards south and decreases northward as indicated by the dashed line.

Conclusions and some discussion of the results

Before starting to draw any conclusions, it should be clearly mentioned that what follows is based on the average values obtained from a statistical treatment of seven days of wind data. As we know, the wind speed is far from being uniform along the axis of the two jets. This is seen when plotting the wind speed of different stations having the same distance from the jet at the same level. However, much more regular variations are observed along an axis perpendicular to the jet. This is the reason why in this study the axis of the jets has been chosen as reference coordinates. As the fluctuations of the jet axis means the advection of different air masses it seems in order to obtain any coherent picture of the large scale motions one simply has to follow the jets.

From this study of the assemblage of upper air data and as far as this statistical result can support the conclusions, one can say that the average maximum speed of *polar* jet is about

50 m/sec for *winter* and this maximum is located at an average height of 300 mb. For the *subtropical* jet the value obtained is around 60 m/sec at a height of 220—230 mb.

DEFANT has computed (1959 to be published) the average wind maximum at the axis of the *subtropical* jet for a period of 6 days in the summer (July 15—20, 1957). He has obtained a value of about 70 m/sec. As one can see, this value is about 10 m/sec more than the winter average obtained in this study.

This may be somewhat surprising and the major question is whether it may be due to the fact that no data from Asia and particularly Japan have been included in this study (as pointed out by Professor E. PALMÉN). In view of the quite large difference obtained it seems, however doubtful, whether this is sufficient to explain this reversed seasonal variation.

If for a moment we accept the idea that the maximum average subtropical jet is stronger in summer than in winter and then search for the mechanism which is responsible for this difference, we see that:

1) In the mean meridional cross sections constructed by DEFANT (DEFANT 1959 to be published) for the same period as the wind was computed, he finds that the subtropical front separating the subtropical air from middle air is much stronger in summer than winter. Now the question is whether the solenoidal field which goes together with this front can be an indication of the strong wind field. As the value of the average wind obtained from this study is not very different from what is needed for the geostrophic balance, it seems that the increase of the wind maximum of the jet could be related to the existing horizontal temperature field of the subtropical front. However, it is difficult to identify and isolate the cause and effect.

2) The second essential difference between Defant's summer profile and this winter profile is that in summer the level of zero wind is at a height of 80 mb and from there upward the winds are from east whereas in the winter the speed at 50 mb still is not less than 10 m/sec. Evidently this decrease of the height of the easterlies in summer relative to winter is due to the fact that in summer the subtropical jet is on the average in much higher latitude than in winter. Consequently, the reversed horizontal temperature field in the stratosphere is more intense. It seems possible that this decrease of the thickness of the layer of westerlies in summer relative to winter might be the cause of redistribution of existing momentum and as a result the sharpness of the peak.

Part II

Introduction

It was ROSSBY's suggestion (1939), that the large scale atmospheric motions could be considered as two dimensional and non-divergent. Following this hypothesis CHARNEY (1949) formulated the problem more precisely. In his study Charney uses the simplified vorticity equation

$$\frac{\partial \zeta}{\partial t} + \mathbf{v} \cdot \nabla \eta = f \frac{\partial \omega}{\partial p} \qquad (1)$$

with the boundary conditions

$$\omega = 0 \text{ at } P = 0 \text{ and } P = P_0$$

Here $\eta = f + \zeta$ is the absolute vorticity and ∇ indicates $\mathbf{i}\frac{\partial}{\partial x} + \mathbf{j}\frac{\partial}{\partial y}$ where $\mathbf{i}$, $\mathbf{j}$ are unit vectors.

Furthermore he assumes that in studying large scale atmospheric motions, the wind increases in magnitude with height while the pattern of the streamlines remains almost the same from level to level. In other words the wind at any level is given by the relation

$$\mathbf{v} = A(p) \cdot \bar{\mathbf{v}} \qquad (2)$$

where $\bar{\mathbf{v}}$ is defined as

$$\bar{\mathbf{v}} = \frac{1}{p_0} \int_0^{p_0} \mathbf{v} \cdot dp \qquad (3)$$

we also have $\zeta = A(P)\bar{\zeta}$. Introducing this into the vorticity equation (1) and integrating over the whole atmosphere, we can eliminate ω and obtain the prognostic equation

$$\frac{\partial \bar{\zeta}}{\partial t} + \overline{A^2}\,\bar{\mathbf{v}} \cdot \nabla \bar{\zeta} + \bar{\mathbf{v}} \cdot \nabla f = 0$$

Using (2) and (3) one gets

$$\frac{\partial \zeta}{\partial t} + \frac{\overline{A^2}}{A}\mathbf{v} \cdot \nabla \zeta + \mathbf{v} \cdot \nabla f = 0$$

This equation indicates that there must be a certain intermediate level (or levels) where

the ratio $\frac{\overline{A^2}}{A}=1$ and all vorticity changes are the result of advection. If such a level exists, the motion at this level can be said to be non-divergent. This intermediate level is very often mentioned to be in the vicinity of 500 mb. It is the purpose of this work to study the accuracy of this assumption and to find out the horizontal variation of the so-called equivalent barotropic level.

The equivalent barotropic level

From each vertical wind profile the average wind is computed. In evaluating the integral

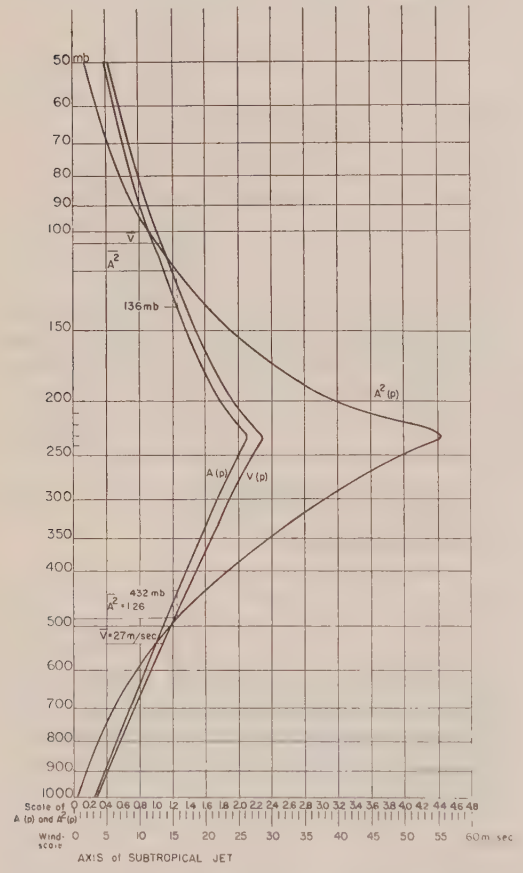

Fig. 11. The vertical wind profile at the axis of the subtropical jet together with the profiles of $A(p)$ and $A^2(p)$. The mean wind is indicated by $\overline{v}=27$ m/sec. The equivalent barotropic levels are at 432 and 136 mb respectively. $\overline{A^2}=1.26$. The wind speed is given in m/sec along the horizontal axis. The scale of $A(p)$ and $A^2(p)$ is also indicated along the horizontal axis.

(3) use has been made of the so-called trapezoidal rule. Due to the vertical wind structure, there are naturally two levels at which the wind and the average wind have the same value. By dividing the wind at any level by the mean wind the profile of $A(p)$ and by multiplying the A value by itself $A^2(p)$ is obtained. Finally using a similar integral as (3) the value of $\overline{A^2}$ is computed.

Fig. *11* shows the vertical wind profile at the axis of subtropical jet together with the graphs of the function $A(p)$ and $A^2(p)$. For this profile the mean wind is 27 m/sec and the corresponding heights are at 540 and 106 mb. The value of $\overline{A^2}=1.25$ and the levels at which $\overline{A^2}=A$, that means the equivalent barotropic levels, are at 432 and 136 mb respectively.

The computation has been repeated for all wind profiles to the south and north of the subtropical jet and distances of 100 km. As one would expect, away from the axis of the jet, $\overline{v}$, $A(p)$, $A^2(p)$, $\overline{A^2}$ and the height of the equivalent barotropic level all vary. The details of this variation is tabulated in the following table.

Fig. *12* shows the wind profile at the axis of the polar jet together with the functions $A(p)$ and $A^2(p)$. As the graph of $A(p)$ and the wind profile coincide in all the levels, both are represented by the same curve. The mean wind for this profile is 25 m/sec. The levels at which the wind is equal to the mean wind is at 570 and 144 mb. In this case $\overline{A^2}=1.26$ and the corresponding equivalent barotropic levels are at 485 and 188 mb respectively. In the case of polar jet as well, the height of the equivalent barotropic level changes as the distance from the axis of the jet increases. The details of these variations are also presented in table 1.

The variation of the height of equivalent barotropic level

Table 1 contains four different parts:

a) South of the subtropical jet
b) North of the subtropical jet
c) South of the polar jet
d) North of the polar jet

The details of variations of $\overline{v}$, $\overline{A^2}$ and the heights of E.B.L. can be studied from table 1.

Discussion of the results

To obtain a general picture of how the lower equivalent barotropic level varies in the space Fig. *13* is presented. The important features of this figure are:

1) In the average the equivalent barotropic level has a higher altitude for the wind structure which represents subtropical jet than the polar jet.

2) At the axis of both jets, the equivalent barotropic level has its maximum height.

3) Away from the axis of the subtropical jet on either side, the height of the E.B.L. decreases rapidly at first and slowly later on.

4) Towards the north of the polar jet, the height of the E.B.L. decreases rapidly first and less rapid later on.

5) To the south of the polar jet the level drops rather sharply at first, and slower later on until 600 km horizontal distance is reached. From there on the height of E.B.L. increases again. It seems that this increase should continue so much that the E.B.L. to the south of the polar jet joins the part to the north of the subtropical jet in such a way that there is no discontinuity in between.

General Conclusions

From this study one can easily see to what extent the assumption that 500 mb is the equivalent barotropic level is correct. The

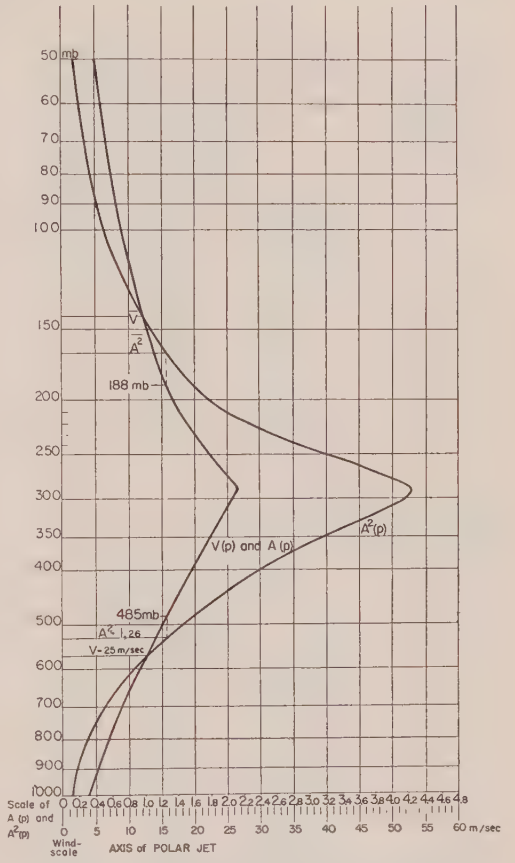

Fig. 12. The vertical wind profile at the axis of the polar jet together with the function $A^2(p)$. Notice that as the profile of $v(p)$ and $A(p)$ coincide in all levels, they are both given by the same curve. Here $\overline{v} = 25$ m/sec. $\overline{A^2} = 1.26$ and the equivalent barotropic levels are at 485 and 188 mb respectively.

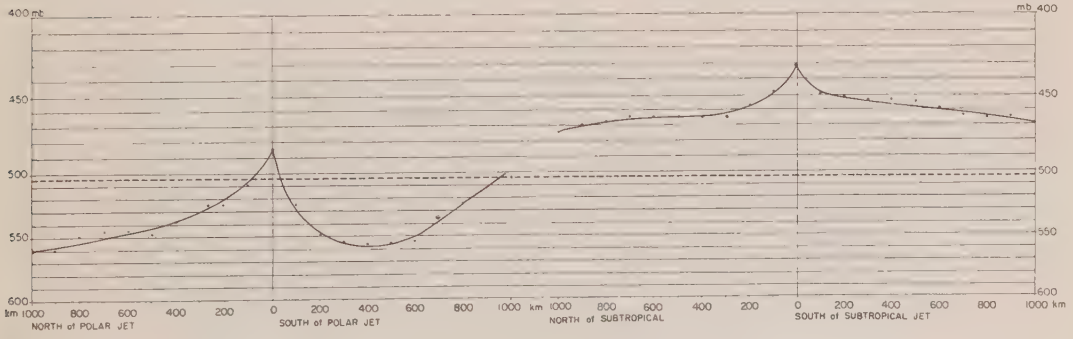

Fig. 13. The variation of the height of the equivalent barotropic level. Axis of the two jets are indicated by the two vertical lines. The dashed line indicates the height of the mean equivalent barotropic level.

Table 1

SOUTH OF SUBTROPICAL JET

distance from jet km	$\overline{A^2}$	lower E.B.L.	upper E.B.L.	$\overline{v}$ m/sec
0	1.26	432 mb	136 mb	27.0
100	1.22	450 "	113 "	23.9
200	1.20	452 "	111 "	20.4
300	1.19	454 "	111 "	18.2
400	1.17	454 "	111 "	16.5
500	1.17	455 "	111 "	15.1
600	1.43	460 "	108 "	14.0
700	1.13	464 "	106 "	13.0
800	1.11	465 "	101 "	12.3
900	1.11	465 "	100 "	11.6
1000	1.10	470 "	89 "	11.0

NORTH OF SUBTROPICAL JET

distance from jet km	$\overline{A^2}$	lower E.B.L.	upper E.B.L.	$\overline{v}$ m/sec
0	1.26	432 mb	136 mb	27.0
100	1.24	449 "	131 "	23.6
200	1.21	459 "	127 "	20.5
300	1.19	465 "	127 "	18.5
400	1.18	465 "	123 "	16.8
500	1.17	465 "	121 "	15.4
600	1.14	465 "	120 "	14.5
700	1.13	465 "	120 "	13.6
800	1.13	468 "	120 "	13.0
900	1.12	470 "	120 "	12.8
1000	1.11	474 "	120 "	12.7

SOUTH OF POLAR JET

distance from jet km	$\overline{A^2}$	lower E.B.L.	upper E.B.L.	$\overline{v}$ m/sec
0	1.26	485 mb	188 mb	25.0
100	1.12	525 "	191 "	22.6
200	1.11	550 "	185 "	20.1
300	1.14	555 "	183 "	17.4
400	1.13	556 "	180 "	15.7
500	1.12	556 "	168 "	14.3
600	1.11	555 "	165 "	13.4
700	1.10	535 "	157 "	12.6
800	1.11	525 "	158 "	12.2
900	1.12	512 "	160 "	11.8
1000	1.13	505 "	161 "	11.7

NORTH OF POLAR JET

distance from jet km	$\overline{A^2}$	lower E.B.L.	upper E.B.L.	$\overline{v}$ m/sec
0	1.26	485 mb	188 mb	25.0
100	1.16	510 "	168 "	20.6
200	1.14	515 "	167 "	17.7
300	1.13	515 "	165 "	16.3
400	1.12	528 "	164 "	15.2
500	1.10	538 "	165 "	14.4
600	1.10	545 "	160 "	13.4
700	1.09	545 "	147 "	12.6
800	1.08	550 "	145 "	11.7
900	1.07	560 "	135 "	11.0
1000	1.06	560 "	118 "	10.4

E.B.L. computed from this seven days mean has a maximum height of 432 mb and a minimum height of 560. This amounts to a difference of 128 mb or approximately 1,800 meters. It should be remembered that 130 mb is based on the average winds of seven days. This might be considerably less than what one may encounter in the study of a single day. From this discussion one can also say that the gradient of vorticity in the prognostic

Table 2

Pressure mb	1000	950	900	850	800	750	700	650	600	550
$\frac{\overline{A^2}}{\overline{A}}$	3.03	2.50	2.14	1.89	1.70	1.52	1.41	1.30	1.19	1.08

Pressure mb	500	450	400	350	300	250	200	150	100	50
$\frac{\overline{A^2}}{\overline{A}}$	1.00	0.91	0.84	0.77	0.72	0.73	0.77	0.93	1.21	2.38

equation should be multiplied by a different wind than what the equation suggests in different regions of the map. At least part of the inaccuracy of the results of barotropic forecasts can be due to incorrectness of the assumption that 500 mb is the E.B.L.

As one should expect, the greatest error in forecasts can be made over the regions of the map where the subtropical jet approaches the polar jet, as in these regions the height of the E.B.L. changes very much within a rather short horizontal distance.

To get an idea where the *mean* equivalent barotropic level is, a mean profile of $A(p)$ and $A^2(p)$ from all the individual values has been constructed. Fig. *14* shows the functions of $A(p)$ and $A^2(p)$. From the figure one can see that the level at which $A = \overline{A^2}$ is equal to 505 mb and 135 mb respectively.

One can conclude by saying that as long as we use such a simple model and so far as we cannot include the horizontal variation of the function A into the equation, the 500 mb is the closest approximation to the non-divergent level.

Finally, the ratio $\frac{\overline{A^2}}{A}$ computed from the profile of mean $A(p)$ and $A^2(p)$ is tabulated and given in Table 2. It is possible to apply the equivalent barotropic model at any level provided the advection of the gradient of the vorticity is multiplied by the factor $\mathbf{v} \cdot \frac{\overline{A^2}}{A}$ corresponding to that level.

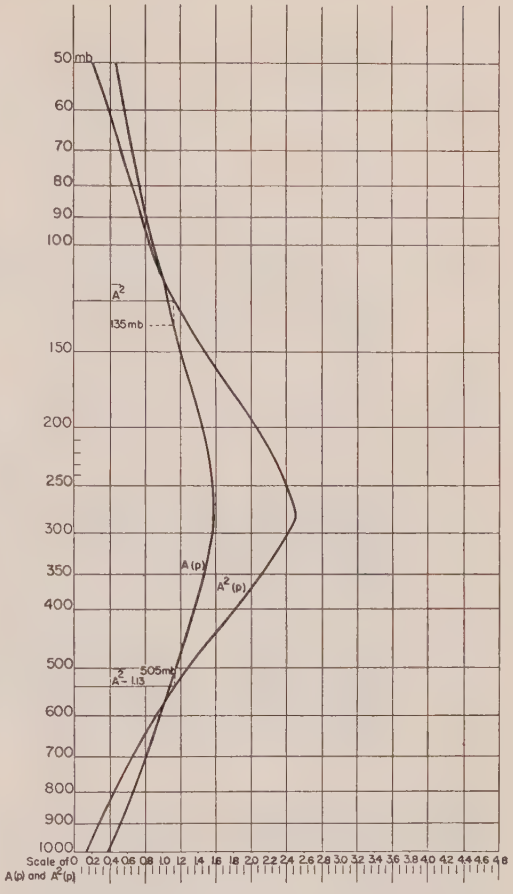

Fig. 14. The profiles of mean $A(p)$ and $A^2(p)$. The level at which $\overline{A^2} = A$ is 505 mb and 135 mb respectively. The mean $\overline{A^2}$ is equal to 1.13.

Acknowledgement

I would like to express my thanks to Dr. B. Bolin for suggesting the study of this problem and to Professor Friedrich Defant for the stimulating discussions throughout the work.

REFERENCES

Charney, J. G., 1949: On a physical basis for numerical prediction of large-scale motions in the atmosphere. *J. Met.* **6**, No. 6.

Defant, Fr., and Taba, H., 1957: The threefold structure of the atmosphere and the characteristics of the tropopause. *Tellus* **9**, pp. 259—274.

— 1958: The details of wind and temperature field and the generation of the blocking situation over Europe. *Beitr. z. Physik d. Atmosphäre.*

— 1958: The strong index change period from January 1 to January 7, 1956. *Tellus* **10**, pp. 225—242.

— 1958: The break down of zonal circulation during the period January 8—13, 1956, the characteristics of temperature field and tropopause and its relation to atmospheric field of motion. *Tellus* **10**, pp. 430—450.

Rossby, C.-G. et al., 1939: Relation between the intensity of the zonal circulation of the atmosphere and the displacements of the semipermanent centers of actions. *J. Mar. Res.* **2**, No. 1.

The Diurnal Variation of the Wind

By G. J. HALTINER, U.S. Naval Postgraduate School, Monterey, California

(Manuscript received March 9, 1959)

Abstract

The equations of motion are numerically integrated under assumptions which represent the diurnal variation of the wind. The coefficient of eddy viscosity varies periodically with time as well as nonlinearly with height. The time variation is represented by two trigonometric terms giving a 20-fold change between maximum and minimum eddy viscosity. Several different functions were used to depict the vertical variation of the eddy viscosity, among which were an increasing, but bounded, exponential function, and also an exponential function which first increased with height and then decreased to a residual value. The boundary conditions imposed were, firstly, that the wind vanishes (or approaches a constant value) at the lower boundary; and, secondly, that the wind becomes geostrophic at some arbitrarily selected upper level.

The solutions were in general agreement with observed data and showed the spiral characteristic of the planetary boundary layer. However, there is disagreement between theory and observation in some important features.

1. Introduction

The wind structure in the lowest several thousand feet is of interest in large-scale processes as well as in micrometeorology. Because of the difficulties involved in attempting to obtain analytical solutions to the general Reynolds' equations for turbulent motion, various simplifying assumptions have been devised. The introduction of a coefficient of eddy viscosity K has provided a substantial simplification. Moreover, the layer of frictional influence has been subdivided into the laminar, surface, and spiral layers, each possessing certain characteristic properties. Steady state analytical solutions have been provided for the spiral layer, or the combined surface-spiral layers, for which K is a constant or a simple function of height. More recently, BUAJITTI and BLACKADAR (1957) have provided numerical solutions for the case of a coefficient of eddy viscosity which varies periodically with time as well as with height. By expressing vertical variations of the variables as finite difference ratios, the partial differential equations are reduced to a system of ordinary differential equations, which, in turn, is solved by electrical analogue. The accuracy of such results will ordinarily increase with decreasing size of the increment of height over which the derivatives are approximated by finite differences. On the other hand, decreasing the height interval increases the number of equations necessary to represent a given layer, thus requiring a greater number of integrators and potentiometers in the analogue computer. Buajitti and Blackadar were able to consider 5 levels, the first and last of which were specified boundary conditions. A two-fold time variation of the coefficient of eddy viscosity was provided by a single cosine term, while the vertical variation consisted of a nonlinear decrease or increase with height. Empirical data (for example, see MILDNER 1932) indicates that the coefficient of eddy viscosity first increases with height, reaching a maximum near 250 meters; and then it decreases to a residual value. Observations of the coefficient of eddy conductivity (1956) indicate diurnal variations between 10 and 100-fold (depending on the height) which require two

or more trigonometric terms for representation. In order to provide such variations in the eddy viscosity, a very large analogue computer would be needed. Buajitti and Blackadar essentially deal with the upper portion of the friction layer and show that better agreement is obtained between theory and observation when both the mean eddy viscosity and its diurnal variation decrease with height.

It was the purpose of this investigation to consider theoretical solutions for the diurnal variation of the wind which provide for a greater resolution and range in the vertical. Because of the complexity of the differential equations, numerical solutions were sought by means of CRC 102A electronic digital computer.

2. The Fundamental Equations

Since we are primarily concerned with the diurnal variation of the wind in the friction layer, horizontal differences are to be neglected and also the vertical variation of the geostrophic wind. Hence the equations of motion may be written in the form

$$\begin{aligned} \frac{\partial U}{\partial \tau} &= fV + \frac{\partial}{\partial Z}\left(K\frac{\partial U}{\partial Z}\right) \\ \frac{\partial V}{\partial \tau} &= f(V_g - U) + \frac{\partial}{\partial Z}\left(K\frac{\partial V}{\partial Z}\right) \end{aligned} \tag{1}$$

where U and V are the horizontal velocity components; f, the Coriolis parameter; K, the kinematic coefficient of eddy viscosity; and V_g is the geostrophic wind. For a simpler and broader interpretation of results, the following transformation of coordinates is made:

$$\begin{aligned} \tau &= \sigma t & Z &= 100qz \\ u &= U/V_g & v &= V/V_g \end{aligned} \tag{2}$$

The transformed equations are

$$\begin{aligned} \frac{\partial u}{\partial t} &= \sigma f v + \frac{10^{-4}\sigma}{q^2}\frac{\partial}{\partial z}\left(K\frac{\partial u}{\partial z}\right) \\ \frac{\partial v}{\partial t} &= \sigma f(1-u) + \frac{10^{-4}\sigma}{q^2}\frac{\partial}{\partial z}\left(K\frac{\partial v}{\partial z}\right) \end{aligned} \tag{3}$$

The boundary conditions imposed are that the wind vanishes (or is constant) at some reference level, $z=0$, presumably at or near the ground; and secondly, that the wind becomes geostrophic at an arbitrarily selected upper level. Thus

$$\begin{aligned} u &= 0, & v &= 0, & &\text{at } z = 0 \\ u &= 1, & v &= 0, & &\text{at } z = z_n \end{aligned} \tag{4}$$

The coefficient of eddy viscosity is assumed to have the form

$$K = g(t)\ k(z) \tag{5}$$

where

$$g(t) = 1 + b\ (\sin \omega t + c \sin 2\omega t) \tag{6}$$

Several different forms were tried for $k(z)$

$$k_1 = q^2 a_1[1 - a_2 \exp(-10^2\, a_3 q z)] \tag{7}$$

$$k_2 = q^2 a_1\{a_4 + a_5 \exp[-10^4\, a_6 q (z - z_m)^2]\} \tag{8}$$

With the exception of a_2, the a_i, b, c, and ω are constants chosen to give a variation of K comparable to observed values. Two different choices were made for a_2; in Case 1, a_2 is constant; in Case 2, a_2 is of the form $a_2 = a_2' + a_2''(\sin \omega t + c \sin 2\omega t)$. The latter choice gives a greater variation of K with height during the time when K is maximum. Estimations (Staley, 1956) of the coefficient of eddy conductivity have indicated a 100-fold increase with height during the daytime, but only a 10-fold increase during night-time. A similar variation may apply to the eddy viscosity.

The second form $k_2(z)$ gives a K which first increases with height, reaching a maximum at z_m, then decreases and becomes essentially constant at still greater heights. Such a distribution is similar to that found by Mildner (1932).

For purposes of solving the equations numerically, the vertical derivatives of Equation (3) may be replaced by centered finite differences, giving the system of equations

$$\begin{aligned} \frac{du_i}{dt} &= \sigma f v_i + \frac{10^{-4}\sigma}{q^2}\left[\left(\frac{\partial K}{\partial z}\right)\frac{u_{i+1} - u_{i-1}}{2h} + \right. \\ &\left. + K_i\frac{u_{i+1} - 2u_i + u_{i-1}}{h^2}\right] \\ \frac{dv_i}{dt} &= \sigma f\,(1 - u_i) + \frac{10^{-4}\sigma}{q^2}\left[\left(\frac{\partial K}{\partial z}\right)_i\frac{v_{i+1} - v_{i-1}}{2h} + \right. \\ &\left. + K_i\frac{v_{i+1} - 2v_i + v_{i-1}}{h^2}\right] \end{aligned} \tag{9}$$

The levels $i=0$ and $i=n$ correspond to the lower and upper boundary conditions, respectively. Thus, (9) and (4) constitute a system of $2n$ equations. Now the friction layer may extend

to several thousand meters. On the other hand, good resolution of the wind field, at least near the surface, probably requires a vertical increment of less than 10 meters, which leads to a system containing several hundred equations. In addition, a small time increment is required to maintain computational stability in the numerical solution; thus, the services of a large, high-speed computer are needed.

By transforming the vertical coordinate to $\ln z$, it is possible to obtain better resolution at low levels and still keep the number of equations to a more practicable value for the computer on hand. The transformation is straightforward (see HALTINER, 1958); and the resulting equations are similar in form to (9).

3. Constants

For convenience, consider the units of (1) to be of the c.g.s. system. Then a choice of $\sigma = 3{,}600$ makes the unit of time in (3) an hour. The parameter q essentially disappears from the final equations; however, its value is related to the overall magnitude of the eddy viscosity by Eqs. (7) and (8) and the size of the vertical height increment. The parameter q implies units of q-meters for z; i.e., $q=2$ gives 2-meter units for z, etc. Thus, as q increases, the coefficient of eddy viscosity increases, but the vertical height increment over which the finite differences are taken also increases. It was necessary to resort to this scaling because typical values of the eddy viscosity required prohibitively small integration time increments for the capacity of the computer available. With l representing the vertical increment of $\ln z$, a choice of $l=\ln 2$, together with $q=3$ would imply successive levels in a geometric series; i.e., 3, 6, 12, 24, . . . meters.

The choices $c=0.3$ and $b=0.8$ give rise to a 20-fold diurnal variation of the eddy viscosity, with $\omega = 2\pi/24$. With regard to the vertical variation of k, the constant value $a_2=0.9$ gives a ten-fold variation of K with height. On the other hand, if a_2 is allowed to vary with time as indicated in Section 2, a choice of $a_2'=0.95$ and $a_2''=.0352$ (Case 2) gives a 10-fold vertical variation of K with its minimum diurnal value, and a 100-fold variation with height at the time of maximum K. The maximum value of K obtained in this case is $1.13 \times 10^3\ q^2$ cm^2/sec.

In connection with the function k_2 of Eq. (8), the values $a_4=.01$ and $a_5=.09$ give essentially a 10-fold variation with height first increasing to a maximum at $z=z_m$ and then decreasing as the altitude increases further. The choice of $z_m=64$ q-meters will be referred to as Case 3, and $z_m=16$ q-meters as Case 4. The maximum value of K which was practicable on the available computer was $256\ q^2$ cm^2/sec in Case 3 and $64\ q^2$ cm^2/sec in Case 4. To obtain a magnitude of K comparable to observed values of the order of 10^4 to 10^5 cm^2/sec, it is necessary to put q in the range 10 to 20. For the former value and $l=\ln 2$, the vertical spacing will correspond to the sequence of heights 5, 10, 20, 40 . . . etc. meters, while the latter gives the sequence . . . 10, 20, 40, . . . meters.

The initial point corresponds to the lower boundary at which the velocity is assumed to vanish. This point may be considered an arbitrary reference level from which the points above are measured. It is apparent that as q increases, the vertical resolution decreases, particularly in the "surface layer" near the lower boundary. One may retain a greater degree of resolution at lower levels by decreasing the value of l; however, the vertical extent is correspondingly decreased, assuming no increase in the total number of equations. In all the cases studied the latitude was taken to be 45°.

4. Results and Conclusions

The velocity distributions obtained for Cases 1 through 4, representing the different forms of the coefficient of eddy viscosity, have very similar patterns. At any particular hour, the vertical variation of the wind shows the characteristic spiral; however, the shape varies significantly from the time of maximum to minimum K, as indicated by Figure 1. Note here that velocities are expressed relative to the geostrophic wind V_g which is represented as 100 units in all figures. The time scale is arbitrary except that 0600 and 1400 correspond to the times of minimum and maximum K, respectively. In agreement with observation, the "night-time" cross-isobar angle exceeds the "daytime" case at low levels. Figures 2 and 3 show the diurnal variation of the wind at successive levels for Cases 1 and 3, respectively. The results are very similar in spite of the different vertical variation of the eddy viscosity. This is partly due to the fact that most of

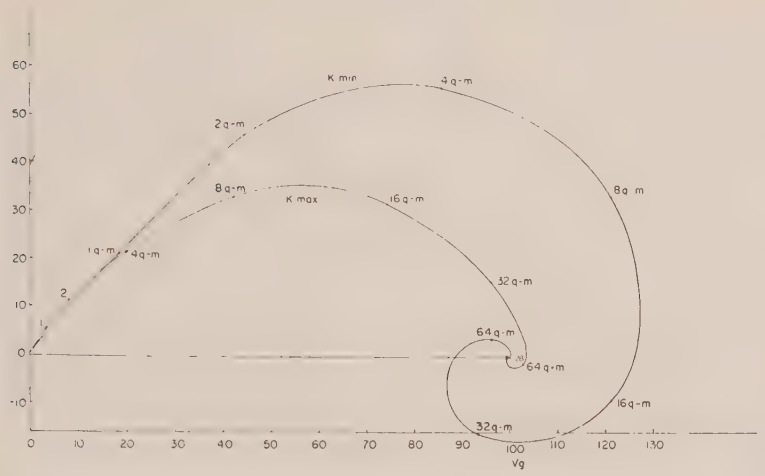

Fig. 1. Theoretical wind distributions as functions of height at the times of maximum and minimum eddy viscosity for Case 1.

the variation in the wind field takes place below the 64 q-meter level where K is assumed to reach a maximum for Case 3.

Since the selection of q is arbitrary, it is of interest to note the effect of varying this parameter. An increase in q corresponds to an increase in the overall magnitude of the eddy viscosity and an increase in the elevations to which the ellipses of Figures 2, 3 and 4 apply. It is apparent that as the eddy viscosity increases, the height at which the wind becomes geostrophic also increases, as well as the height of the maximum diurnal variation of the wind. A comparison of Figures 2 and 3 shows that the diurnal variation of the wind is smaller in Case 1 than in Case 3, even though the overall magnitude of K is less in the latter. However, the vertical extent to which deviations from the geostrophic are observed is greater in Case 1 than in Case 3. Figure 4 shows some observational data evaluated by Buajitti and Blackadar. Note that the shape and orientation of the ellipses of Case 3 from 8 q-m upward agree with the observed orientation from 15 ft. upward moderately well. However, the position of the wind vector at the time of maximum eddy viscosity (presumed to be near midday) is approximately opposite to the position of the observed wind vector at 1400. This disagreement is brought out in Figure 5 which shows the wind speed as a function of height for Case 3. Note that the low-level wind speed corresponding to the time of minimum eddy viscosity exceeds that corresponding to the maximum eddy viscosity. This condition is observed to hold above the "crossover", but not in the surface layer immediately adjacent to the ground. The zero momentum at the lower boundary tends to be propagated upward and the maximum penetration is observed at the time of maximum eddy diffusivity. This is similar to the diurnal temperature wave which is propagated upward from the lower boundary where heating takes place. Here there is in addition a source of momentum in the pressure and Coriolis forces. In passing, it may be noted in Figure 5 that at the time of minimum eddy viscosity the wind speed exceeds the geostrophic value by 25 % at one level and the strong shear occurs in the jet-type profile. Figure 6 shows the results for Case 4. The overall pattern is similar to Case 3 especially at and below 8 q-meters. A comparison of the 32 q-m ellipse of Case 3 and the 16 q-m ellipse of Case 4 shows a similarity in general shape; however, the time positions of the wind vectors have shifted clockwise on the ellipse about 60°. At 16 q-m in Case 4, the position of the wind vectors at the time of maximum and minimum eddy viscosity agree moderately well with the observed 1400 and 0600 winds at 3,650 feet; however, the orientation of the ellipse is only in fair agreement with observed orientation.

At the 32 q-m level there appears to be about $1\frac{1}{4}$ cycles to the ellipse during the 24 hr.

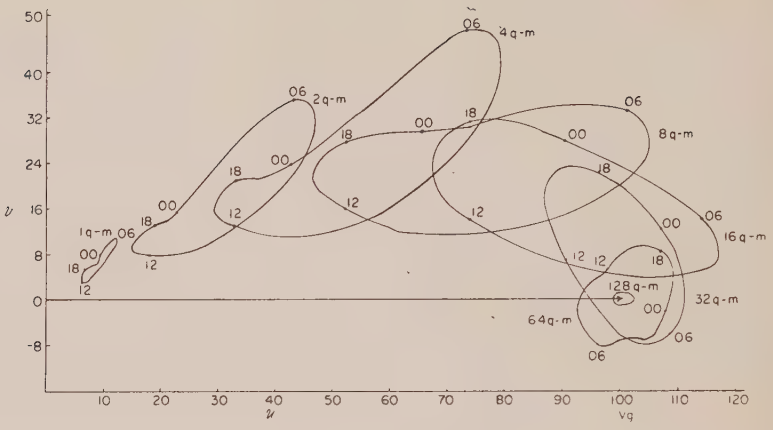

Fig. 2. The theoretical diurnal variation of the wind for Case 1.

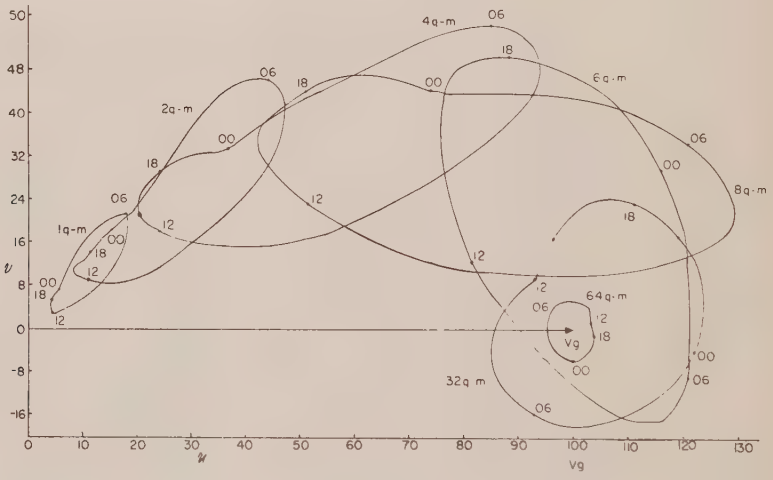

Fig. 3. The theoretical diurnal variation of the wind for Case 3.

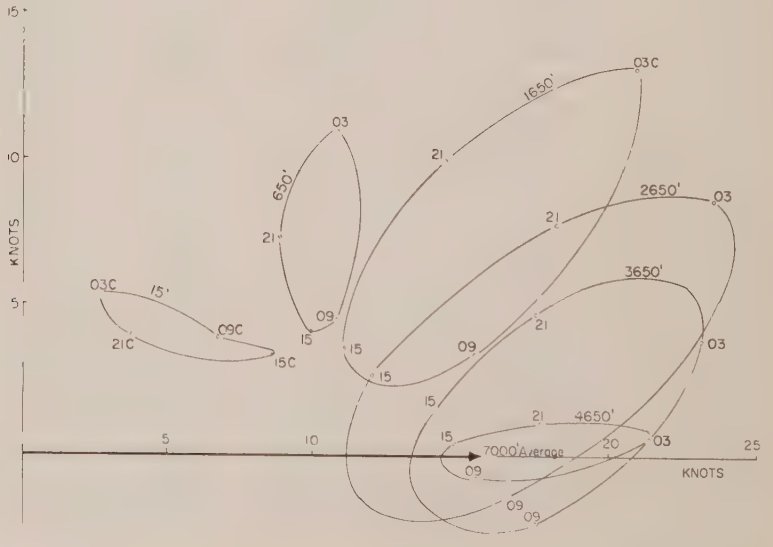

Fig. 4. The observed diurnal variation of the wind, after Buajitti and Blackadar (1957).

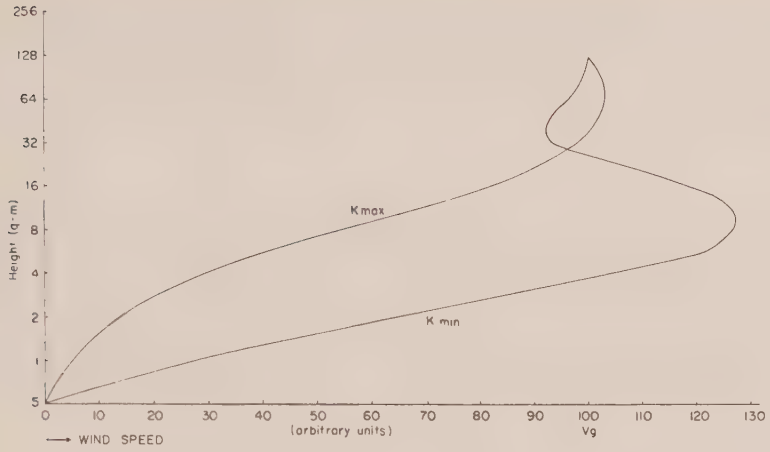

Fig. 5. The wind speed as a function of height at the times of maximum and minimum eddy viscosity in Case 3.

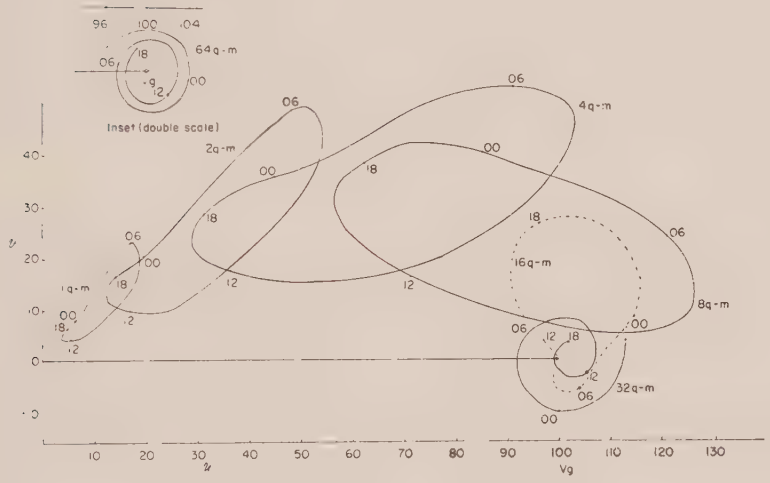

Fig. 6. The theoretical diurnal variation of the wind for Case 4.

period, while at 64 q-m the wind vector appears to pass through two complete cycles in a 24 hour period. These features did not occur in Case 3 even though the vertical variation of the eddy viscosity is similar. This phenomenon may be due to the initial conditions which were taken from Case 3 at 0600 hrs; however, this does not appear to be very likely. Time restrictions did not permit another 24 hour computation. Some computations were also made in which the geostrophic wind was allowed to vary linearly with height; however the resulting differences were minor and did not correct any of the significant discrepancies described above.

The results of this study show some agreement between observation and the theoretical models representing the diurnal variation of the wind. However, there is disagreement in some significant features of the wind field.

One may infer that coefficients of eddy viscosity of the type used here are inadequate to fully explain the diurnal variation of the wind. Perhaps some other type of function for K will provide better agreement or a two-layer model may be necessary. A study of this problem is being conducted at present and will be reported on at a later date.

REFERENCES

Buajitti, K. and Blackadar, A. J., 1957: Theoretical studies of diurnal wind variations in the planetary boundary layer, *Quarterly Journal of the Royal Meteorological Society*, **83**, pp. 486—500.

Haltiner, G. J., 1958: The diurnal temperature wave with a coefficient of diffusivity which varies periodically with time and exponentially with height, *Journal of Meteorology*, **15**, pp. 317—323.

Mildner, P., 1932: *Beitr. Phys. frei Atmos.*, **19**, pp. 151.

Staley, D. O., 1956: The diurnal temperature waver of bounded eddy conductivity, *Journal of Meteorology*, **13**, pp. 13—20.

Uninodal Seiches in the Oscillation System Baltic proper —Gulf of Finland

By EUGENIE LISITZIN, Institute of Marine Research, Helsinki

(Manuscript received December 22, 1958; revised version February 3, 1959)

Abstract

Seventeen cases of regular sea level oscillations with at least four distinctly developed periods recorded at Hamina (Fredrikshamn) in the east part of the Gulf of Finland during the years 1952—1954 were selected and the period corresponding to the maximum amplitude computed numerically. The results show that this period is fairly constant with an average of 26.2 (± 0.2) hours. Sea level records at Władysławowo on the Polish coast confirm this period as a uninodal seiche in the oscillation system Baltic proper—Gulf of Finland.

In the paper is also discussed the possible occurrence of transversal oscillations in the Gulf of Finland and the probability of the participation of the Bay of Kiel at the named seiches in the Baltic.

1. General survey

Witting (1911) was the first to determine an approximate value for the oscillation period of a standing wave in the Baltic proper and the Gulf of Finland. He based his computations on a number of theoretical assumptions and different simplifications of the bottom profile, getting for the particular cases considerably deviating results. The final conclusion made by Witting was that the period of the uninodal oscillation amounts to about 28—31 hours, a result which must be considered a comparatively good approximation. After a lapse of 30 years Neumann (1941) took the problem up again, trying to solve it on the one hand with the aid of selected representative sea level records, on the other hand, and this is the most important part of his paper, on the basis of extensive calculations involving the numerical methods developed by Defant (1918) and Hidaka (1936).These two methods require an exact knowledge of the size and depth of the sea basin. The correspondence between the individual results attained at by Neumann in different ways is surprisingly good. Thus, the average value of the oscillation period for the Baltic including the Gulf of Finland determined from sea level records amounts to 27.6 hours, while theoretical calculations on the basis of the two methods mentioned above gave 27.5 hours. The principal condition for the reliability of this value is, however, the assumption that the Baltic is enclosed in the south-west at the Fehmarn Belt.

The results of Neumann's calculations are without doubt excellent, however, a few factors influencing the data may be pointed out in this connection. Only six readings a day were used from the sea level records for the stations on the Swedish, Finnish, Estonian and Latvian coasts. The amplitudes of the oscillation being generally at their highest and the phenomenon as a whole most distinct for the stations situated in the Gulf of Finland, the determination of the period is based mainly on these comparatively incomplete data. In ad-

dition, Neumann computed, as a rule, the oscillation period only with the aid of the time difference between the first and last maximum taking into consideration the number of the interjacent extremes. This procedure, in cases with occasional and local irregularities in the course of the sea level variations, especially towards the end of the oscillation period where the amplitudes are generally slight, may cause considerable deviations. In fact, the length of the period estimated by Neumann for the separate cases varies between 26 and 28 hours and is thus only approximate.

The theoretical calculations of the oscillation period with the aid of the methods of Defant and Hidaka form a very instructive and interesting part of Neumann's paper. The complete agreement between the results is, without doubt, the best proof of the exactitude and reliability of the two methods. The principal difficulty in solving the problem lies, however, as Neumann himself pointed out in his paper, in the irregular configuration of the Baltic and especially in the difficulty of determining exactly the limits of the oscillation basin. As already mentioned above, in his first attempt to determine the oscillation period Neumann considered the Baltic to be closed at the Fehmarn Belt. Including the shallow region of the Bay of Kiel in the oscillation system, using the method of Defant, he arrived at an oscillation period of 29.5 hours; the method of Hidaka gave a period 0.2 hours shorter. The excellent correspondence with the results attained with the aid of the sea level records is thus lost in this case. The example suffices also to show the pronounced dependence of the oscillation period on the sea basin and gives a distinct picture of the difficulties involved. It may be pointed out, moreover, that Neumann's tables show, as a rule, a considerable deviation between the computed amplitudes and the corresponding recorded values. The location of the nodal line is also different according to the theoretical results and for the actual cases considered in Neumann's paper.

These discrepancies prove that the problem is far from solved. The best way to approach it once more is to base the research on a great number of adequate sea level records. This, however, presents a considerable difficulty. In some of the countries bordering the Baltic, sea level data have not been published since the beginning of the Second World War. The work had therefore inevitably to be planned and carried out with the Finnish sea level records, which in their entierety were at the disposal of the author, constituting the principal and essential part of the research. In a limited number of cases the results for the Finnish coast had, however, to be compared with representative results for the southern part of the Baltic. In this connexion the author expresses her sincere thanks to Commander K. Zagrodzki of the "Zaklad Oceanografii Panstwowego Instituta Hydrologiczno-Meteorologicznego" in Gdynia and to President J. M. Lorenzen of the "Küstenausschuss Nord- und Ostsee" in Kiel-Wik for having supplied her for a few shorter periods with hourly sea level data for Władysławowo (off the peninsula Hel) and Strande (outside Kiel). The institute in Poland also sent supplementary records for the sea level stations Kołobzreg and Swinoujscie.

2. Uninodal oscillation at Hamina

As starting point and basis for the research were chosen the hourly records for Hamina (Fredrikshamn) which is now the easternmost Finnish sea level station in the Gulf of Finland. From the records of the years 1952—1954 a number of cases was selected characterized by a distinct and regular oscillation with an approximate period of 26—28 hours. These cases seem on the whole to be unexpectedly frequent, but only cases which fulfilled the following three main conditions were taken into account in the present research:

a) the number of consecutive, distinctly developed oscillation periods had to be at least four,

b) a rough estimation of the average (double) amplitude of the oscillation concerned had to give a result of at least 12 cm, and

c) in order to ascertain that the phenomenon represented a uninodal standing oscillation, corresponding records were used to check that a more or less pronounced inverse seiche oscillation appeared simultaneously at Ystad situated on the Swedish coast in the south part of the Baltic.

Moreover, the possibility was always kept in mind that a strong wind may induce a new oscillation which could influence the period computed. It was therefore in all the cases

with an increase of amplitude during the selected period checked that no apparent dislocation of the extreme values has occurred.

It was rather surprising to establish that uninodal seiches fulfilling the above conditions occur fairly frequently in the oscillation system Baltic proper — Gulf of Finland. For the three years in question, on an average almost nine per cent of the total number of sea level variations, covering an cumulative time of three months, were characterized by a prolonged uninodal oscillation. The number of less pronounced cases or cases with a fewer periods and a more restricted average amplitude is, of course, considerably higher. The distribution of the selected cases over the particular years is, however, fairly uneven. For the year 1952 there were used in this study no less than nine cases with altogether 51 periods, in 1953 only three cases, corresponding to 12 periods and, finally, in 1954 five cases resulting in 25 periods. These cases cover in round figures 15, 4 and 7 % respectively, of the corresponding year.

Once the cases were selected the harmonic constants were computed numerically. Starting from different lengths of the oscillation period the one corresponding to the maximum amplitude could be determined with considerable accuracy. The computed data are collected in Table 1. Although the period lengths used cover a time from 25 to 27 hours, the period connected with the highest value of the amplitude generally varies between 26.0 and 26.4 hours only. In reality, we find in Table 1 only two exceptions from the above statement. For the oscillation recorded in January 1952 the computed period is distinctly shorter than the average, approximately 25.5 hours. The number of consecutive periods used for the determination of the harmonic constants is, however, in this case exceptionally high, reaching 12, against the usual total of 4 or 5 periods. It is thus by no means out of the question that a certain dislocation of the phenomenon occurred in the course of this comparatively prolonged time, influencing the result accordingly. The other exception in Table 1 is the case recorded at the beginning of April 1952, where the maximum amplitude corresponds to a period of 26.6 hours. The deviation from the generally computed period length is thus rather insignificant. Table 1 shows in many cases that the maximum of the amplitude is by no mean

Table 1. The harmonically determined average amplitudes (cm) of a uninodal seiche at Hamina for different lengths of the oscillation period

Length of the period, h.	1952									1953			1954					
	I 16. 29. 12 periods	II 10. — 14. 4 periods	II 16. — 21. 5 periods	III 16. — 21. 5 periods	III 26. — 31. 5 periods	IV 2. — 8. 5 periods	IV 15. — 20. 5 periods	VII 31. — VIII 5. 5 periods	XI 18. — 23. 5 periods	III 23. — 27. 4 periods	X 22. — 26. 4 periods	XII 2. — 6. 4 periods	I 15. — 20. 5 periods	VI 27. — VII 1. 4 periods	X 14. — 21. 7 periods	XI 10. — 15. 5 periods	XI 27. — XII 1. 4 periods
25.0	7.9	17.5	—	8.9	—	—	—	—	—	—	—	—	—	6.4	—	—	11.7
25.5	*8.8*	18.1	—	9.1	7.0	—	—	—	8.3	—	7.6	—	—	7.0	18.5	26.4	12.5
26.0	7.4	*18.7*	7.3	*9.3*	*7.9*	8.9	8.9	5.6	*9.0*	12.1	*7.8*	26.9	14.9	*7.1*	18.8	28.2	*12.6*
26.2	6.6	*18.7*	7.5	9.1	7.6	8.8	*9.4*	*5.8*	8.5	13.1	7.6	*28.2*	*15.2*	6.8	*18.9*	27.8	11.9
26.4	4.7	18.3	6.5	9.0	*7.7*	9.2	9.1	5.5	7.9	*13.3*	7.2	26.8	15.0	6.7	18.7	*28.3*	11.6
26.6	—	—	—	—	—	*9.3*	—	—	—	12.8	—	—	—	—	17.1	26.8	—
27.0	—	—	—	—	—	9.2	—	—	—	—	—	—	—	—	—	—	—

pronounced, indicating the presence of occasional perturbations. We seem therefore to be entitled to consider 26.2 (± 0.2) hours as the average length of the oscillation period for the seventeen representative cases given in Table 1.

The deviation between the theoretically computed period of Neumann and the result of this paper depends probably on the difficulty to reproduce for mathematical purposes the irregular boundaries of the sea basin.

3. The results for Władysławowo

In order to complete the results and check the character of the oscillation as a uninodal seiche in the Baltic proper and the Gulf of Finland, the Polish sea level records for Władysławowo were considered for four of our cases. The harmonic constants computed are given in Table 2 and compared with the corresponding data for Hamina. This table shows that for Władysławowo, too, the oscillation period referring to the maximum amplitude is in three of the four cases to be found between the limits of 25.7 and 26.4 hours. In addition, the differences between the phase angles for the two stations (last column in Table 2) indicate in these three cases a distinct inversity of the oscillation being fairly close to 180°. The amplitudes for Władysławowo form the 3.0 to 4.7 parts than those for Hamina, which, of course, makes the harmonic constants for the former sea level station less reliable. Concerning the fourth case given in Table 2 (for March

Table 2. Harmonic constants for Hamina and Władysławowo for different lengths of the oscillation period

Length of the period, hours	Hamina		Władysławowo		Phase angle difference
	Amplitude, cm	Phase angle	Amplitude, cm	Phase angle	
			1952, February 10.—14.		
25.2	17.5	354°	4.8	191°	163°
25.5	18.1	344°	5.5	179°	165°
25.7	18.0	336°	6.4	171°	165°
26.0	18.7	329°	6.0	167°	162°
26.2	18.7	322°	5.8	152°	170°
26.4	18.3	315°	5.7	152°	163°
27.0	17.9	295°	5.2	137°	158°
			1952, April 15.—20.		
26.0	8.9	260°	3.1	93°	167°
26.2	9.4	258°	3.3	81°	177°
26.4	9.4	252°	3.4	77°	175°
26.7	9.4	238°	3.4	67°	171°
27.0	9.3	227°	3.3	60°	167°
			1953, March 23.—27.		
23.5	—	—	3.6	176°	—
23.8	—	—	3.8	165°	—
24.0	9.5	354°	3.6	157°	163°
24.5	—	—	3.4	137°	—
25.0	11.7	319°	2.9	115°	156°
25.5	—	—	2.7	97°	—
26.0	12.1	297°	2.2	88°	151°
26.2	13.1	288°	2.1	83°	155°
26.4	13.3	285°	1.8	75°	150°
26.6	12.8	279°	—	—	—
			1953, December 2.—6.		
26.0	26.9	108°	5.9	293°	175°
26.2	28.2	100°	6.0	286°	174°
26.4	26.8	97°	5.9	281°	176°

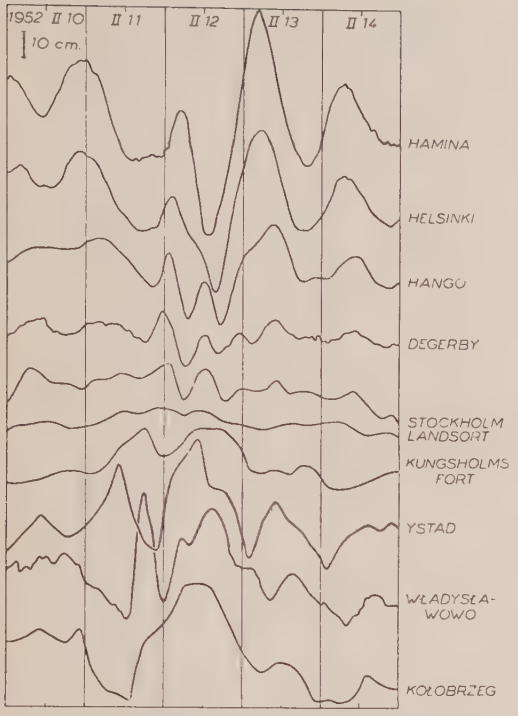

Figure 1. Sea level variations 10—14 February 1952.

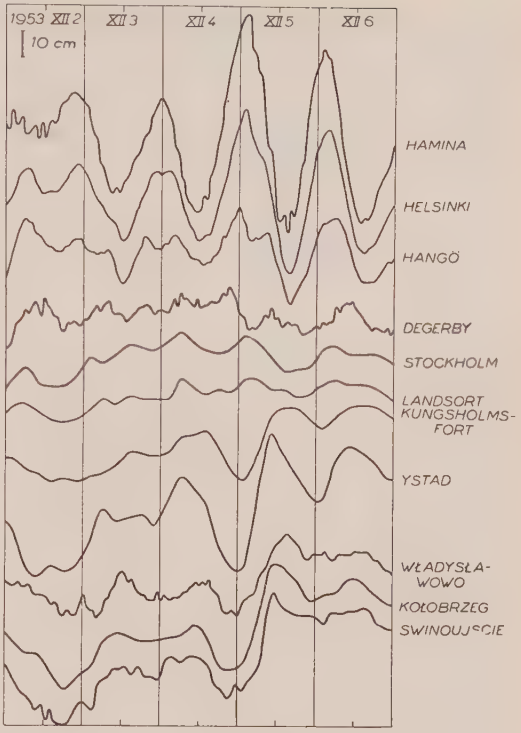

Figure 2. Sea level variations 2—6 December 1953.

1953), the correspondence is not quite satisfactory. On the one hand, the oscillation period for Władysławowo is considerably shorter than for Hamina, amounting to 23.75 hours only, on the other hand the condition for inversity of the phenomenon at the two stations is fulfilled only approximately. As, finally, the amplitudes for Władysławowo are comparatively small in this case, the presence must be presumed of a more or less local factor disturbing the regular course of the phenomenon and influencing the results.

In order to give a graphical representation of the data used above, the sea level records for 10—14 February, 1952, and 2—6 December, 1953, are reproduced in Figures 1 and 2, respectively. Besides the values for Hamina and Władysławowo, the figures give the hourly records for three additional Finnish sea level stations: Helsinki (Helsingfors), Hangö (Hanko) and Degerby. The curves representing the Swedish stations Stockholm, Landsort, Kungsholmsfort and Ystad and the Polish station Kołobrzeg are based on six readings daily and the curve for Swinoujscie in Figure 2 on twelve readings daily. The position of these stations appears in Figure 3.

Figures 1 and 2 show that the oscillation is fairly distinct at Hamina and Helsinki; at Hangö the phenomenon has on the whole a similar character, but the amplitudes are slight and a disturbance in the feature of a supplementary maximum can be noted, for instance, in Figure 1 on 12 February. At Landsort the

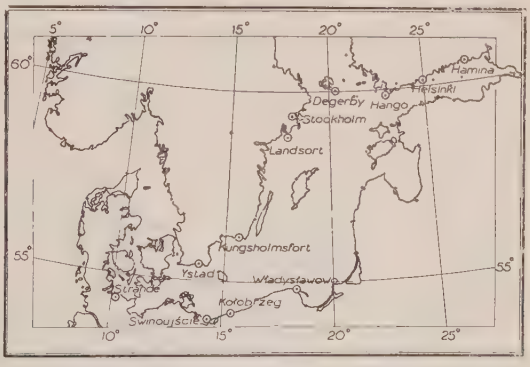

Figure 3. Position of the sea level stations.

oscillation is hardly perceptible owing to the proximity of this sea level station to the nodal line. The inversity of the phenomenon in the south part of the Baltic is indisputable, but the number of different local and regional perturbations is considerable, as appears from the curves given in Figures 1 and 2.

4. Transversal oscillation in the Gulf of Finland

Following the coast from east to west, the general outline of the seiche oscillation in the Gulf of Finland indicates a slight retardation of the occurrence of the extreme sea levels. This retardation can be explained only with the aid of transversal oscillations in the basin caused by the effect of the Coriolis force. In order to obtain some idea of the average value of the time lag the harmonic constants for an oscillation period of 26.2 hours were computed for Hangö for all the cases given in Table 1, however with the exception of the case noted in April 1954 which is missing from the records at Hangö. Table 3 reproduces these constants and the corresponding data for Hamina. Also to be found in the table are the ratios between the amplitudes and the differences between the phase angles. The general impression of Table 3 is the lack of conformity in the individual cases. Thus the ratio between the amplitudes for Hamina and Hangö varies from 1.7 to 10.1. According to the theoretical determinations made by Neumann this ratio should be about 2.5. The limits for the fluctuations of the phase differences are 33° and – 25°. The cases where the extreme sea levels at Hangö appear earlier than at Hamina must be omitted in this connexion as they can not be caused by a transversal oscillation but are due to other disturbances, probably of more local character. The remaining cases are, without doubt, also influenced by disturbing effects. The average value for the positive phase differences in Table 3 is 12°, corresponding to a time lag of approximately 55 minutes. This value is self-evidently a rough approximation only, as the number of cases is far too restricted to allow a more exact determination. It is, for instance, about 35 % too low in comparison with the time lag attained by Neumann (1941). This author, on the basis of theoretical determinations, com-

Table 3. Harmonic constants for Hamina and Hangö corresponding to an oscillation period of 26.2 hours

Time	Hamina		Hangö		Ratios of the amplitudes	Phase angle difference
	Amplitude, cm	Phase angle	Amplitude, cm	Phase angle		
1952						
I 16.—29.	6.6	86°	3.9	108°	1.7	22°
II 10.—14.	18.7	322°	4.7	355°	4.0	33°
II 16.—21.	7.5	233°	3.7	235°	2.0	2°
III 16.—21.	9.1	210°	1.4	202°	6.5	— 8°
III 26.—31.	7.6	159°	3.3	146°	2.3	—13°
IV 2.—8.	8.8	108°	2.9	117°	3.0	9°
IV 15.—20.	9.4	258°	3.9	269°	2.4	11°
VII 31.—VIII 5.	5.8	64°	2.8	78°	2.1	14°
XI 18.—23.	8.5	332°	3.3	331°	2.5	— 1°
1953						
III 23.—27.	13.1	288°	5.9	274°	2.2	—14°
X 22.—26.	7.6	130°	3.1	137°	2.5	7°
XII 2.—6.	28.2	100°	2.8	103°	10.1	3°
1954						
I 15.—20.	15.2	235°	3.8	233°	4.0	— 2°
X 14.—21.	18.9	250°	5.1	264°	3.7	14°
XI 10.—15.	27.8	176°	7.0	151°	4.0	—25°
XI 27.—XII 1.	11.9	27°	5.4	32°	2.2	5°

Table 4. Harmonic constants for Hamina and Strande for different lengths of the oscillation period

Length of the period, hours	Hamina		Strande		Phase angle difference
	Amplitude, cm	Phase angle	Amplitude, cm	Phase angle	
			1954, November 10.—15.		
25.5	26.4	204°	—	—	—
26.0	28.2	182°	13.8	310°	128°
26.2	27.8	176°	15.3	306°	130°
26.4	*28.3*	167°	16.5	300°	133°
27.0	28.0	146°	19.2	288°	142°
28.0	27.9	111°	22.0	270°	159°
28.4	26.6	99°	*22.4*	262°	163°
28.8	24.8	83°	21.9	252°	169°
			1955, January 7.—12.		
26.0	16.3	321°	8.0	155°	166°
26.2	17.0	313°	—	—	—
26.4	17.6	306°	9.0	132°	174°
26.6	18.7	296°	—	—	—
27.0	20.0	286°	10.0	112°	174°
27.5	21.3	275°	*10.9*	100°	175°
28.0	22.1	256°	10.7	76°	180°
28.4	22.1	245°	10.3	65°	180°
28.8	*22.3*	233°	9.2	46°	173°
29.4	20.9	218°	—	—	

puted that the retardation between Koivisto (Björkö), in the Gulf of Finland about 100 km east of Hamina, and Hangö amounts to 1.8 hours. Using this value, we get by interpolation a retardation of 85 minutes between Hamina and Hangö.

5. The results for Strande

The results of this study have shown that the period of the uninodal oscillation in the system Baltic proper — Gulf of Finland is, according to the sea level records, on an average 26.2 hours, i.e. 1.3 hours shorter than the period calculated by Neumann when demarcating the south-west basin of the Baltic at the Fehmarn Belt. If the Bay of Kiel is included in the oscillation area the correspondence deteriorates still more and the difference between the lengths of the periods increases to somewhat more than 3 hours. It is thus possible that the shallow bay plays, as a rule, no part in the oscillation. Its cooperation may depend on the direction of the impulse. The question, however, requires more thorough study. For this purpose, two series of sea level records for Strande were used. Unfortunately these cases had to be chosen from among records covering a time of one year only, i.e. from 1 November, 1954, to 31 October, 1955. No comparison could therefore be made with the records examined above for Władysławowo which all refer to the years 1952 and 1953. The results of the harmonic analysis for the two cases for Strande and Hamina, each covering five periods, are given in Table 4. The amplitudes are fairly marked, but in spite of this the correspondence between the oscillation periods is not satisfactory. For the case in November 1954, concerning which the results for Hamina have already been studied in Table 1, there is the prolonged maximum of the amplitudes corresponding to periods lying between 26.0 and 26.4 hours. The maximum at Strande, on the contrary, may be located comparatively exactly as corresponding to an oscillation period of 28.4 hours. The deviation between the period lengths is too marked to permit consideration of the two series of sea level variations as an identical uninodal seiche oscillation, especially as the condition for inversity is hardly fulfilled. The second case given in Table 4 is of considerable interest, principally owing to the discrepancy between its oscillation period

for the maximum amplitude at Hamina and the results of Table 1. This period amounts to 28.8 hours. We could therefore presume that in this special case a larger part of the Baltic participates in the seiche, i.e. that the Bay of Kiel is engaged in the phenomenon, too. Unfortunately, the records for Strande confirm this supposition only approximately. According to Table 4, the oscillation period for Strande can be determined by interpolation at roughly 27.7 hours.

The available records thus do not suffice to solve the problem. A much more extensive material is needed. The possibility that the Bay of Kiel occasionally influences the phenomenon must nevertheless always be kept in mind. It is just this effect and the occurrence of possible coincident oscillations in the bay, probably with a period of 28.4—28.8 hours, that present the most interesting question concerning the uninodal seiches in the Baltic and should be studied more closely.

REFERENCES

Defant, A., 1918: Neue Methode zur Ermittlung der Eigenschwingungen (Seiches) von abgeschlossenen Wassermassen (Seen, Buchten usw). *Annalen der Hydrographie und Maritimen Meteorologie* **46**, pp. 78—85.

Hidaka, K., 1936: Application of Ritz's Variation Method to the Determination of Seiches in a Lake. *The Memoirs of the Imp. Marine Observatory* **VI**, No. 2.

Neumann, Gerhard, 1941: Eigenschwingungen der Ostsee. *Aus dem Archiv der Deu.schen Seewarte und des Marineobservatoriums* **61**, No. 4.

Witting, Rolf, 1911: Tidvattnet i Östersjön och Finska viken. *Fennia* **29**, No. 2.

On Systematic Errors in the Least Squares Regression Analysis, with Application to the Atmospheric Effects on the Cosmic Radiation

By HARALD TREFALL and JACK NORDÖ[1], Universitetet i Bergen, Bergen, Norway

(Manuscript received January 2, 1959)

Abstract

It is shown that if the variables employed in a least squares regression analysis are subject to random errors of measurement, the expectation values of the partial regression coefficients, of the partial correlation coefficients and of the multiple correlation coefficient may all differ from those which would have existed, had no errors been present. If there is no intercorrelation between the errors of different variables, random errors in a given variable always reduce the numerical expectation values of the corresponding partial regression and correlation coefficients. Coefficients corresponding to other variables may, however, be influenced in either direction depending on the intercorrelations between the variables. The expectation value of the multiple correlation coefficient is reduced by errors in any variable. The general case, in which the errors of different variables are intercorrelated, has also been briefly discussed.

The problem of determining the atmospheric effects on the cosmic radiation is then discussed. It is shown that some previously unexplained discrepancies between empirical and theoretical estimates, and also between empirical estimates obtained from the study of day-to-day variations, and such obtained from the seasonal variations of the cosmic-ray intensity, are probably due to systematic effects of random errors in the aerological data employed in the regression analysis.

Estimates of error variances and covariances of aerological data from the upper troposphere and the lower stratosphere have been obtained by analysing differences between data from two closely situated stations on Spitzbergen. They have then been used to obtain corrected estimates of the cosmic-ray atmospheric effects, which are now found to agree fairly well with the theoretical ones.

I. General considerations

1. *Introduction*

A least squares regression analysis is frequently used when a possible linear relationship between two or more measured quantities is investigated. The simplicity of the method is, perhaps, the main reason why it is so commonly used. It does not appear, however, to be generally appreciated that random errors in the independent variables will not only increase the variances of the correlation and regression coefficients, but will also change their expectation values.

This effect is very easily seen in the case of only one independent variable. The relation between the measured values x_1 of the independent variable and x_0 of the dependent variable is then given by

$$x_0 = b_1 x_1 + \xi \qquad (1)$$

where b_1 is the regression coefficient and ξ is the residual in the regression equation between the measured quantities. If the measurements are subject to random errors we may write

$$x_i = x_i' + \varepsilon_i \qquad (2)$$

[1] Now at Det Norske Meteorologiske Institutt, Oslo.

where x_i' is the true value of x_i and ε_i is the random error of measurement, the corresponding regression equation between the true values being

$$x_0' = b_1' x_1' + \xi'. \tag{3}$$

For the sake of simplicity, but without loss of generality we may assume that all variables have zero mean.

We shall assume that the errors are always random with respect to the true variables, i.e.

$$\overline{\varepsilon_i x_j'} = 0 \tag{4}$$

for all i and j, which implies that

$$\overline{x_i x_j} = \overline{x_i' x_j'} + \overline{\varepsilon_i \varepsilon_j}. \tag{5}$$

A bar denotes the mean value of an infinitely large sample.

The expectation values of the regression coefficients b_1 and b_1' are then

$$b_1' = \frac{\overline{x_0' x_1'}}{\overline{x_1'^2}} \tag{6}$$

and

$$b_1 = \frac{\overline{x_0' x_1'} + \overline{\varepsilon_0 \varepsilon_1}}{\overline{x_1'^2} + \overline{\varepsilon_1^2}}. \tag{7}$$

For the corresponding correlation coefficients they are

$$R' = \frac{\overline{x_0' x_1'}}{\left(\overline{x_0'^2} \cdot \overline{x_1'^2}\right)^{\frac{1}{2}}} \tag{8}$$

and

$$R = \frac{\overline{x_0' x_1'} + \overline{\varepsilon_0 \varepsilon_1}}{\left[\left(\overline{x_0'^2} + \overline{\varepsilon_0^2}\right)\left(\overline{x_1'^2} + \overline{\varepsilon_1^2}\right)\right]^{\frac{1}{2}}}. \tag{9}$$

From these equations it follows that the expectation values of the regression and correlation coefficients are always affected by random errors in the independent variable x_1. Regarding errors in the dependent variable, the correlation coefficient R is, of course, always influenced, whereas the regression coefficient b_1' is affected only if this error is correlated with the error in the independent variable. We see that b_1 may be smaller or larger than b_1', depending on the correlation which exists between ε_0 and ε_1. Even for the correlation coefficient it may happen that $R > R'$, which is rather surprising as one intuitively expects that the presence of errors would invariably reduce the magnitude of this statistical parameter. The case of $R > R'$ can, however, occur only in the rather unusual situation when the correlation between the errors is stronger than between the true variables themselves.

If the errors are not correlated with each other, i.e.

$$\overline{\varepsilon_i \varepsilon_j} = 0 \text{ for all } i \neq j, \tag{10}$$

it is easily seen that the expectation value of R is always less than that of R', and that the numerical expectation value of b_1 is always less than that of b_1'. This effect of random errors of measurement on the correlation coefficient was first noted by SPEARMAN (1904).

2. *Several variables with uncorrelated errors*

We shall now consider regression equations with several independent variables. As these variables may well be correlated with each other, they are often only formally independent. If the errors of the different variables are also correlated with each other, the situation becomes so complicated that very few conclusions can be drawn regarding the effect of the errors on the regression and correlation coefficients. However, in many (and perhaps in the majority) of the cases of practical interest the errors are not correlated with each other. We shall, therefore, begin with a discussion of this restricted case. On the other hand, the regression between cosmic-ray intensity and atmospheric conditions, which is to be discussed in the second part of this paper, presents a case in which the errors *are* intercorrelated.

Let x_0 be the dependent variable, and x_i, $i = 1, 2, \ldots n$, be the "independent" ones. Let us denote by A the determinant with elements

$$a_{ij} = \overline{x_i x_j}, \quad i = 0, 1, \ldots . n, \text{ and}$$
$$j = 0, 1, \ldots . n, \tag{11}$$

and by A_{ij} the corresponding cofactors. The empirical multiple regression coefficients are then given by

$$b_i = -A_{0i}/A_{00}, \tag{12}$$

the corresponding partial correlation coefficients by

$$r_i^2 = A_{0i}^2/(A_{00}A_{ii}), \tag{13}$$

and the multiple correlation coefficient by

$$R^2 = 1 - A/(a_{00}A_{00}). \tag{14}$$

The corresponding true values b_i', r_i' and R' are obtained by substituting for a_{ij} the true covariances

$$a_{ij}' = \overline{x_i' x_j'}, \tag{15}$$

based on the true values of the variables.

For the variances of errors we shall find it convenient to introduce the notation $\overline{\varepsilon_i^2} = \varepsilon_{ii}$. In order to see how the errors influence the expectation values of regression and correlation coefficients, we first note that in the restricted case under consideration we have, according to (5) and (10), that

$$\partial a_{kk}/\partial \varepsilon_{kk} = 1, \tag{16}$$

whereas

$$\partial a_{ij}/\partial \varepsilon_{kk} = 0 \text{ if either } i \neq k \text{ and/or } j \neq k. \tag{17}$$

Eq. (16) holds, however, also in the most general case, but not (17). By means of (16) and (17) we now find that

$$\partial A/\partial \varepsilon_{kk} = A_{kk} \tag{18}$$

and

$$\partial A_{ij}/\partial \varepsilon_{kk} = (A_{ij})_{kk}, \tag{19}$$

where $(A_{ij})_{kk}$ denotes the cofactor of the element a_{kk} as it appears in the determinant A_{ij}. If a_{kk} is not an element of A_{ij}, $(A_{ij})_{kk}$ is identically zero, and it should be noted that this occurs whenever i or j equals k.

If we differentiate (12) we find, by means of (18) and (19), that

$$\frac{\partial b_i}{\partial \varepsilon_{kk}} = -b_i\left[\frac{(A_{00})_{kk}}{A_{00}} - \frac{(A_{0i})_{kk}}{A_{0i}}\right]. \tag{20}$$

If $k=0$, we have $(A_{00})_{kk} = (A_{0i})_{kk} = 0$, and thus $\partial b_i/\partial \varepsilon_{00} = 0$. Consequently, *the expectation values of the regression coefficients are not influenced by errors in the dependent variable.*

If $k=i$ we still have $(A_{0i})_{kk} = 0$, but as i cannot here be zero, $(A_{00})_{kk} \neq 0$, and we get

$$\frac{1}{b_i}\frac{\partial b_i}{\partial \varepsilon_{ii}} = -\frac{(A_{00})_{ii}}{A_{00}}. \tag{21}$$

As $(A_{00})_{ii}$ and A_{00} are both positive definite we conclude that *random errors in an independent variable always tend to reduce the numerical value of the corresponding regression coefficient.* However, as nothing definite can be said about the sign of $\partial b_i/\partial \varepsilon_{kk}$ when $0 \neq k \neq i$, the regression coefficients corresponding to other independent variables may be influenced in either direction depending not only on the intercorrelation between the "independent" variables, but also on their correlations with the dependent variable. Consequently, *if several variables contain random errors, no general rule can be formulated regarding the combined effect of these errors on a given regression coefficient.*

Differentiating (13), we obtain

$$\frac{\partial r_i}{\partial \varepsilon_{kk}} = -\frac{r_i}{2}\left[\frac{(A_{00})_{kk}}{A_{00}} + \frac{(A_{ii})_{kk}}{A_{ii}} - 2\frac{(A_{0i})_{kk}}{A_{0i}}\right] \tag{22}$$

If $k=0$ the first and the third quotients within the brackets vanish, but as i cannot be zero the second term remains, and we find that $(1/r_i) \cdot (\partial r_i/\partial \varepsilon_{00})$ is always negative. Consequently, *errors in the dependent variable reduce the numerical expectation values of all partial correlation coefficients.* If $k=i$ only the first term remains, and we find that also $(1/r_i)(\partial r_i/\partial \varepsilon_{ii})$ is negative, whereas if $0 \neq k \neq i$ the sign depends on the correlations between all variables. We thus see that *random errors in an independent variable also tend to reduce the numerical value of the corresponding partial coefficient, whereas the expectation values of the other partial correlation coefficients may be changed in either direction.*

Finally, differentiation of (14) gives for $k \neq 0$

$$2R\frac{\partial R}{\partial \varepsilon_{kk}} = -\frac{(A_{00})_{kk}}{A_{00}}\left[\frac{A_{kk}}{a_{00}(A_{00})_{kk}} - \frac{A}{a_{00}A_{00}}\right] =$$

$$= -[(A_{00})_{kk}/A_{00}]\,[(1 - R_k^2) - (1 - R^2)], \tag{23}$$

where R_k denotes the multiple correlation coefficient which would have been obtained without the variable x_k. As the correlation cannot improve if one of the independent variables is discarded, we conclude that $\partial R/\partial \varepsilon_{kk} < 0$ for all $k \neq 0$. (It might have been zero if x_0 had not been correlated with x_k, but then there would have been no need for x_k as an independent variable.) Consequently, *random errors in any independent variable reduce the expectation value of the multiple correlation coefficient.* It is obvious that the same applies to errors in the dependent variable when these are not correlated with the errors in the independent variables.

If the independent variables are not intercorrelated, the situation is much simpler. We then have $a_{ij} = 0$ whenever $ij(i-j) \neq 0$, and find that (12), (13) and (14) reduce to

$$b_i = a_{0i}/a_{ii}, \tag{24}$$

$$r_i^2 = \frac{a_{0i}^2}{a_{00}a_{ii}\left[1 - \sum\limits_{j \neq 0,\,i} a_{0j}^2/(a_{00}a_{jj})\right]}, \tag{25}$$

and

$$R^2 = \sum_{i \neq 0} a_{0i}^2/(a_{00}a_{ii}). \tag{26}$$

We thus see that b_i can only be influenced by ε_{ii}, whereas r_i and R are still influenced by random errors in any variable.

3. *Several variables with correlated errors*

In the more general case when the errors in different variables are correlated and (10) is no longer satisfied, (18) and (19) do not hold and the rules formulated on the basis of the equations (20), (22) and (23) no longer apply. The following can, however, be said:

A. If, but only if, the errors in the dependent variable are correlated with the errors in one or more of the independent variables, the expectation values of all regression coefficients will be influenced also by the errors in the dependent variable, but not necessarily in such a way as to reduce their numerical values.

B. The numerical expectation value of a partial regression or correlation coefficient is no longer necessarily reduced by errors in the corresponding independent variable, nor will errors in the dependent variable always reduce the numerical expectation values of all partial correlation coefficients.

C. Even the multiple correlation coefficient may have its expectation value increased.

It is not difficult to convince oneself about the truth of the statements (A) and (B), but (C) is at first sight rather surprising. It can, however, be shown that the residual variance has still an absolute minimum when random errors of measurement are absent.

The residual ξ of the empirical regression equation

$$x_0 = \sum_{i \neq 0} b_i x_i + \xi \tag{27}$$

can be written in the form

$$\xi = \xi' + (\varepsilon_0 - \sum_{i \neq 0} b_i \varepsilon_i) + \sum_{i \neq 0} (b_i' - b_i)\, x_i', \tag{28}$$

where ξ' is the residual of the regression equation

$$x_0' = \sum_{i \neq 0} b_i' x_i' + \xi' \tag{29}$$

between the true variables. As $\xi' x_i' = 0$ for all $i \neq 0$ and, according to (4), $\overline{\xi' \varepsilon_i} = 0$ for all i, we find that

$$\overline{\xi^2} = \overline{\xi'^2} + \Big[\varepsilon_0 - \sum_{i \neq 0} b_i \varepsilon_i\Big]^2 + \Big[\sum_{i \neq 0} (b_i' - b_i)\, x_i'\Big]^2, \tag{30}$$

which clearly demonstrates that in all cases the residual variance has an absolute minimum at zero errors.

If we express the residual variances $\overline{\xi^2}$ and $\overline{\xi'^2}$ by means of the respective multiple correlation coefficients and total variances of the dependent variables, and use the relation $\overline{x_0'^2} = \overline{x_0^2} - \overline{\varepsilon_0^2}$, we get from (30) that

$$(R'^2 - R^2)\,\overline{x_0^2} = -(1 - R'^2)\,\overline{\varepsilon_0^2} + \Big[\varepsilon_0 - \sum_{i \neq 0} b_i \varepsilon_i\Big]^2 + \Big[\sum_{i \neq 0} (b_i' - b_i)\, x_i'\Big]^2. \tag{31}$$

If $\overline{\varepsilon_0 \varepsilon_i} = 0$ for all $i \neq 0$, (31) reduces to

$$(R'^2 - R^2)\,\overline{x_0^2} = R'^2 \overline{\varepsilon_0^2} + \overline{\Big[\sum_{i \neq 0} b_i \varepsilon_i\Big]^2} + \Big[\sum_{i \neq 0} (b_i' - b_i)\, x_i'\Big]^2. \tag{32}$$

From the equations (31) and (32) we can now draw the following conclusions:

A′. If the errors in the dependent variable are either absent or uncorrelated with the errors in the independent variables, the multiple correlation coefficient has an absolute maximum at zero errors. This does not, however, imply that all partial derivatives of R with respect to the error variances will be negative or zero everywhere in error space.

B′. If the errors in the dependent variable are correlated with the errors in the independent variables, R may in special cases be greater than R', provided that the correlation between the errors is stronger than that between the true variables. It would, for example, happen if the partial regression coefficients between the errors are approximately equal to those between the corresponding true variables, as the third term of (31) is then close to zero and the second term approximately equal to $(1 - R_\varepsilon^2)\overline{\varepsilon_0^2}$, where R_ε denotes the multiple correlation coefficient between ε_0 as dependent variable and the other errors as independent variables. It would also happen if all error variances are large compared to the variances of the corresponding true variables, as the empirical regression coefficients will also then be approximately equal to those between the errors, again making the first and second terms of (31) dominant and their sum approximately equal to $(R_\varepsilon^2 - R'^2)\,\overline{\varepsilon_0^2}$.

Even though peculiar cases such as those discussed in (B′) may be very rare in practical applications, they serve to demonstrate how careful one should be when judging the quality of empirical relationships established between variables with unknown errors.

The important consequence of these considerations is that when some relationship is expected to exist between two or more physical quantities for theoretical reasons, empirically determined regression coefficients are never strictly comparable to the theoretically estimated ones. The expected discrepancies may, of course, be small or even negligible if the measurements are very accurate, but it should never be forgotten that significant and otherwise unexplainable discrepancies may arise in this way. In the second part of this paper we shall present what we believe to be such a case.

It should especially be noted that if some of the "independent" variables are very strongly correlated with each other, the empirical regression coefficients may be widely different from the true ones if one of those variables contains even relatively small errors.

However, if we can in some way or other obtain estimates of the variances and covariances of errors which we know to be present in empirical data, we can use eq. (5) to compute true variances and covariances of the variables. Having thus removed the influence of the errors, the true regression and correlation coefficients can be found. This we shall now try to do in the case of the atmospheric effects on the hard component of the cosmic radiation.

II. Application to the cosmic-ray atmospheric effects

1. *Introduction*

As an application of the preceding general considerations we shall discuss the problem of determining the regression coefficients representing the atmospheric effects on the hard component of the cosmic radiation at sea-level. This component is usually defined as that part of the radiation which is able to penetrate 10 cm of lead. It consists of nearly only μ-mesons, and their number depends on the atmospheric conditions. The intensity of the hard component is usually correlated with the barometric pressure B at sea-level, the height H_1 of the 100 mb level and the temperature T_1 at or near that level. The barometer effect is mainly due to the absorption of the radiation in the atmosphere. The correlation with the height of the 100 mb level is due to the dependence of the disintegration probability of the μ-mesons on the distance between their production levels and sea-level, whereas the origin of the (positive) temperature effect is more complicated.

The interpretations of these effects have been discussed by Trefall (1955 a, 1955 b and 1956), and theoretical estimates of the regres-

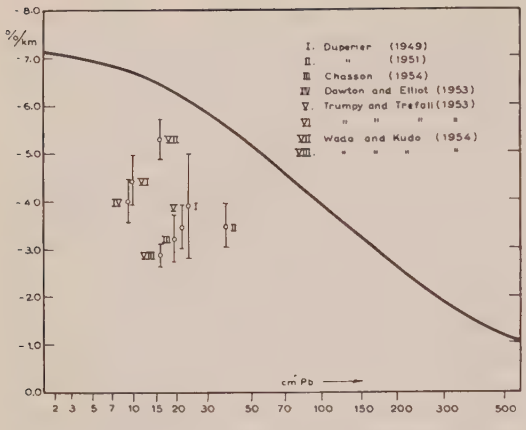

Fig. 1. In this figure are plotted theoretical estimates and empirical values of the height coefficient belonging to the set of independent variables B, H_1 and T_1, as functions of the amount of absorbing material in the cosmic-ray recording apparatus. The recordings in Manchester were performed with about 10 cm of lead.

sion coefficients have been calculated and compared with empirical results. It was then found (Trefall 1956) that the empirically determined values of the height coefficient (the partial regression coefficient with respect to H_1, often also called the negative temperature coefficient) had usually too small numerical values to be compatible with the theoretical estimate. This is clearly shown in Figure 1, where curve B gives the theoretically expected dependence of the height coefficient on the amount of absorbing material in the meson recorder. At that time no satisfactory explanation could be found for the discrepancy, but it now appears that it is probably due to errors in the aerological data which have been used as independent variables in the regression equation for the determination of the atmospheric effects.

2. *Estimation of errors in aerological data*

The observational errors in radiosonde data have been studied in later years by several authors. Some of their results are given in Tables 1 a, b and c. Raab and Rodskjer (1950) used twin soundings, and obtained the error standard deviations given in Table 1 a. From night soundings Rossi (1952) obtained similar results (Table 1 b). From the Payerne comparison of radiosondes Nyberg (1952) computed the standard deviations given in Table 1 c

Table 1 a. Estimates of error standard deviations for the Finnish radiosonde
(Raab and Rodskjer 1950)

Meteorological element	Isobaric levels	
	350 mb—150 mb	≧ 150 mb
Temperature	0.57 °C	0.61 °C
Pressure.....	6.3 mb	4.5 mb

Table 1 b. Error standard deviations for night twin soundings with the Finnish radiosonde
(Rossi 1952)

Meteorological element	Isobaric levels		
	275 mb	162 mb	96 mb
Temperature.....	0.68 °C	0.72 °C	0.78 °C
Pressure.....	4.1 mb	3.0 mb	3.2 mb

Table 1 c. Error standard deviations for the Payerne data of 1950
(Nyberg 1952)

Meteorological element	Radiosonde type	Isobaric levels	
		500 mb—300 mb	300 mb—200 mb
Temperature	Finnish	0.54 °C	0.86 °C
	All six tested	0.47 °C	0.81 °C
Pressure....	Finnish	5.4 mb	5.9 mb
	All six tested	5.2 mb	5.8 mb

for the errors in night releases. These values are probably lower than the errors of aerological data obtained under ordinary working conditions, when there is less careful inspection of the instruments and less reliable conversion of transmitted data. In addition all aerological records incorporate influences from small-scale systems such as cumulus convection, gravity waves and others. Such disturbances are "noise" on the synoptic scale, and effectively increase the errors beyond those obtained from twin soundings.

A better method for determining the total error variance would be to perform simultaneous or approximately simultaneous soundings at stations separated by a distance of the order of 10 km. Such a pair of stations now exist on Spitzbergen, where the Norwegian station at Isfjord Radio and the Russian station

at Barentsburg are situated only 18 km apart. If Y_i and Y_j denote the deviations of two meteorological elements from their respective mean values, we have

$$Y_{i,I} - Y_{i,B} \approx \varepsilon_{i,I} - \varepsilon_{i,B} \tag{33}$$

and

$$Y_{j,I} - Y_{j,B} \approx \varepsilon_{j,I} - \varepsilon_{j,B}, \tag{34}$$

where subscripts I and B refer to Isfjord Radio or Barentsburg data, respectively. As there can be no significant correlation between the errors in corresponding data from the two stations, we find that the error covariances of the stations are related by the equation

$$\overline{\varepsilon_{i,I}\varepsilon_{j,I}} + \overline{\varepsilon_{i,B}\varepsilon_{j,B}} \approx \overline{(Y_{i,I} - Y_{i,B})\,(Y_{j,I} - Y_{j,B})}. \tag{35}$$

Putting $i=j$ we obtain an equally valid relation for error variances.

In order to separate the error variances of the two stations some assumption must be made regarding their relative reliability. As there is nothing to suggest that one station is more reliable than the other, our best estimate of the error covariance of a pair of meteorological elements observed at any station is, according to the method of maximum likelihood,

$$\overline{\varepsilon_i\varepsilon_j} = \frac{1}{n}\sum (Y_{i,I} - Y_{i,B})\,(Y_{j,I} - Y_{j,B}) \tag{36}$$

where the summation has been performed over the n available data. Error variances are again obtained by putting $i=j$. Having thus estimated both variances and covariances of errors, correlation coefficients between errors may also be computed. The results are presented in Tables 2 and 3. In order to check the stability of these statistical parameters the data were divided in two groups of approximately equal sizes. The variances are apparently very stable, as was confirmed by means of the F-test. The correlation coefficients are not so stable, even though none of the differences are statistically significant at the 5 % level.

The existence of correlations between errors is, of course, due to the fact that the heights of the isobaric levels are not measured directly, but are computed from records of the atmospheric temperature distribution as a function of pressure. Any error in the temperature measured at a given pressure level will, therefore, contribute to the error in the heights of

Table 2. Estimated error variances for heights and temperatures

Period	300 mb			200 mb			100 mb		
	$\overline{\varepsilon_T^2}$ $(C°)^2$	$\overline{\varepsilon_H^2}$ m^2	n	$\overline{\varepsilon_T^2}$ $(C°)^2$	$\overline{\varepsilon_H^2}$ m^2	n	$\overline{\varepsilon_T^2}$ $(C°)^2$	$\overline{\varepsilon_H^2}$ m^2	n
17 Sept.—29 Oct. 1957	2.74	1743	40	5.09	2862	33	5.25	5229	19
1 Nov. 57—6 Jan. 1958	2.42	1991	46	4.39	2434	36	4.51	4986	17
Both combined	2.56	1898	86	4.69	2772	69	5.04	5074	36

Table 3. Correlation coefficients between errors

Period	Errors of:		
	H_1 and T_1	H_1 and H_2	H_1 and H_3
17 Sept.—29 Oct. 1957	0.589	0.766	0.728
1 Nov. 57—6 Jan. 1958	0.495	0.508	0.252
Both combined	0.560	0.628	0.465

all higher levels. Only errors in the thicknesses of not overlapping atmospheric layers are expected to be uncorrelated. A further check on the correlations obtained could therefore be performed by computing correlation coefficients between the errors in the height H_2 of the 200 mb level and the thickness $H_1 - H_2$ of the 100 – 200 mb layer, and between the errors in the height H_3 of the 300 mb level and the thickness $H_1 - H_3$. The values obtained for the combined periods were – 0.050 and + 0.188, respectively, none of which are significantly different from zero.

Eliassen (1954), who analysed data from British stations, estimated by means of a different method the error variance of the height of the 300 mb level to be 2,092 m². This agrees very well with the results that are given in Table 2, and indicates that the error estimates in Table 2 can be used in the following discussion.

3. *Evaluation of corrected cosmic-ray regression coefficients*

After having thus obtained estimates of the error variances and covariances of the necessary meteorological elements, corrections were applied according to (5) to the aerological data used in the analysis of some cosmic-ray records from Manchester. The errors in the sea-level pressure records could be neglected because their variance was negligible compared to the total pressure variance. The aerological data came from the Liverpool station some 50 km away, whereas the pressure data were recorded in Manchester. As the cosmic-ray data represented the integrated intensity throughout a day, corresponding mean values were used for the meteorological elements. The daily mean of the barometric pressure was based on 24 hourly readings, and the aerological data on 4 radiosonde ascents per day. Only days on which all soundings reached the 100 mb level were used. When the corrections for errors were applied, allowance was made, of course, for the fact that we were using daily mean values of the meteorological elements.

Two periods were selected for analysis, one from July 13th to September 11th 1950, and another from September 1st to November 7th 1951, containing 34 and 40 useful days respectively. The total variances of the meteorological elements were quite different for the two periods, being very low in 1950 and rather high in 1951. This is clearly shown in Table 4, where we have given ratios between total variances of aerological data for each of the two periods and our estimated error variances. We therefore expect the regression coefficients from the 1950 period to be much more affected by the random errors of measurement than those from 1951.

In Table 5 we have given uncorrected and corrected regression and correlation coefficients corresponding to three different sets of independent variables. The reasons for introducing the second and third sets of variables will be given later. It should here only be noted that the theoretical estimates of the height coefficient b_2' are nearly equal for all three sets of variables, its numerical value increasing only slightly as we go from the first to the third set. The temperature coefficient b_3' will, however, depend critically on the choice of variables and is, in fact, expected to change from positive to negative values as we go from the first to the third set. The corresponding change in b_1' is negligible.

The differences between the uncorrected and corrected height coefficients for the 1950 period are remarkable. Even though the values of b_2 obtained with the three different sets of variables are on the average only about 60 % of the corresponding theoretical values, the corrected coefficients b_2' agree very well

Table 4. Ratios between total variances and estimated error variances for the Liverpool aerological data

Period	Variable					
	T_1	H_1	H_2	H_3	H_1—H_2	H_1—H_3
1950.....	5.6	2.1	11.9	21.2	6.4	6.6
1951.....	11.4	18.7	45.0	58.8	10.3	11.0

Table 5. Regression and correlation coefficients for cosmic-ray atmospheric effects

Variables	Period	Uncorrected				Corrected			
		b_1 %/km	b_2 %/km	b_3 %/°C	R	b_1' %/km	b_2' %/km	b_3' %/°C	R'
B, H_1, T_1	1950	— 1.46	— 3.48	+ 0.079	0.849	— 1.37	— 6.38	+ 0.067	0.860
	1951	— 0.84	— 5.95	+ 0.116	0.966	— 0.80	— 6.28	+ 0.124	0.971
$B, H_2, (H_1—H_2)$	1950	— 1.34	— 4.13	— 0.003*	0.865	— 1.25	— 6.70	— 0.059*	0.875
	1951	— 0.86	— 6.00	— 0.032*	0.961	— 0.83	— 6.27	— 0.035*	0.965
$B, H_3, (H_1—H_3)$	1950	— 1.15	— 4.72	— 0.019*	0.870	— 1.08	— 6.99	— 0.099*	0.879
	1951	— 0.85	— 6.52	— 0.091*	0.958	— 0.85	— 6.78	— 0.102*	0.963

* In order to facilitate comparisons between the regression coefficients b_3 or b_3' obtained with different sets of independent variables, all coefficients marked by asterisks have been given in terms of equivalent variations of the mean temperature of the atmospheric layer under consideration.

with the theoretical estimate presented in Figure 1. Further, the rather high values of the barometer coefficient b_1 obtained with the first and second sets of variables are somewhat reduced when the corrections are applied. The temperature coefficient b_3 obtained with the first set seems, however, to be adversely affected by the correction.

The results from 1951 are not quite so satisfactory. This period is characterized by abnormally low values of the barometer coefficient b_1, and the even lower values of b_1' are not encouraging. The height coefficients b_2 behave better, as they already before the correction agree fairly well with the theoretical estimates and the slight changes after the correction bring them into very good agreement with the corresponding coefficients for the 1950 period. The reason why the height coefficients of the 1951 period are so much less affected by our correction is, no doubt, that the total variances of the heights of all isobaric levels are greater in 1951 than in 1950. The temperature coefficients b_3 have quite reasonable values both before and after the correction.

Our correction has in all cases led to an increase of the multiple correlation coefficient. However, it was shown in the first part of this paper that only under very special circumstances would such a correction not lead to an increase in the multiple correlation coefficient. This would hold even if error variances and covariances were arbitrarily chosen within the range permitted by the general laws of statistics. The observed differences between R' and R cannot, therefore, be made the basis for any conclusion regarding the correctness of the estimated error variances. The real tests are that the variability of the regression coefficients obtained for different periods should be reduced and the agreement between empirical values and theoretical estimates should be improved.

The view that the low empirical height coefficients obtained by most workers may have been caused by the large errors in the height H_1 of the 100 mb level, is supported by the fact that higher values are usually found when monthly means of cosmic-ray intensity are correlated with corresponding meteorological data than when daily means are used (Bachelet and Conforto, 1956). As we expect the ratio of error variance to total variance to be smaller for monthly means than for daily means, such a trend in the empirically determined coefficients is to be expected. It must, however, be remembered that the characteristics of the day-to-day variations of the atmospheric temperature distribution differ from those of the seasonal variations. As the atmospheric temperature distribution is far from uniquely determined by the chosen variables, differences between "seasonal" and "day-to-day" regression coefficients may arise also in this way.

III. Conclusion

The results obtained demonstrate how drastically empirical regression coefficients may

be influenced by random errors of measurement. Therefore, if one out of a number of measured quantities can select different sets of variables, which would have contained approximately equal amounts of information had no errors been present, one should use that set for which the ratios between the error variances and the true variances of the variables are the lowest.

In Table 4 we gave ratios between the total variance and the estimated error variance of the quantities which have been employed as independent variables in the present analysis. It is not surprising to find that this ratio is much smaller for H_1 than for H_2 or H_3. The decrease of the ratio with increasing height is mainly due to the negative correlation between stratospheric and tropospheric temperatures, which makes the true variance of H_1 less than the corresponding variances for levels closer to the tropopause. As the error variance steadily increases with increasing height as shown in Table 2, the relative error variance (the ratio between error variance and total variance) increases very rapidly as we go from the troposphere to the stratosphere.

From the statistical point of view the height H_1 of the 100 mb level is, therefore, a poor variable. Actually, the extensive use of H_1 in the study of the atmospheric effects on the cosmic radiation seems to be somewhat fortuitous. It is true that Duperier, who was the first one to correlate cosmic-ray intensity with heights of isobaric levels, obtained a better correlation with H_1 than with heights of lower levels (Duperier 1945). However, later results by Duperier and others (Duperier 1949, Wada 1951, Bachelet and Conforto 1956) do not generally show this preference for the 100 mb level, and actually indicate that on the average the correlation is better with the 200 mb level than with the 100 mb level. This is really not surprising, as the mean level of meson production appears to lie near 150 mb.

Even though it might be desirable to avoid the 100 mb level altogether and use only data from lower levels, theoretical considerations show that some information about higher levels is also needed for a really satisfactory representation of the cosmic-ray atmospheric effects. This is the reason why H_1 has been retained in our second and third sets of variables, and only the temperature T_1 at the 100 mb level has been replaced by the height of some lower isobaric level. From the statistical point of view and according to Table 4 these sets should certainly be better than the first one. The results given in Table 5 show that the corrected regression coefficients are most stable when the third set of variables is employed, but no final conclusion should be based on the results obtained from these two small samples only.

The reasons why we have used the thickness of a certain layer (the difference between two heights) as the third variable of the second and third sets rather than the single height H_1 are threefold: Firstly, these sets of variables are essentially the same type as the first one because the third variable is a measure of the mean temperature of that layer, and this makes the comparison of regression coefficients very easy. Secondly, we now avoid the intercorrelation between errors which makes the detailed study of their effects so difficult. Finally, with this type of regression equation each term has a more direct physical significance than in the other case.

As a final remark we mention that the relative error variance of the atmospheric temperature has a minimum near the 200 mb level, where it is less than half the value at 100 mb (Nordö, 1958). Remembering that the mean level of meson production lies near 150 mb, one would expect the barometric pressure B, the height H_2 of the 200 mb level and the temperature T_2 at this level to be a very good set of variables for the representation of the cosmic-ray atmospheric effects. The reason why we have not tried this set is that the main purpose of the present paper was to point out the important effects which random errors of measurements generally may have on empirical regression coefficients. The cosmic-ray case should mainly serve as an example indicating the applicability of the mathematical considerations given above.

IV. Acknowledgments

We are indebted to Mr. P. Breistein of the Arctic Group, Det Norske Meteorologiske Institutt, Oslo, for providing aerological data from Isfjord Radio and from Barentsburg, and to Dr. H. Elliot, Imperial College, London,

for the use of cosmic-ray records from Manchester. The aerological data from Liverpool were taken from the Daily Aerological Record of the Meteorological Office, London.

Finally, we wish to express our best thanks to Forskningsfondet av 1919 for financial support of this work obtained by one of the authors (Trefall).

REFERENCES

Bachelet, F., and Conforto, A. M., 1956: Atmospheric Effects on the Cosmic Ray Total Intensity at Sea Level, *Il Nuovo Cimento, Series X*, **4**, p. 1479.

Duperier, A., 1945: The Geophysical Aspects of Cosmic Rays. *Proc. Phys. Soc. A*, **57**, p. 464.

Duperier, A., 1949: The Meson Intensity at the Surface of the Earth and the Temperature at the Production Level. *Proc. Phys. Soc. A*, **62**, p. 684.

Eliassen, A., 1954: Provisional Report on Calculation of Spatial Covariance and Autocorrelation of the Pressure Field. *Videnskapsakademiets Institutt for Vær- og klimaforskning, Oslo. Rapport nr* **5**, 1954.

Nordö, J., 1958: Unpublished manuscript.

Nyberg, A., 1952: On the Comparison of Radiosonde Data in Payerne, May 1950. *Sveriges Met. Hydr. Inst. Medd., Serie B, nr* **9**.

Raab, L. and Rodskjer, N., 1950: A Study of the Accuracy of Measurements of the Väisälä Radiosonde. *Arkiv för Geofysik*, **1**, No. 2.

Rossi, V., 1952: On the Accuracy of the Finnish Radiosonde. *Geophysica*, **4**, No. 2.

Spearman, G., 1904: The Proof and Measurement of Association between two Things. *Amer. J. Psych.*, **15**, p. 88. (See also Yule and Kendall: *An Introduction to the Theory of Statistics*. Charles Griffin Co., Ltd., London 1949.)

Trefall, H., 1955 a: On the Positive Temperature Effect in the Cosmic Radiation and the μ-e Decay. *Proc. Phys. Soc. A*, **68**, p. 893.

— 1955 b: On the Barometer Effect on the Hard Component of the Cosmic Radiation. *Proc. Phys. Soc. A*, **68**, p. 953.

— 1956: On the Interpretation of the Atmospheric Effects on the Hard Component of the Cosmic Radiation. *Universitetet i Bergen, Årbok 1956, Naturvitenskapelig rekke, nr* **10**.

Wada, M., 1951: The Relation between Cosmic-Ray Intensities and Heights of Isobar Levels. *J. Sci. Res. Inst., Tokyo*, **45**, p. 77.

Isotopic Composition of Sulfur in Precipitation and Sea-Water

By GÖTE ÖSTLUND, Radioactive Dating Laboratory, Geological Survey of Sweden, Stockholm

(Manuscript received May 14, 1959)

Introduction

As an attempt to approach the question of the origin of airborne sulfur, it was intended to make measurements of natural S^{35} and determine the S^{32}/S^{34}-ratio of sulfur in rain-water. For different reasons the S^{35} counting had to be omitted, but the S^{32}/S^{34}-ratio, and the sulfur contents of a number of samples of precipitation and sea-water were made.

Experimental

The rain, snow, and lake water samples were percolated through a cotton-wool filter and then through a chloride saturated anion exchange column with a volume of 175 ml, at a rate of 100 ml/min. The sulfate was eluted with sodium chloride solution and the column washed several times with distilled water. Barium sulfate was precipitated in the usual manner from the eluate, and the sulfur content was calculated from its weight and the original volume of water. In one case (Sample S 4) the efficiency of the sorption step was tested by using two columns in series. No trace of sulfate could be detected in eluate from the second column. The figures for sulfur content in Table 1 are thus reproducible within ± 2 % of their values. From the sea-water samples, barium sulfate was precipitated directly.

In collecting rain-water from roofs, each sample was taken after the rain had washed the roof thoroughly. Between 50 and 300 liters were taken, corresponding to at least 50 mg of sulfate sulfur.

For mass-spectrometric analysis the barium sulfate samples were converted to cadmium sulfide, which was mixed with vanadium-V-oxide. By heating this mixture gave sulfur dioxide for the mass-spectrometer. This procedure is described by GAVELIN et al. (1959).

Description of locations

Stockholm: A copper roof at the Royal Institute of Technology in the NE part of central Stockholm. Snow taken from ground. Lat. 59° 21′ N, Long. 18° 05′ E.

Huddinge: A tile roof in Huddinge, a scattered residential area 13.5 km SSW of the above locality. Lat. 59° 14′ N, Long. 17° 59′ E.

Köping: A felt roof in the E part of the city of Köping on Lake Mälaren, 120 km W of Stockholm. Lat. 59° 31′ N, Long. 16° 01′ E.

Flahult: A tile roof at a farm in Flahult, Småland, 7.5 km S of Jönköping. Lat. 57° 42′ N, Long. 14° 08′ E.

Texas: Rain-water taken with a plastic funnel at the Institute of Marine Research, Port Aransas, Texas, on the coast of the Gulf of Mexico. Lat. 27° 50′ N, Long. 97° 04′ W.

Table 1. Assay and isotopic composition of sulfatic sulfur in various waters

Sample No.	Date y/m/d	Sample of	Location	Sulfur content mg/l	Isotope ratio	
					$\delta S^{34}/S^{32}$	S^{32}/S^{34}
S 1	57/02/11—16	Snow	Stockholm	0.49	+ 0.7	22.21
S 2	57/02/16—17	”	”	1.34	+ 1.8	22.18
S 3	57/06/23—24	Rain	Köping	1.08	+ 3.4	22.15
S 4	57/09/00—02*	”	Stockholm	2.63	— 1.7	22.26
S 5	57/09/12	”	”	6.27	+ 0.3	22.22
S 6	57/09/13	”	”	2.40	— 0.1	22.23
S 7	57/09/19	”	”	1.70	— 0.9	22.25
S 8	57/09/24	”	”	2.04	+ 2.2	22.18
S 9	57/10/17	”	”	3.18	+ 1.8	22.18
S 10	57/10/17	”	Huddinge	1.75	+ 1.8	22.18
S 11	57/10/18	”	”	0.93	+ 1.4	22.19
S 12	57/10/18—20	”	Flahult	2.54	+ 2.6	22.17
S 17	58/01/11 } 58/02/10 }	”	Texas	—	+ 1.4	22.19
S 18	58/01/— —**	”	Washington	—	+ 0.6	22.21
S 13	57/04/xx***	Sea water	Arctic Sea	914	+ 15.1	21.89
S 14	57/09/30	”	North Sea	722	+ 14.7	21.90
S 15	57/10/10	”	Bothnia	150	+ 15.6	21.88
S 16	57/10/24	Lake water	Mälaren	15.5	— 2.2	22.27

* Aug. 31 to Sept. 2
** Actual day unknown
*** Various days during April

Washington: Rain-water taken with a plastic funnel in Nahcotta, Washington, on the Pacific Coast. Lat. 46° 31′ N, Long. 124° 02′ W.

Arctic Sea: Various small quantities of surface water taken during a cruise from the Shetland Islands to North of Iceland. April 1957.

North Sea: Surface water taken at the lightship of Fladen, 55 km SSW of Göteborg in Cattegat. Lat. 57° 12′ N, Long. 11° 48′ E.

Bothnia: Surface water at the lightship of Finngrundet in the Gulf of Bothnia, 190 km NNE of Stockholm. Lat. 61° 15′ N, Long. 18° 39′ E.

Mälaren: Untreated water for Stockholm municipal water system. The intake is at a depth of 18 m in Lake Mälaren, 25 km W of Stockholm. Lat. 59° 20′ N, Long. 17° 48′ E.

Results

In Table 1 are given the results obtained. The exact locations are given above. The isotope ratios refer to the average-meteorite standard, used by the University of Hamilton group, accepted to have a S^{32}/S^{34}-ratio of 22.225 (Gavelin 1959). If R_s is the S^{34}/S^{32}-ratio for the standard (1/22.225) and R_x the corresponding ratio for the unknown sample, δ is defined according to

$$\delta = \frac{R_x - R_s}{R_s} \cdot 1000$$

The reproducibility of the values are ± 2 % of the value in sulfur assay, ± 0.9 in δ, and ± 0.02 in S^{32}/S^{34}-ratio.

Discussion

The most striking result to be recognized by looking at Table 1, is the marked constancy of the isotopic ratio of the sulfur in precipitation, regardless of location and time of year, and despite large differences in sulfur concentration. Even the coast rains at the Gulf of Mexico and the Pacific give the same ratio as the east wind snow over Scandinavia. The mean of all isotopic ratios in precipitation is 22.20 and the extremes are 22.26 and 22.15. The average isotopic ratio obtained for sea-water sulfate, 21.91, differs slightly from the average of 21.80, compiled by Rankama (1954), and measurements by Feely and Kulp (1957). Our values are much closer to the higher ratios given by Thode et al. for the Pacific

(also partly referred by Rankama).* The unexpected high S^{32}/S^{34} value for Lake Mälaren is probably due to local conditions in the soil and ground of the Mälar basin.

There is a large difference in isotopic ratio between sea-water and precipitation, but very little probability of chemical or other fractionation processes on the path of the sulfur from the sea-water drops to the rain. It can therefore be considered quite true, that the sulfate sulfur in precipitation is *not* likely to originate principally from sea-water spray. Natural materials having isotope ratios closer to those of precipitation, and which are possible sources of airborne sulfur, are among others volcanic gases, sulfur in coal and petroleum used industrially, and biogenic hydrogen sulfide e.g. from marshes and swamps. More comprehensive estimates of the sulfur isotope balance of the atmosphere, surface waters, and the earth's crust might perhaps throw some light on which source could be the most important.

* In a recent paper (Geochim. et Cosmochim. Acta **16**, p. 213 (1959)) Ault and Kulp have obtained a very small spread around an avergage of 21.76. Our primary standard was a Sudbury nickel sulfide ore submitted 1956 by Jan Monster at the University of Hamilton (Sample No. 10708), stated to have the value 21.203. In Table 6 in Ault's paper Sudbury sulfides are measured to 22.11. It is thus extremely likely that the difference between our and Ault's values of sea-water is a question of standards.

Acknowledgements

The valuable technical assistance by Mr L. Lundgren at this laboratory and Mr A. Parwel at the Mineralogic Institute of the Riksmuseet in making the preparations, and by Mr R. Ryhage at the Karolinska Institutet for the mass-spectrometric determinations is hereby appreciated. Dr E. Eriksson at the International Meteorological Institute in Stockholm kindly provided the two American samples.

REFERENCES

Feely, H. W. and Kulp, J. L., 1957: Origin of Gulf Coast Salt-Dome Sulfur Deposits. *Bull. Ass. Am. Petr. Geol.* **41**, p. 1816.

Gavelin, S., Parwel, A., and Ryhage, R., 1959: Sulfur Isotope Fractionation in Sulfide Mineralization. *Econ. Geol.* in press.

Rankama, K., 1954: *Isotope Geology*, London, Pergamon Press Ltd., p. 279.

Thode, H. G., Macnamara, J., and Fleming, W. H., 1953: Sulfur Isotope Fractionation in Nature and Geological and Biological Time Scales. *Geochim. et Cosmochim. Acta*, **3**, pp. 235—243.

Further Statistics Concerning the General Circulation

By VICTOR P. STARR

Massachusetts Institute of Technology, Cambridge, Massachusetts[1]

(Manuscript received March 31, 1959)

During the past few years it has become increasingly clear that the newer outlook upon the fundamental processes of the general circulation continues to flourish and prosper. It bids fair to become the essential starting point for all rational discussion of the large motions of the atmosphere, as indeed it must if its principal ideas are correct. This stage has been reached not without much debate about logical matters, much effort to reinstate older schemes through secondary adjustments, and much examination of evidence. Also, any number of theoretical solutions, most of which lend support to the new views, have been advanced to illustrate the workings of the general circulation.

It likewise is worth our while to note that the trends of thought which have led us to what seems a more just view of this large subject do not find their entire application here, but have shown relevance also for smaller structures present in synoptic flow patterns. Here again consideration of the flow of momentum and the associated transfer of kinetic energy from one scale of motion to another seems to be a primary concept in the rational investigation of the behavior of synoptic systems. This is shown in a recent paper by SALTZMAN (1959). Another recent paper by KUO (1959) purports to show that, just as is the case for the circumpolar vortex, certain other large circulation systems may not release convectively their solenoidal energy. They presumably can be maintained in the atmosphere only through the action of still smaller eddies which do have associated baroclinic releases of energy in them. A general interpretation of all these developments has been given by STARR (1959).

Let us return to the larger problem, however. The writer (STARR, 1948) has long ago pointed out that the processes of gathering statistics concerning the new view of the general circulation would require much time and effort. We are still thus occupied, but since the results are quite gratifying, these labors are not so much of a burden as one might suppose judging merely from the amount of time and drudgery which is entailed. On the other hand, such work must be done, if we are to build solidly, because no other source of information can be equivalent to it (see STARR 1958 in this regard).

One activity which has its aim in this general direction is the work of SALTZMAN (1957, 1958). This consists of a plan to study the transfers of kinetic energy from the eddies to the mean zonal motions by use of the technique of spectral analysis, in order to examine the role played in this action by eddies corresponding to various wave numbers around the hemisphere. In addition, the process of convective kinetic energy release

[1] This research has been supported by the Geophysics Research Directorate, Air Force Cambridge Research Center, Air Research and Development Command, under Contract AF 19 (604)—2242.

through vertical motions may also be brought within the ambit of the scheme. Aside from the partial results already presented earlier, new findings in this area, obtained from the analysis of a complete year of geostrophic data are now being reported by SALTZMAN and FLEISHER (1959). Still more extensive results are expected at a later date.

Since they serve as an interesting comparison to the Saltzman and Fleisher statistics, the writer wishes to make available the outcome of computations from actual wind data for an additional year, similar in an over-all fashion to those published several years ago (STARR, 1953) for the year 1950. The new findings are for the calendar year 1951—the same period as was used by SALTZMAN and FLEISHER.

The 1950 study concerned itself with the evaluation of an integral over the atmosphere in the northern hemisphere of the form

$$2\pi r^2 \int\int \varrho\,[u'v']\,\cos^2\phi\,\frac{\partial}{\partial\phi}\left(\frac{[u]}{r\cos\Phi}\right)d\phi dz \quad (1)$$

u, v being the eastward and northward wind components, ϱ density, r earth's radius, Φ latitude, z elevation, the square brackets denoting averages along complete latitude circles, and the primes indicating deviations from such averages. Since the integrand contains, in proper form, the product of the eddy stress into the meridional shear of angular velocity of the mean flow, (1) gives the instantaneous rate of conversion of eddy kinetic energy into mean flow kinetic energy through the action of the horizontal wind. In almost all details the procedures used for the 1951 study are a duplication of those for the 1950 study (to which the reader is referred). The chief differences are due to the somewhat better quality and quantity of the 1951 data, so that it seemed desirable to make use of compilations for the 100- and 1,000-mb levels which were omitted previously. The following are the results.

(1) The expression above was evaluated on a daily basis. The average of these 365 values was $(5.8\pm1.0)\times10^{20}$ erg sec^{-1}. All individual monthly values were positive. Since these calculations were made by levels and by days, this figure is comparable to that obtained in the previous study in paragraph (3) under »Critique and further computations», for the first half of 1950, namely 9.8×10^{20} erg sec^{-1}. The confidence limits are twice the standard error of the mean. The 70° N latitude data were included for 1951 in all studies.

(2) The use of a vertically-averaged momentum transport and a vertically-averaged shear (on a daily basis) in evaluating (1) resulted in a value of $(4.8\pm0.7)\times10^{20}$ erg sec^{-1} for the year. All individual monthly values were again positive. This is comparable to the value $(4.5\pm1.0)\times10^{20}$ erg sec^{-1} reported previously in paragraph (2) under "Critique, etc.", for the first half of 1950.

(3) When one resorts to computations based upon mean profiles for the year averaged vertically as well as with respect to time (comparable to those shown in Fig. 1 of the previous study), one gets the value of 4.6×10^{20} erg sec^{-1}. This is in good agreement with the value of 4.4×10^{20} erg sec^{-1} calculated for the entire year of 1950.

(4) Use of the 500-mb data alone for the momentum transport and shear, assuming these to be representative of the average for the atmosphere (on a daily basis) resulted in the quantity $(6.2\pm1.2)\times10^{20}$ erg sec^{-1} for the year (all monthly values positive). A figure to be compared with this, based upon 500-mb geostrophic data, was obtained by SALTZMAN and FLEISHER, also for the year 1951. Their figure is $(3.8\pm1.2)\times10^{20}$ erg sec^{-1} with all months positive. It is tempting to assume that the lower figure for the geostrophic calculations is mainly a result of a smoothing process in the drawing of maps of the contours from which gridpoint data were read.

It must not be lost sight of, that the present calculations are subject to all the strictures and qualifications enumerated in the discussion of the previous study. Such features as the probable underestimation of the total effects computed here, due to selectivity favoring more frequent observation of lighter winds at higher levels, is as true for the present data as for the previous compilations. Added to these, it should be borne in mind that individual years may vary greatly one from another in regard to the properties here studied. Shorter periods may of course show even more striking differences.

The data compiled for the year 1951 afforded an opportunity to repeat another calculation which the writer had the privilege to communicate some years ago in the pages of this

journal, again using an assemblage of statistics for the calendar year 1950 (see STARR 1954). These two studies pertain to the measurement from actual wind data of the efficacy in the atmosphere of the classical mechanism for the maintenance of the kinetic energy of the mean zonal motions. As explained in the former paper such efforts are afflicted with great difficulties, but since a new set of extremely extensive and in many ways better observations offered another independent occasion to execute the computation, the resulting figures are given herewith.

For our present purpose it is needed to evaluate the effect of the mean meridional circulations in producing kinetic energy of the mean zonal motions through the action of Coriolis forces. This action is given by

$$\varrho f[\overline{u}]\,[\overline{v}[\qquad (2)$$

per unit volume of air. Here ϱ is density, f the Coriolis parameter, u the eastward and v the northward component of velocity, while the brackets denote zonal averages and bars time averages. The reader is directed to the former paper for added details. The volume integrals by latitude belts and for the hemisphere are given in the accompanying table together with a reproduction of the corresponding numbers for 1950. The figures for the hemisphere for both years show a net destruction of kinetic energy of mean zonal motions.

Since the kinetic energy stored in the mean meridional circulations themselves is always extremely small, and since the mean zonal motions are sensibly geostrophic, the negative value of the figures given above for the hemisphere possess the implication that the mean meridional circulations convert kinetic energy back into potential and internal. This has been commented upon, for example, by LORENZ (1955).

Excluding the figure quoted from Saltzman and Fleisher's study, the amount of data on which the results given for 1950 and 1951 are based is enormous. About a quarter million winds were processed—a task which has required the sustained efforts of a crew of skilled computers for several years. In view of the fact that much of the labor in this type of study consists in the tabulating of the initial observations, not much is gained through the use of electronic calculators, unless the input can be secured in a form already recorded on magnetic tape. Fortunately this is the case for the International Geophysical Year observations which are now being processed so as to obtain further information from data which no doubt are significantly better than either those for 1950 or 1951.

TABLE 1.

Volume integral for the atmosphere from 1 000 to 100 mb of the quantity $\varrho f[\overline{u}]\,[\overline{v}]$ in 10^{20} erg sec^{-1}.

Lat. Belt	0—13°	13—31°	31—42°	42—55°	55—70°	70—90°	Hemisphere
Int. 1950	+ 0.01	— 0.35	— 3.55	— 2.65	+ 2.69	+ 1.76	— 2.09
Int. 1951	+ 0.27	— 0.00	— 4.79	— 3.93	+ 3.61	+ 1.68	— 3.16

REFERENCES

KUO, H. L., 1959: Finite amplitude three-dimensional harmonic waves on the spherical earth. *J. Meteor.*, **16**, p. 524.

LORENZ, E. N., 1955: Available potential energy and the maintenance of the general circulation. *Tellus*, **7**, p. 157.

SALTZMAN, B., 1957: Equations governing the energetics of the large scales of atmospheric turbulence in the domain of wave number. *J. Meteor.*, **14**, p. 513.

— 1958: Some hemispheric spectral statistics. *J. Meteor.*, **15**, p. 259.

— 1959: On the maintenance of the large-scale quasi, permanent disturbances in the atmosphere. *Tellus*, **11**- pp. 425—431.

SALTZMAN, B., and FLEISHER, A., 1959: Hemispherci kinetic energy transfer spectrum (to be published in Tellus 1960).

STARR, V. P., 1948: An essay on the general circulation of the earth's atmosphere. *J. Meteor.* **5**, p. 39.

— 1953: Note concerning the nature of the large-scale eddies in the atmosphere. *Tellus*, **5**, p. 494.

— 1954: Commentaries concerning research on the general circulation. *Tellus*, **6**, p. 268.

— 1958: What constitutes our new outlook on the general circulation? *J. Met. Soc. of Japan*, **36**, p. 167.

— 1959: Trends of thought concerning meteorological research. *Geof. Pura e* **43**, p. 269.

INDEX

Aarons, J.: Effects of the solar flares of 7 July 1958, 319.
Adiabatique, taux de variation, Dufour, 1.
Alfvén, H.: Momentum spectrum of cosmic radiation, 106.

Baltic, uninodal seiches in, Lisitzin, 459.
Baroclinic atmosphere, Monin, Obukhov, 159.
— models, Wiin-Nielsen, 45.
Baus, R. A.: Fission product radioactivity in the air along the 80th meridian — January—June 1957, 83.
Be^7, Goel, Narasappaya, Prabhakara, Thor, Zutshi, 91.
Bleichrodt, J. F.: The dependence of artificial radioactivity in rain on rainfall rate, 404.
Blifford, Jr., I. H.: Fission product radioactivity in the air along the 80th meridian — January—June 1957, 83.
Blok, J.: The dependence of artificial radioactivity in rain on rainfall rate, 404.
Boric acid evaporation, Gast, Thompson, 344.
Bray, J. R.: An analysis of the possible recent change in atmospheric carbon dioxide concentration, 220.
Bryan, K.: A numerical investigation of certain features of the general circulation, 163.
Båth, M.: Book Review, 257.

Chloride, yearly circulation of, Eriksson, 375.
Cloud nucleus population, Twomey, Squires, 408.
CO_2 concentration, Bray, 220.
—, current data, 145, 265, 373.
Coalescence in shallow cumulus, Mason, 216.
Convection, influence of rotation on, Starr, 360.
Convective clouds, Twomey, Squires, 408.
— currents, Haltiner, 4.
Cooley, D. S.: Letter to the Editor, 257.
Cosmic radiation, Alfvén, 106.
— —, Dattner, Venkatesan, 239.
— —, Johansson, 101.
— —, Trefall, Nordö, 467.
— ray, Goel, Narasappaya, Prabhakara, Thor, Zutshi, 91.
— — intensity, Venkatesan, Dattner, 116.
Current data, air, and precipitation, 139, 259, 366.
— —, CO_2, 145, 265, 373.
Currents in the Baltic, Svansson, 231.
Cumulus clouds, Durbin, 202.

Dattner, A.: Long term changes in the daily variation of cosmic ray intensity, 116.
—: Anisotropies in cosmic radiation, 239.
Dekker, R. H.: The dependence of artificial radioactivity in rain on rainfall rate, 404.
Droplet sampling, Durbin, 202.
Dufour, L.: Sur le taux de variation adiabatique de la température en fonction de la pression dans une masse d'air contenant un cristal de glace sphérique, 1.
Durbin, W. G.: Droplet sampling in cumulus clouds, 202.

Earthquakes, Nishimura, Kishimoto, Tanaka, 130.
Equivalent barotropic level, Taba, 441.
Eriksson, E.: The yearly circulation of chloride and sulfur in nature; meteorological, geochemical and pedological implications. Part I, 375.
Evaporation-precipitation cycle, Kraus, 147.
Exchange models, Welander, 348.

Fischer, G.: Ein numerisches Verfahren zur Errechnung von Windstau und Gezeiten in Randmeeren, 60.
Fonselius, S.: Natural radiocarbon measurements on surface water from the North Atlantic and the Arctic Sea, 77.

Gast, J. A.: Evaporation of boric acid from sea water, 344.
General circulation, Bryan, 163.
— —, Starr, 481.
Gezeiten in Randmeeren, Fischer, 60.
Goel, P. S.: Study of cosmic ray produced short-lived P^{32}, P^{33}, Be^7 and S^{35} in tropical latitudes, 91.
Growth of cloud droplets, Mordy, 16.

Haltiner, G. J.: On the theory of convective currents, 4.
—: The diurnal variation of the wind, 452.
Hemmingsen, E.: Permeation of gases through ice, 355.
Hultqvist, B.: Effects of the solar flares of 7 July 1958, 319.
—: On the interpretation of ionization in the lower ionosphere occurring on both day and night side of the earth within a few hours after some solar flares, 332.

Ice, permeation of gases, Hemmingsen, 355.
Integral constraints, Wiin-Nielsen, 45.
Ionization in the lower ionosphere, Hultqvist, 332.
Ionized gas in magnetic field, Åström, 249.
Isotopic composition of elements, Johansson, 101.

Jet wind-profiles, Taba, 441.

Kishimoto, Y.: Observed secular tilting motion of the ground which preceded the occurrence of several destructive earthquakes, 130.
Kraus, E. B.: The evaporation-precipitation cycle of the trades, 147.
Kuettner, J.: The band structure of the atmosphere, 267.
Kuo, H. L.: Integration of four-level prognostic equations over the hemisphere, 412.

Large-scale disturbances, Saltzman, 425.
Lisitzin, E.: Uninodal seiches in the oscillation system Baltic proper—Gulf of Finland, 459.
Lock, C. J. H.: The dependence to artificial radioactivity in rain on rainfall rate, 404.
Lockhart, Jr., L. B.: Fission product radioactivity in the air along the 80th meridian — January—June 1957, 83.

Mason, B. J.: The formation of rain by coalescence in very shallow cumulus, 216.
Momentum spectrum of cosmic radiation, Alfvén, 106.
Monin, A. S.: A note on general classification of motions in a baroclinic atmosphere, 159.
Mordy, W. A.: Computations of the growth by condensation of a population of cloud droplets, 16.

Narasappaya, N.: Study of cosmic ray produced short-lived P^{32}, P^{33}, Be^{7} and S^{35} in tropical latitudes, 91.
Nishimura, E.: Observed secular tilting motion of the ground which preceded the occurrence of several destructive earthquakes, 130.
Nordö, J.: Integration of four-level prognostic equations over the hemisphere, 412.
—: On systematic errors in the least squares regression analysis, with application to the atmospheric effects on the cosmic radiation, 467.

Obukhov, A. M.: A note on general classification of motions in a baroclinic atmosphere, 159.
Oceanic thermocline, Robinson, Stommel, 295.
— —, Welander, 309.
Ortner, J.: Effects of the solar flares of 7 July 1958, 319.

P^{32}, P^{33}, Goel, Narasappaya, Prabhakara, Thor, Zutshi, 91.
Power-law distribution of drops, Welander, 197.
Prabhakara, C.: Study of cosmic ray produced short-lived P^{32}, P^{33}, Be^{7} and S^{35} in tropical latitudes, 91.

Radioactivity in fission products, Lockhart, Baus, Blifford, 83.
— — rain, Bleichrodt, Blok, Dekker, Lock, 404.
Radiocarbon measurements, Fonselius, Östlund, 77.
Rain formation, Mason, 216.
Robinson, A.: The oceanic thermocline and the associated thermohaline circulation, 295.

S^{35}, Goel, Narasappaya, Prabhakara, Thor, Zutshi, 91.
Seiches, Lisitzin, 459.
Solar flares, Hultqvist, Aarons, Ortner, 319.
— —, Hultqvist, 332.
Squires, P.: The influence of cloud nucleus population on the microstructure and stability of convective clouds, 408.
Starr, V. P.: Hydrodynamical analogy to $E = mc^2$, 135.
—: Note concerning the influence of rotation on convection, 360.
—: Further statistics concerning the general circulation, 481.
Stern, M. E.: The moving flame experiment, 175.
Stommel, H.: The oceanic thermocline and the associated thermohaline circulation, 295.
Sulfur, isotopic composition, Östlund, 478.
—, yearly circulation of, Eriksson, 375.
Svansson, A.: Some computations of water heights and currents in the Baltic, 231.

Taba, H.: The horizontal and vertical wind profiles of the subtropical and polar jet for January 1—7, 1956, and the variation of the equivalent barotropic level, 441.
Tanaka, Y.: Observed secular tilting motion of the ground which preceded the occurrence of several destructive earthquakes, 130.
Thompson, T. G.: Evaporation of boric acid from sea water, 344.
Thor, R.: Study of cosmic ray produced short-lived P^{32}, P^{33}, Be^{7} and S^{35} in tropical latitudes, 91.
Trajectory methods, Wiin-Nielsen, 180.

TREFALL, H.: On systematic errors in the least squares regression analysis, with application to the atmospheric effects on the cosmic radiation, 467.
TWOMEY, S.: The influence of cloud nucleus population on the microstructure and stability of convective clouds, 408.

VENKATESAN, D.: Long term changes in the daily variation of cosmic ray intensity, 116.
—: Anisotropies in cosmic radiation, 239.
Vertical velocity, Wiin-Nielsen, 432.

Water heights in the Baltic, Svansson, 231.
WELANDER, P.: A theoretical power-law for the size distribution of small particles or drops falling through the atmosphere, 197.
—: An advective model of the ocean thermocline, 309.
—: On the frequency response of some different models describing the transient exchange of matter between the atmosphere and the sea, 348.
WIIN-NIELSEN, A.: On certain integral constraints for the time-integration of baroclinic models, 45.
—: On the application of trajectory methods in numerical forecasting, 180.
—: On a graphical method for an approximate determination of the vertical velocity on the mid-troposphere, 432.
Wind, diurnal variation of, Haltiner, 452.
Windstau, Fischer, 60.
WURTELE, M. G.: Letter to the Editor, 256.

ZUTSHI, P. K.: Study of cosmic ray produced short-lived P^{32}, P^{33}, Be^{7} and S^{35} in tropical latitudes, 91.

ÅSTRÖM, E.: On density and isotropy of an ionized gas in a magnetic field, 249.

ÖSTLUND, G.: Natural radiocarbon measurements on surface water from the North Atlantic and the Arctic Sea, 77.
—: Isotopic composition of sulfur in precipitation and sea-water, 478.

Errata

In Volume 11, Number 2 in the article "A theoretical power-law for the size distribution of small particles of drops falling through the atmosphere" by P. WELANDER, the following corrections should be made: page 198, line 2: change A to r; page 200, line 8: change r^{-3} to r^{-5}; page 201, formula (17): change $\varepsilon^{\frac{1}{3}}$ to $\varepsilon^{-\frac{1}{3}}$.